

Methanation of Carbon Dioxide

Experimental research of separation enhanced methanation of CO₂

G. Granitsiotis

Methanation of Carbon Dioxide

Experimental research of separation enhanced methanation of CO₂

by

G. Granitsiotis

to obtain the degree of Master of Science
at the Delft University of Technology,
to be defended publicly on Wednesday April 26, 2017 at 14:30 PM.

Student number: 4422627
Project duration: March 1, 2016 – April 26, 2017
Daily supervisor: Dr. K. Anastasakis, TU Delft
Dr. W. G. Haije, TU Delft
Thesis committee: Prof. dr. ir. W. De Jong, TU Delft, supervisor
Prof. dr. J. J. C. Geerlings, TU Delft
Dr. ir. J. W. Haverkort, TU Delft
Dr. W. G. Haije, TU Delft

An electronic version of this thesis is available at <http://repository.tudelft.nl/>.

Abstract

The ever growing use of renewable sources of energy led to a need for energy storage. Mainly due to the intermittency nature of applications like solar and wind. In addition, the need for regulation of the greenhouse gases led to the development of carbon capture and storage applications. Thus, the combination of those two factors accelerated the production of renewable fuels (called also solar fuels). Renewable fuels is a power-to-x solution of storing the surplus electric energy produced from renewable sources, via multiple steps processes. Hence, solar fuels can contribute immensely in a long-term, large-scale energy storage solution. Those fuels are synthetic hydrocarbon that derive from hydrogen (produced from renewables) and the CO_2 captured. Some possible fuels are methanol, methane and liquid hydrocarbons.

Amongst, those, methane is the most promising solution. It can be synthesized with a single reaction, it has high energy density and can be easily distributed. The methanation of CO_2 is an exothermic catalytic reaction and takes place in multiple fixed bed reactors in row. In order for this renewable methane to be used as SNG, high purity levels are required. Hence, novel techniques are researched to achieve the necessary purity of methane in fewer process steps.

The present study focuses on one of those techniques called separation enhanced methanation of CO_2 . The principle behind this technique is the removal, in situ, of the vapor produced by the reaction, to increase the conversion of reactants. This topic is approached experimentally. A fixed bed reactor built in house is used for the experiments. For the hydrogenation of CO_2 a nickel catalyst is used, coupled with two different zeolites (3A and 4A) for the adsorption of water vapor. Initially, the pure catalyst's performance was tested. Subsequently, the combinations of catalyst-zeolites (physical mixture) followed to determine the enhancement of the process. Two GHSV were applied in the experiments, for different temperatures in the range of $200^\circ C$ - $360^\circ C$. Also, different combinations of catalyst-zeolite 4A were deployed, regarding the size of the catalyst particles.

From the results, it was concluded that the proximity of the catalytic sites to the zeolites surface plays the most dominant role in the performance of the process. This proximity is linked to the average particle size and the uniformity of the bed. The highest conversion rates were achieved in the range of $260^\circ C$ to $280^\circ C$, with values of up to 98,5% of conversion.

Acknowledgement

During the time I spent working on this MSc thesis project, I realized the importance of co-operation and guidance. This project wouldn't be finished without the assistance of other people. Thus, under the completion of this study, I would like to give my acknowledgements to those people who were involved in different ways with their presence.

First of all, I would like to thank two people, Dr. Kostas Anastasakis and Dr. Wim Haije, my daily supervisors. The first one for his help and guidance on all the technical matters and not only. The completion and operation of the experimental set up wouldn't be feasible without his great contribution and knowledge. I would like to thank Dr. Haije for all the valuable help and knowledge he offered regarding all the aspects of this thesis. From the design of the experiments to writing my report and applying new ideas. His contribution was nonetheless crucial.

Secondly, I would like to extend my gratitude to my supervisor Dr. ir. Wiebren de Jong for accepting me initially to his group and offering this very interesting thesis topic to me.

Lastly, a special thanks goes to my colleagues in the department for all our fun times and help they offered in many occasions for my thesis and to my family for their support and patience along all this while.

Contents

List of Symbols	ix
List of Figures	xi
List of Tables	xv
1 Introduction	1
1.1 Thesis outline	3
2 Literature	5
2.1 Sabatier Reaction	5
2.1.1 General Knowledge	5
2.1.2 Applications	6
2.2 Catalysts.	6
2.3 Sorption.	8
2.4 Sorption enhanced methanation studies	10
3 Materials and methods	11
3.1 Experimental set-up	11
3.1.1 Reactor	15
3.1.2 Micro-GC Calibration	16
3.2 Materials	18
3.2.1 Aluminum oxide pellets	18
3.2.2 Catalyst	18
3.2.3 Sorbents	19
3.3 Experiments	20
3.3.1 Experiments with catalyst	20
3.3.2 Experiments with the combination catalyst/zeolites	23
4 Modelling and calculations	33
4.1 Pressure Drop in the Reactor	33
4.2 Thermodynamics of the reaction.	34
4.2.1 Aspen model.	34
4.2.2 Calculations based on Factsage	37
4.3 Thermodynamics of Sorption.	39
5 Results of experiments	45
5.1 Experiments with $Ni/Al_2O_3 - Al_2O_3$	45
5.2 Experiments with Ni/Al_2O_3 -zeolite 3A.	47
5.2.1 6000 GHSV	47
5.2.2 2400 GHSV	50

5.3	Experiments with <i>Ni/Al₂O₃</i> -zeolite 4A	52
5.3.1	Experiments without CH ₄ as an inlet gas	52
5.3.2	Experiments with CH ₄ in the inlet stream	55
5.4	Experiments with ground <i>Ni/Al₂O₃</i> (2,5mm in size) and zeolite 4A	55
5.4.1	Experiments without CH ₄ as an inlet gas	55
5.4.2	Experiments with CH ₄ in the inlet stream	58
5.5	Experiments with ground <i>Ni/Al₂O₃</i> (1mm in size) and zeolite 4A	59
5.5.1	Experiments without CH ₄ as an inlet gas	59
5.5.2	Experiments with CH ₄ in the inlet stream	62
6	Concluding remarks	67
6.1	Conclusions	67
6.2	Recommendations	68
	Bibliography	71
A	Appendix	77
A.1	77
A.2	78
A.3	78
A.4	79
A.5	79
A.6	80
A.7	82

List of Symbols

Ni/Al_2O_3	Nickel supported on Aluminum oxide (catalyst)
$Ni/Al_2O_3 - 3A$	Physical mixture of catalyst and zeolite 3A
$Ni/Al_2O_3 - 4A$	Physical mixture of catalyst and zeolite 4A
$Ni/Al_2O_3 - Al_2O_3$	Physical mixture of catalyst and alumina pellets
λ	Mean free path
T	Temperature
d	Kinetic diameter
P	Pressure
L	Bed length
D_p	Particle diameter
ϵ	Porosity
μ	Dynamic viscosity
v	Fluid velocity
ρ	Density
P_{tot}	Overall pressure
P_{ref}	Reference pressure
P_{H_2O}	Partial pressure of water vapor
x	Number of mols
ΔH	Enthalpy difference
ΔS	Entropy difference
K	Chemical equilibrium constant

List of Figures

1.1	Process scheme of the concept(Schaaf et al. [46])	2
2.1	Comparison of conversion of CO_2 and yield of CH_4 between different catalysts (as taken from Wei et al. [54])	7
2.2	"Equilibrium sorption of water vapor from atmospheric air at 25°C on (A) alumina (granular), (B) alumina (spherical), (C) silica gel, (D) 5A zeolite, (E) activated carbon." (as taken from Deng et al. [26])	9
3.1	Process flow diagram of the setup:1.Gas tanks, 2.Electronic ball valves, 3.Needle valves, 4.Mass flow controllers, 5.Reactor, 6.Condensation vessels, 7.Volume flow meter, 8.Micro GC	12
3.2	Reactor and tripod	14
3.3	Calibration line of H_2 , $R^2 = 0,9993$ (points in table 3.1)	17
3.4	Reactor composition-1st series of experiments	22
3.5	Reactor composition-2nd series of experiments	24
3.6	A representation of the old and new catalytic particles and their interaction with the zeolite pellets (numbers in mm)	28
3.7	Combination of zeolite 3A/Ni	30
3.8	Combination of zeolite 4A/Ni	30
3.9	Combination of zeolite 4A/2,5mm Ni	31
3.10	Combination of zeolite 4A/1mm Ni	31
4.1	Pressure Drop for various porosities and flow rates. All pressures are in <i>bar</i>	34
4.2	Gibbs Reactor model in AspenPlus	35
4.3	Theoretical Conversion of CO_2	36
4.4	Theoretical Conversion of CO_2 , for different values of pressure, as calculated from <i>AspenPlus</i>	36
4.5	Theoretical Conversion of CO_2 , for different values of pressure, as calculated from <i>Factsage</i>	37
4.6	Gas composition in mols as a function of temperature	38
4.7	Influence of P_{H_2O} in conversion of H_2	39
4.8	Isosteres of 3A and operational lines of the present process	41
4.9	Isosteres of 3A and operational lines of the present process	41
4.10	Isosteres of 4A and operational lines of the present process	42
4.11	Isosteres of 4A and operational lines of the present process	43
5.1	Conversion of CO_2 , $Ni/Al_2O_3-Al_2O_3$ (temperature range 200–380°C), (GHSV=6000, table 3.4)	46
5.2	Conversion of H_2 , $Ni/Al_2O_3-Al_2O_3$ (temperature range 200–380°C), (GHSV=6000, table 3.4)	46

5.3	Conversion of CO_2 , Ni/Al_2O_3-3A , (temperature range 200–360°C),(GHSV=6000, table 3.4)	48
5.4	Conversion of H_2 , Ni/Al_2O_3-3A , (temperature range 200–360°C),(GHSV=6000, table 3.4)	48
5.5	Conversion of H_2 , comparison between pure Ni/Al_2O_3 and Ni/Al_2O_3-3A , (GHSV=6000, table 3.4)	49
5.6	Conversion of H_2 , Ni/Al_2O_3-3A (temperature 240°C),(GHSV=2400, table 3.7)	50
5.7	Conversion of H_2 , Ni/Al_2O_3-3A (temperature 260°C),(GHSV=2400, table 3.7)	51
5.8	Conversion of H_2 , Ni/Al_2O_3-3A (temperature 280°C),(GHSV=2400, table 3.7)	51
5.9	Conversion of H_2 , Ni/Al_2O_3-4A (temperature 240°C),(GHSV=2400, table 3.7)	53
5.10	Conversion of H_2 , Ni/Al_2O_3-4A (temperature 260°C),(GHSV=2400, table 3.7)	53
5.11	Conversion of H_2 , Ni/Al_2O_3-4A (temperature 280°C),(GHSV=2400, table 3.7)	54
5.12	Conversion of H_2 , Ni/Al_2O_3-4A (temperature 300°C),(GHSV=2400, table 3.7)	54
5.13	Conversion of H_2 , Ni/Al_2O_3-4A (temperature 260°C and CH_4 in inlet),(GHSV=2400, table 3.8)	56
5.14	Conversion of H_2 , Ni/Al_2O_3-4A (temperature 280°C and CH_4 in inlet),(GHSV=2400, table 3.8)	56
5.15	Conversion of H_2 , Ni/Al_2O_3 2,5mm – 4A (temperature 260°C),(GHSV=2400, table 3.7)	57
5.16	Conversion of H_2 , Ni/Al_2O_3 2,5mm – 4A (temperature 280°C),(GHSV=2400, table 3.7)	57
5.17	Conversion of H_2 , comparison between Ni/Al_2O_3 2,5mm–4A and Ni/Al_2O_3-4A , (GHSV=2400, table 3.7)	59
5.18	Conversion of H_2 , Ni/Al_2O_3 2,5mm – 4A (temperature 260°C and CH_4 in inlet),(GHSV=2400, table 3.8)	60
5.19	Conversion of H_2 , Ni/Al_2O_3 2,5mm – 4A (temperature 280°C and CH_4 in inlet),(GHSV=2400, table 3.8)	60
5.20	Conversion of H_2 , comparison between Ni/Al_2O_3 2,5mm–4A and Ni/Al_2O_3-4A , with CH_4 as inlet, (GHSV=2400, table 3.8)	61
5.21	Conversion of H_2 , Ni/Al_2O_3 1mm – 4A (temperature 260°C),(GHSV=2400, table 3.7)	61
5.22	Conversion of H_2 , Ni/Al_2O_3 1mm – 4A (temperature 280°C),(GHSV=2400, table 3.7)	62
5.23	Conversion of H_2 , comparison between Ni/Al_2O_3 2,5mm – 4A, Ni/Al_2O_3-4A and Ni/Al_2O_3 1mm – 4A, (GHSV=2400, table 3.7)	63
5.24	Conversion of H_2 , Ni/Al_2O_3 1mm – 4A (temperature 260°C and CH_4 in inlet),(GHSV=2400, table 3.8)	64
5.25	Conversion of H_2 , Ni/Al_2O_3 1mm – 4A (temperature 280°C and CH_4 in inlet),(GHSV=2400, table 3.8)	64
5.26	Conversion of H_2 , comparison between Ni/Al_2O_3 2,5mm – 4A, Ni/Al_2O_3-4A and Ni/Al_2O_3 1mm – 4A, with CH_4 as inlet,(GHSV=2400, table 3.8)	65
A.1	Calibration line of CO_2	80
A.2	Calibration line of CH_4	81
A.3	Calibration line of N_2	81
A.4	Calibration line of CO	82
A.5	Fraction yield of CH_4 , Ni/Al_2O_3 2,5mm-4A, (at 260°C),(GHSV=2400, table 3.7)	83

A.6	Fraction yield of CH_4 , Ni/Al_2O_3 2,5mm-4A, (at 280°C),(GHSV=2400, table 3.7)	84
A.7	Fraction yield of CH_4 , Ni/Al_2O_3 1mm-4A, (at 260°C),(GHSV=2400, table 3.7)	85
A.8	Fraction yield of CH_4 , Ni/Al_2O_3 1mm-4A, (at 280°C),(GHSV=2400, table 3.7)	86

List of Tables

3.1	Calibration points:Gases fractions	17
3.2	Composition of Molecular Sieve 4A. As given by manufacturer.	20
3.3	Catalyst/alumina oxide bed	21
3.4	Flow characteristics of 1st series of experiments	21
3.5	Catalyst/zeolites bed	24
3.6	Experiment with presence of CH ₄ as inlet, zeolite 3A	26
3.7	Flow characteristics for the minimum volumetric flow rates	26
3.8	Experiment with CH ₄ as inlet and minimum flow rates, zeolite 4A	26
5.1	Corvesion of H ₂ for experiments with catalyst-alumina and catalyst-zeolite 3A	49
A.1	Mols reacted based on stoichiometry	78

Introduction

In the introductory chapter, an overview of the current thesis work is presented. In particular, the background of the thesis is illustrated, together with the objectives and motivation that it was based upon. Finally, the scope of the current work is presented and the outline of the thesis.

The world's population is growing each year by a rate of approximately 1,18% [27]. This number corresponds to an additional 83 million people per year. That increase lead to an exponential growth in the energy demands. Specifically, the energy consumption, for the same time frame (2010-2015), has risen globally by 7%, from 12540 to 13423 Mtoe [4]. Subsequently, the CO_2 emissions reached more than 35000 Mt for the year 2015 only [3], [44]. So, this increase in energy demands coupled with the ever growing concerns about the future of the environment have led to a boost in the usage of “cleaner” solutions. Moreover, those solutions are forced into the market and established due to the strict regulations and goals set by many countries and organizations. Especially, in EU many agreements have been signed, like the EU 20-20-20 strategy. Which, refers to 20% in emissions, 20% energy from renewables and 20% increase in efficiency.

Many alternatives to classical fossil fuels have risen due to the reasons mentioned above. Those, mainly focus on renewable sources of electricity. Like wind turbines, solar panels tidal power etc. The problem with many of those solutions is the need for storage of the energy produced. The reason is the intermittency nature of applications like solar and wind. This reason created the need of storing energy on large scale and over longer times (whole seasons). But, the technology of storing electricity in such a large scale with the use of batteries is not yet economically and practically feasible, solutions like electrolysis of water have been used for the production of hydrogen.

Regardless of the usage of renewable sources, fossil fuels still play a dominant role for the production of energy and, generally, in the process industry. Hence, capture and storage technologies of carbon dioxide have been developed and are being developing furthermore, to reduce the emissions. Specifically, capture technologies for post and pre-combustion are economically feasible in many occasions and industrial separation of CO_2 (from natural gas processing and ammonia production) is an already mature market [43].

Hydrogen is a carbon neutral fuel and possesses the highest energy density possible, with 142 MJ/kg. Nonetheless, the complexity and expense in storing and distributing is high, together with the increased hazards when manipulating it. This fact combined with

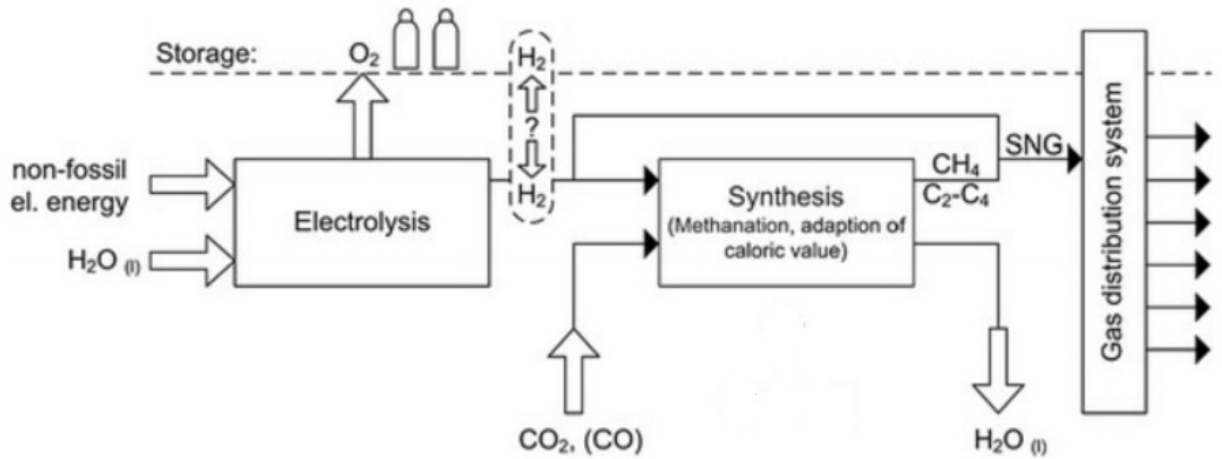
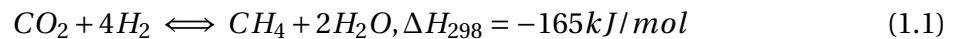


Figure 1.1: Process scheme of the concept (Schaaf et al. [46])

the offer of carbon dioxide (from capturing processes mentioned previously) led to process development activities towards synthetic hydrocarbons. Those hydrocarbons can only have as combustion products CO_2 and water, with the purpose of having an emission neutral production of energy. Also, another requirement is to synthesize a fuel with high energy density. Thus, possible solutions can be methanol, methane and liquid hydrocarbons (C_nH_{2n+2} with $n > 6$) [18]. Methanol's synthesis from CO_2 and H_2 is simple and, almost, energy neutral [15], but its energy density is significantly less than methane's and octane's (19,7 MJ/kg compared to 55,5 and 44MJ/kg respectively). Octane on the other hand, being liquid, is the most convenient in storing and transporting. But synthesizing it is a complex process, by applying reverse water gas swift reaction combined with Fischer-Tropsch synthesis [5]. Lastly, methane has the highest energy density amongst the ones mentioned, it can be synthesized in one step (single catalytic reaction), from carbon dioxide and hydrogen, and (very importantly) it can be accommodated by the already vast distribution network of natural gas and replace it as a renewable source of energy. The reaction can be seen below (equation 1.1).



This concept (methanation of CO_2 and CO) has been, vastly, examined in academia and it has been already applied on different scales. A general scheme of the certain, overall, process can be seen in figure 1.1. As taken from Schaaf et al. [46].

A typical commercial methanation process of carbon dioxide consists of several fixed bed reactors in a row, with intermediate cooling steps and recycle streams, until the sufficiently high methane purity is reached [49]. The reaction occurs in elevated temperatures ($250^\circ C$ - $450^\circ C$). For synthetic natural gas (SNG) from coal or biomass, the methanation occurs up to $600^\circ C$ [38]. The pressure conditions of the last reactor usually reach pressures of more than 20bar [46] in order to reach the high specifications of methane's purity as specified for the gas grid.

The present work focuses in the sorption enhanced methanation process. Specifically,

by applying the Le Chatelier principle and removing in situ one of the products (water vapor) the reaction is led to the right hand side, increasing the conversion of the reactants. Previously, others have applied the Le Chatelier principle in thermodynamic equilibrium based reaction ([17], [22], [34], [23]) and studied the enhancement. Regarding, the separation enhanced methanation of carbon dioxide and carbon monoxide, only very recently has been studied ([51], [15], [13], [25]) and all the studies were focused in micro-scale application.

The current work aims in a large scale process, with a physical mixture of the materials used (catalyst and sorbent material). The scope is to experimentally study the enhancement and detect the parameters, that mainly effect the efficiency of the process. Those parameters are the temperature range, pressure, composition of materials, type of materials and most importantly, uniformity of mixture and proximity of catalytic sites to zeolite's surface.

Those exactly are the questions researched with the present experimental work:

- Feasibility of sorption enhanced methanation of CO_2 , over a physical mixture of catalyst-zeolites, in large scale
- Temperature range of operation for the process
- Which parameters influence the performance of the process.

An adiabatic reactor was used (designed and built in-house), that resembled the last reactor in a multi-reactor step process. The purpose was to achieve the highest possible conversion of the reactants (for a minimum time frame) in atmospheric conditions. Hence, substituting the expensive (in operation and equipment costs) high pressure reactor needed so far for the same conversion values of the reactants.

1.1. Thesis outline

Chapter 2

A theoretical backround is provided in this chapter. This backround regards the catalysts used for this type of work, together with sorbent materials that can be applied for the adsorption of water vapor. Lastly, reactor technologies are presented dedicated for this process and the literature review of the studies focused in the methanation of CO_2 .

Chapter 3

This chapter introduces the materials and methods that were employed to investigate, initially the conventional catalytic Sabatier reaction and subsequently the soption enhancement of the same process. The analysis of the aluminum oxide pellets, catalyst and sorbents used is presented. Along with the analysis of the setup used for the experiments. In addition, a description of the procedure followed during the experiments together with the series of experiments is provided.

Chapter 4

This chapter is devoted in the calculations and modelling performed prior the experiments. The goal was to predict, based on thermodynamics, the progression of the present synergistic process and set the goal (partial pressure of water) for the optimum results. Also, approximate the pressure drop and temperature rise inside the catalytic bed.

Chapter 5

This chapter presents the experimental results along with their interpretation. Firstly, the series of experiments with the combination $Ni/Al_2O_3 - Al_2O_3$ were performed to determine the activity of the present catalyst for a range of temperatures at atmospheric pressure. Subsequently, the experiments with the combination Ni-Al/Zeolities followed. Initially, the pair $Ni/Al_2O_3 - 3A$ was tested, followed by $Ni/Al_2O_3 - 4A$. Lastly, the two combinations of ground Ni/Al_2O_3 (2,5mm and 1mm average sizes) paired with zeolite 4A were put into test.

Chapter 6

The conclusions, drawn from this work, are discussed in this chapter. Also, recommendations for future work in this field is provided.

2

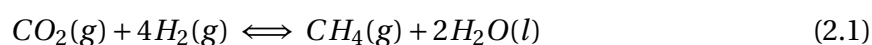
Literature

2.1. Sabatier Reaction

2.1.1. General Knowledge

One process frequently applied in the chemical industry is that of hydrogenation of organic compounds. Specifically, it refers to the reaction between molecular hydrogen and another element or organic compound. The vast majority of those reactions occur in a catalytic environment. The purpose behind hydrogenation is usually to reduce/oxidase an organic compound or change its saturation state. Reduction and oxidation refers to the decrease and increase, respectively, of the number of oxygen molecules in a compound and saturation refers to the absence of double and triple bonds in the compound as well.

Two of the most known hydrogenation reactions are the methanation of carbon dioxide and carbon monoxide. In particular the reaction of either carbon monoxide or carbon dioxide with hydrogen for the synthesis of methane and water (reduction). The conversion of carbon dioxide to methane is called the Sabatier process and is ,probably, amongst the hydrogenation processes the most researched one. Attributed to the French chemist Paul Sabatier, an innovator in the catalytic hydrogenation processes, who discovered it in the 1910s [7]. This reaction proceeds as follows:



The Sabatier process is highly exothermic, with a release of energy of $\Delta H = -165 \text{ kJ/mol}$ for the reaction with carbon dioxide and $\Delta H = -201 \text{ kJ/mol}$ for the reaction with carbon monoxide [14]. It is a thermodynamically favorable reaction ($\Delta G = -113,5 \text{ kJ/mol}$) in a big range of temperatures and pressures[14]. On the contrary, the reduction of a fully oxidized carbon to methane is kinetically limited [54]. Thus, a catalyst is needed to reach acceptable conversion rates and selectivity to methane. Although methanation of CO_2 is a simple reaction, the mechanism that takes place during catalysis for the conversion towards CH_4 is complicated. Two general routs have been proposed. One refers to the conversion of CO_2 to CO and subsequently the formation of carbon monoxide to methane [53]. The second is the direct conversion of CO_2 towards CH_4 , without formation of any intermediates [29].

As a process, the Sabatier reaction has been greatly researched both in academia and the private sector due to the different usages it can display and the fact that it involves some

of the most dominant and abundant chemical compounds on earth. The main topics that have been investigated are the materials that can catalyze this process.

2.1.2. Applications

Life support

One of the usages is the synthesis of water in remote places, where there is no reliable water source. Such a characteristic case is the International Space Station. For example NASA has developed an in house Sabatier reaction system [37] that can produce water and methane from the carbon dioxide of the atmosphere of the station and the hydrogen produced from electrolysis. That methanation process is an intermediate step for the final production of oxygen, from electrolysis of the water produced by the Sabatier reaction.

Energy storage

Another field in which Sabatier process can have a substantial impact is that of energy storage and carbon dioxide management. Despite the efforts been made to reduce the carbon dioxide footprint emitted by the industry, transportation and energy production, we are still unable to reach the strict goals that have been set internationally for the maximum production of CO_2 globally. Lots of focus has gone into carbon storage via the new solutions of CO_2 capturing. But, still carbon dioxide storage is energy costly and inefficient leading to the need for alternative solutions.

Those solutions are the chemical transformation of CO_2 to renewable fuels. These are methanol, liquid hydrocarbons and methane, as mentioned previously. Hence, a solution could be the Sabatier process, which has the benefit not only of carbon dioxide reduction but also the synthesis of methane. A compound vastly used nowadays in the western world, both in households and in the industry. It, also, has the great benefit of an already existent distribution network, especially in Europe. On the topic of energy storage, there is also the benefit of the conversion of hydrogen to the more "practical" (as mentioned above) methane. After the bloom of the renewable energy sources there can be a significant amount of hydrogen produced from electrolysis yearly, which is very challenging to store and distribute compared to methane. Hence, the necessity for a stable Sabatier process to convert to natural gas.

2.2. Catalysts

The methanation of CO_2 is considered a typical catalytic heterogeneous process, since it can only be performed under the presence of a solid (in most cases) catalyst and the reactants are always in gaseous form. The most widely studied material for the hydrogenation of CO_2 is Nickel (Ni). Those Ni catalytic pellets consist, always, of nickel supported on another material to form the end product. The support's material plays a crucial role in the catalysis. Because it influences the interaction between Nickel, the support and CO_2 , determining in this way the catalytic activity and selectivity towards the products [20]. The materials used typically as supports in Nickel catalysts are oxides. Like TiO_2 , SiO_2 , Al_2O_3 , CeO_2 and ZrO_2 . The reason for using those is their high surface area. High surface area is needed for dispersion of the active phase, which is nickel. So, increased dispersion of the active phase has been the main focus of research. Other studies [28] focused on the preparation of Ni/MCM-14 catalysts. MCM-14 is a mesoporous material. Comes from silicate

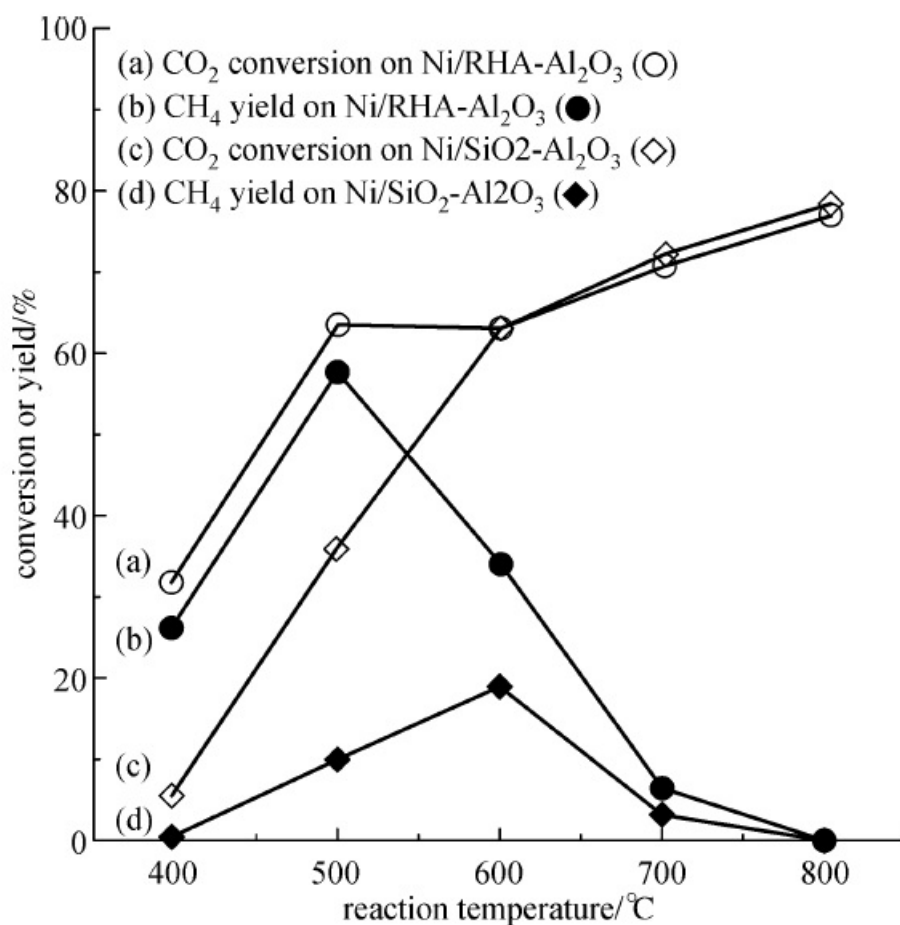


Figure 2.1: Comparison of conversion of CO₂ and yield of CH₄ between different catalysts (as taken from Wei et al. [54])

and aluminosilicate solids. By specific preparation and impregnation of nickel on MCM-14, the catalyst exhibited high selectivity (96%) and space-time yield (91,4 g/kg/h). Better than the performance exhibited by a Ni/SiO₂ catalyst [52]. Another factor that influences the activity of the catalyst is the reduction of NiO to active Ni. Nickel is, always, impregnated on a support in the form of nickel oxide (NiO). Hence, the conditions present at the reduction process are very crucial for the complete activation of nickel. Those conditions are temperature, time and composition of gas stream used for the reduction. Amorphous silica can be used for the methanation of CO₂. Specifically, amorphous silica extracted from rice husk (RHA). Due to its high specific area, porosity and melting point, they can be a solid solution for the hydrogenation of carbon dioxide [20]. Another study focused in the combination of amorphous silica and aluminum oxide for the formation of double material support. Although, increased reduction and calcination temperatures are needed, due to the presence of aluminum oxide trapped in nickel oxide particles, the recorded conversion and selectivity is higher than the Ni/RHA catalyst [19]. Also, the performance of Ni/RHA-Al₂O₃ towards the methanation of carbon dioxide is better than Ni/SiO₂-Al₂O₃. A detailed comparison can be seen in figure 2.1.

Another type of nickel catalyst is Raney nickel. A fine-grained material which consists of traces of Alumina. Raney nickel is thermally and structurally stable and has a large BEP surface area. It has high recorded activity in the methanation reaction of CO_2 [45]. Generally, Ni/Al_2O_3 (nickel/alumina) alloys have a high activity towards the hydrogenation of carbon dioxide, with high selectivity towards methane [41]. Lastly, iron has been also used combined with nickel for methanation processes (of CO and CO_2). The end product is a bimetallic $Ni - Fe/MgAl_2O_3$ catalyst [40]. It has high activity towards the methanation of CO_2 and the benefit that iron is cheaper than nickel. So, the overall catalyst is less costly to produce.

Except nickel other metals, that have been investigated for the hydrogenation of CO_2 (and not only), are group VIII metals (Rh and Ru). Those are supported on the same oxides like nickel (TiO_2 , SiO_2 , Al_2O_3 , CeO_2 and ZrO_2). The main disadvantage of ruthenium and rhodium is that they are very expensive, due their scarcity and the fact that there is so much available quantity until complete depletion. Other than that their activity towards methanation of CO_2 is significantly higher than nickel's [40]. In addition, they can operate at a temperature range where nickel is not active (around $150^\circ C$). The reason is that nickel based catalysts at low temperatures interact with carbon monoxide and form mobile nickel subcarbonyls [11]. The support used for the formation of the catalyst plays a crucial role in the performance of the product towards the methanation process. The effect of the support to the hydrogenation process of carbon dioxide has been studied by Kowalczyk et al. [39]. The results based on the surface-based activities (TOF) of ruthenium are $Ru/Al_2O_3 > Ru/MgAl_2O_4 > Ru/MgO$. Generally, $Ru/\gamma - Al_2O_3$ is used as a base of comparison for all catalysts, due to its high activity for methanation of carbon dioxide at low temperatures.

2.3. Sorption

The second main phenomenon that occurs in the present experimental study (besides catalysis) is that of physisorption. Adsorption occurs when a molecule of the adsorbate bonds on the surface of an adsorbent. There are two types of adsorption (sorption). The first is chemical adsorption or chemisorption. In the case of chemisorption, a chemical reaction occurs between the surface and the adsorbate. Hence, chemisorption is similar to a chemical reaction with a specific constant rate of reaction at each temperature and each pressure. The second type of adsorption is physisorption or physical adsorption. In physisorption the molecules of adsorbate are attracted with Van der Waals force on the surface of the adsorbent. This process in contrast with chemisorption is dynamic. At constant temperature and pressure the adsorption rate changes with the reduction of the capacity of the adsorbent.

There are several materials for the adsorption of water. A study performed by Deng et al. [26] on several novel adsorbent materials, encapsulates the ones suitable for the adsorption of water. Those can be activated alumina, activated carbon, silica gel, selective water sorbent (SWS), metal organic framework (MOF) and molecular sieves (zeolites). A comparison of their capacities towards relative humidity at room temperature can be seen in figure 2.2.

In detail, activated alumina is a form of aluminum oxide, with a high porous surface. Its formula is $Al_2O_3 \cdot nH_2O$. It has a more polar surface than silica gel and higher capacity

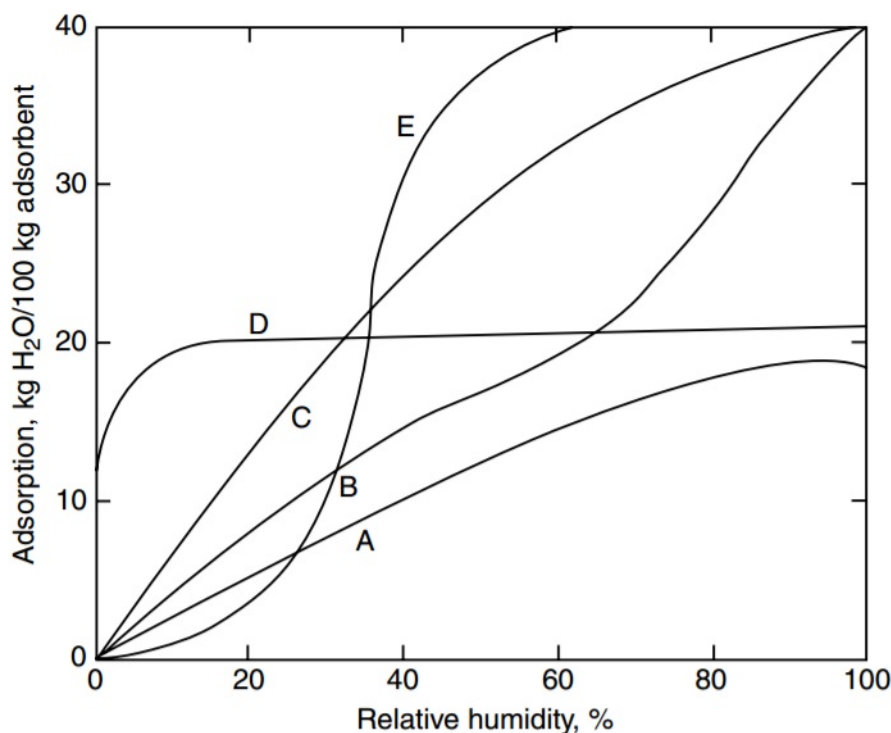


Figure 2.2: "Equilibrium sorption of water vapor from atmospheric air at 25°C on (A) alumina (granular), (B) alumina (spherical), (C) silica gel, (D) 5A zeolite, (E) activated carbon." (as taken from Deng et al. [26])

to water than silica gel at elevated temperatures [26]. Activated carbon has a large surface area. It has a microporous and mesoporous structure, with a high adsorption capacity for non-polar compounds as well. From figure 2.2 one can see its affinity towards water vapor. Silica gel is a very known compound. Silica gel is a granular, porous form of silicon dioxide (SiO_2). It has a high affinity towards water and it is probably the most used desiccant (both in industry and household use). The disadvantage of silica gel is that it deactivates at elevated temperatures. MOFs consist of metal ions coordinated to organic ligands to form up to three dimensional structures. They exhibit high capacity to water at low partial pressures of vapor, plus they are easily regenerated in low temperatures [30]. Also, MOFs exhibit high adsorption capacity to methane, hydrogen, ethylene, ethane and others at elevated ambient pressures. But, no definite data are available in literature for their adsorptive capacity at elevated temperatures. Lastly, zeolites are aluminosilicate minerals. Zeolite is a material with uniform pores. The pore size can be from 3 angstroms up to 10 angstroms in diameter. This property makes it ideal for sieving molecules of a certain kinetic diameter amongst molecules with larger dimension. Zeolites have a high affinity to water due to the increased polarity of the molecule of water and its small size (2,65 Å).

One can conclude, that zeolites are the best choice amongst the ones mentioned for the adsorption of water vapor in experimental conditions present in this study. The main advantages are the adsorptive capacity at low partial pressures of water (low concentration), fast rate of adsorption, separation of molecules by size and (most importantly) the adsorptive capacity at elevated temperature range [15], [51].

2.4. Sorption enhanced methanation studies

Sorption enhanced reactions, where one of the products is removed in situ to shift the equilibrium towards the products side, have been studied before. For example the adsorption of CO_2 to enhance the water gas shift reaction for the production of pure hydrogen [50]. Regarding sorption enhanced methanation process, (where water vapor is removed) four studies have been published.

The first one is that of Walspurger et al. [51]. In this study a combination of zeolite 4A with a nickel/alumina catalyst was deployed. Initially, the adsorption capacity to water vapor at $200^\circ C$, $250^\circ C$ and $300^\circ C$. Subsequently, 3,6 g of catalyst and zeolite 4A combined were ground to powder, mixed together and pressurized in uniform pellets. Onwards, those pellets were placed in a quartz reactor. The performance of this combination was tested out at the same temperatures of the adsorption test. Close to 100% conversion of reactants was achieved at $250^\circ C$. The second study is that of Borgschulte et al. [15]. In this case nickel nitrate aqueous solution was used with different concentrations, combined with zeolite 5A. Hence, nickel particles were impregnated on zeolite 5A (6 wt% of nickel on 5A). The resulted catalyst (13g) was placed in a tubular reactor and tested out. Also, 100% conversion of reactants was reached above $220^\circ C$. Furthermore, an investigation of the reaction's mechanism was proposed. The third study is of Bacariza et al. [13]. In this research paper a USY zeolite was impregnated with 5% nickel, resulting in a Ni-based zeolite catalyst. Several preparation and pre-reduction conditions of the catalyst were tested in order to optimize the performance of the catalyst. The conversion reached 100% at $250^\circ C$. Most recent is the study by Delmelle et al. [25]. In this last study two different catalysts were prepared. The first catalyst was 5% Ni impregnated on zeolite 5A and the second was 5% Ni impregnated on zeolite 13X. Both catalysts yielded pure methane in similar temperature range. But, the 5Ni/13X catalyst performed three times more the maximum compared to 5Ni/5A. The reason is the higher capacity of zeolite 13X for water vapor compared to zeolite 5A. No comparison was made between other types of zeolites with 13X. But, zeolites 3A and 4A are vastly used for dehydration of hydrocarbons [2], [8].

3

Materials and methods

This chapter introduces the materials and methods that were employed to investigate, initially the conventional catalytic Sabatier reaction and subsequently the option enhancement of the same process. The analysis of the aluminum oxide pellets, catalyst and sorbents used is presented. Along with the analysis of the setup used for the experiments. In addition, a description of the procedure followed during the experiments together with the series of experiments is provided.

3.1. Experimental set-up

The experimental setup consists of one main equipment-component which is the heat-integrated fixed bed reactor. Followed by a series of 5 mass-flow controllers for the regulations of the gases, 5 automated electronic valves, 2 vessels for the condensation of the vapor produced by the reaction and a gas chromatography.

Below, follows a process flow diagram that depicts the current setup(fig.3.1).

The experimental setup comprises 9 different groups of equipment. Those are the following and documented based on the enumeration on figure 3.1.

1. **Gas tanks:**The first stage of the setup is the supply of the process gases from the in-house storage facilities. The gases, available for the system, are Nitrogen(N_2), Carbon dioxide(CO_2), Hydrogen(H_2), Methane(CH_4) and Carbon monoxide(CO). The gases are provided in a purity higher than 99% per volume.
2. **Electronic ball valves:**The second stage consists of 5 electronically automated on/off valves. Those are placed there purely for safety reasons. They suspend the inflow of gases in cases of gas leakage, fire etc.
3. **Needle valves:**The on/off valves are followed by 5 accurate pressure control valves to regulate the pressure of each gas prior to the next step. The valves were adjusted to maintain the pressure of the gases at 1,5bar. That value of pressure was imposed by the mass flow controllers (next station of set up).

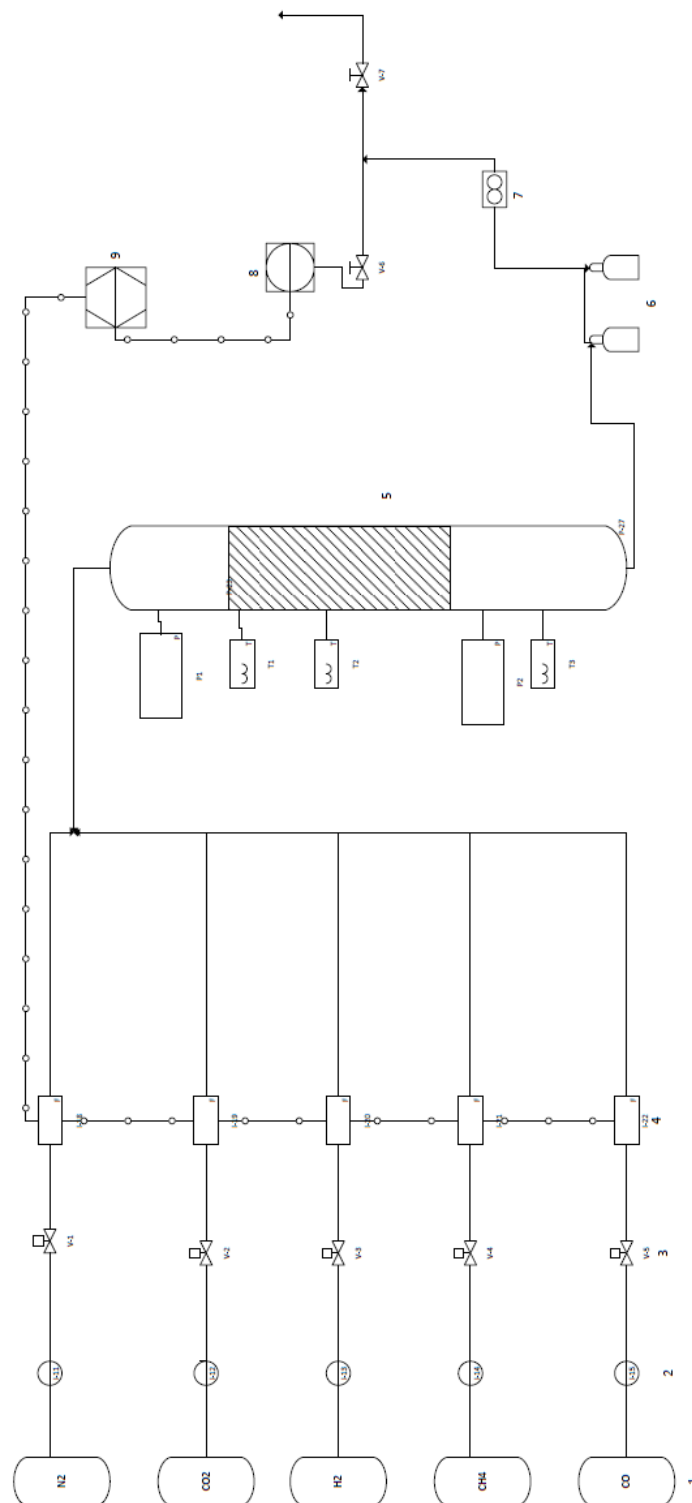
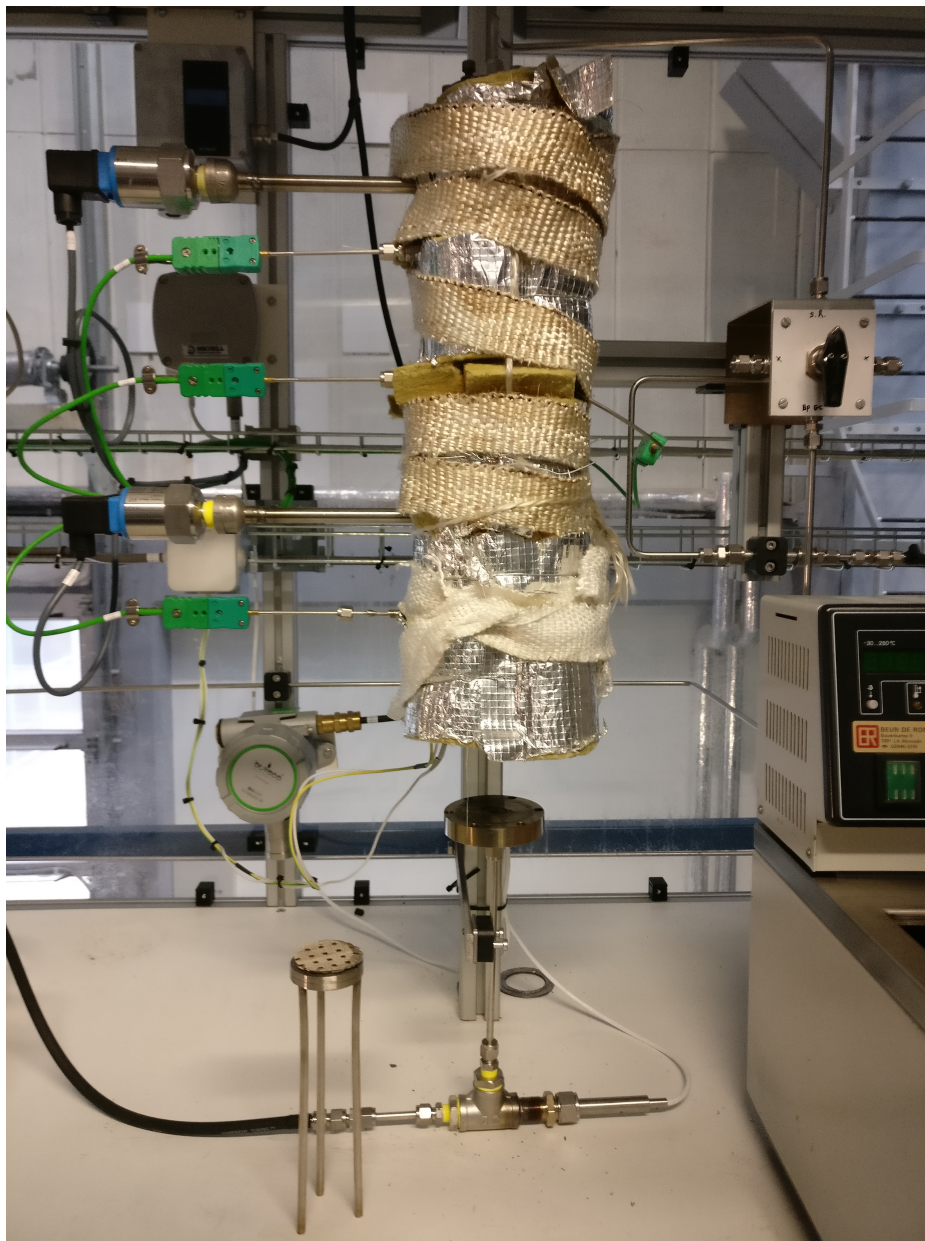


Figure 3.1: Process flow diagram of the setup: 1. Gas tanks, 2. Electronic ball valves, 3. Needle valves, 4. Mass flow controllers, 5. Reactor, 6. Condensation vessels, 7. Volume flow meter, 8. Micro GC

4. **Mass flow controllers:** The last stage of gas regulation in the setup are the 5 mass flow controllers purchased by Bronkhorst. The specific models are the Bronkhorst EL-FLOW F-201CV. They are designed for highly accurate gas flow control (third decimal of mL), with a negligible uncertainty. The flow range, that those can regulate, is 0,1-5 L_n/min . L_n indicates the normal Liters and refer to the volume at $0^\circ C$ and 1 bar. The mass flow controllers can handle an inflow of 1,3-5 bar and provide the outflow at 1 bar. The specific model is considered to be suitable for lab applications.
5. **Reactor:** Due to the importance of this component, the reactor has been analyzed on its own in subsection 3.1.1.
6. **Condensation vessels:** The outlet gases (that exit the reactor at the bottom) pass through 2 continuous flow bottles. The first one is placed in an ice bath and the second contains silica gel. The purpose is to fully condense the vapor been formed by the reaction. So it won't reach the mass flow meter and the micro gas chromatography. The silica gel has recorder adsorption capacity towards CO_2 . But the competitive adsorption between water vapor and CO_2 , favors the first [12]. This can be attributed to the increased polarity of H_2O . Hence, the adsorption of CO_2 can be neglected. The same holds for zeolites [24]. Polyethyleneimine modified silica gel is used for the adsorption of CO_2 [55].
7. **Volume flow meter:** After the condensation containers follows a residential diaphragm gas meter. It is manufactured by the company named Itron and the specific model is "Gallus 2000". The diaphragm displaces positively due to the flow. This displacement is linked with a specific volume, thus measuring the volume of the flow. It is specified for accurate, continuous measurement of volume flow for non-corrosive gases. The flow limits are 0,016 – 2,5 m^3/h with a maximum of $55^\circ C$ for the gases temperature.
8. **Micro GC:** The final, but non the less crucial, component of the setup is the micro gas chromatograph. It is a Micro-GC of the company Varian. The model's name is "CP-4900". It is used for analysing the volumetric composition of the outlet gases from the reactor. The column's type is Hayesep A 40 cm heated column. It works in a continuous mode and takes automatically a sample of gases every 4 min. The amount of gases that do not enter the Micro-GC are bypassed to an exhaust hose and led to the atmosphere. More information regarding the GC are presented in the following section.
9. **Computer:** Next to the setup a computer is placed. All of the electronic devices and sensors are physically connected to the PC. The 3 temperature and 2 pressure sensors on the reactor "give" readings on the PC via a LabView simulator. This simulator is designed and coded inhouse, designated for the specific reactor. The 5 mass flow controllers are handled via the software FlowView (provided also from Bronkhorst). Each one of the controllers has his own control panel. Lastly, the Micro-GC is operated via Galaxie, a software provided by Agilent.

Figure 3.2: Reactor and tripod



3.1.1. Reactor

This is the main equipment-component of the current setup. It is a heat integrated-fixed bed, tubular reactor. The dimensions are 5,2cm of inner diameter and 45cm height. The reactor is made from stainless steel, type 316.

Heat integration

A heating cable is wrapped around the reactor and can reach a maximum temperature of 400°C. The reactor together with the heating cable are covered with a layer (thickness of 7cm) of glass wool to thermally insulate the unit. The whole system can be considered adiabatic, since the outer surface of glass wool is close to room temperature, even when the heating cable is set at the maximum of 400°C. The heating's cable operation panel has two indicated temperatures. The one that the user sets the cable at and the one that indicates in real time the actual temperature of the cable. When the cable reaches the temperature as set by the user, it fluctuates around this value until it stabilizes to the aimed one. The response of the cable can be considered rather slow and needs time to reach the maximum. Also, even after stabilization at the desired temperature it would, sometimes fluctuate by approximately 1°C.

Access and inner design

The bottom and top of the tubular reactor comprises of two removable steel caps, so one can have access to the inside. Gaskets are placed between the caps and the reactor for sealing. The inlet of the gases is at the top of the reactor. Explicitly, a stainless steel tubing of 0,6cm diameter is connected to the upper cap. At the bottom cap a similar tube is connected for the outlet of the gases. Inside of the reactor (at the low end) a removable metallic tripod is placed (15cm height, 5,20cm diameter) for the purpose of supporting the catalytic bed. So, the bed (physical mixture of catalyst/alumina and catalyst/zeolites) is poured from the top of the reactor, with the use of a funnel, on the tripod. As it is mentioned onwards has a height of approximately 16cm. The part above the bed which is approximately 14cm is always filled with Aluminum oxide pellets. The tripod (like the reactor) is made from stainless steel type 316.

Sensors

As it can be seen in the figure 3.2, 5 sensors are placed on the reactor. Two of them are pressure sensors and measure the absolute pressure in bar. The other 3 are temperature sensors and take measurements in Celsius. All of them operate in real time and record 3-4 measurements per 1sec and show it on screen via the software LabView (mentioned previously). The accurate regulation of temperature is difficult because the readings of temperature on LabView variate constantly in a range of 4°C. So all the experimental temperatures mentioned onwards are an approximate average of those readings. The same goes for the readings of the pressure sensors. The essential part of the reactor, which is the catalytic bed, occupies the space between the first temperature sensor (from the top) and the second pressure sensor on the bottom. It can be clearly seen as the crossed line area in figure 3.1. An image of the reactor with the tripod can be seen in figure 3.2.

Regulation of temperature

The temperature forms a very important role in the present study. Thus the regulation of temperature is very crucial. Unfortunately, due to lack of accuracy in the readings of the

thermocouples and the lagging response of the heating cable it was difficult to have reproducibility. Namely to perform different experiments at exactly the same temperature. In addition, there is lack of data for the heat capacity and heat conductivities of all the materials that comprise the reactor and the bed. Also, other properties are, also, unknown like the convection heat transfer coefficient for each fluid (h), the overall heat transfer coefficient (UA) and the heat transfer rate (\dot{Q}). UA is usually calculated by the thermal conductivities of the materials, the convection heat transfer coefficient for each fluid and the contact areas of the fluids to solid particles. But, because inside the reactor is a packed bed of several materials (Ni/Al_2O_3 , zeolites, Al_2O_3), this isn't feasible. Hence, modelling the heat exchange of such a system is a complex procedure even in equilibrium conditions. Hence, before realizing the experiments, tests were performed for the different flow rates, flow composition and bed composition. The purpose was to determine the difference between the cable temperature and the temperature of the middle thermocouple in each case. So, when carrying out an experiment (for each bed composition and flow rate), one can know what the cable's temperature should be in order to achieve the desired temperature inside the bed.

3.1.2. Micro-GC Calibration

As it has been refer prior to section 3.1, a Micro-GC devise is used in this research for the purpose of analysing the outlet process gases of the reactor. Gas chromatography is probably the most common type of chromatographic analytical methods. It is used for separating and analysing gaseous compounds that do not decomposed during vaporization. The GC consists mainly of a metallic or glass column. This column contains, inside of it, a stationary phase. This phase is a liquid or polymer supported on a solid. The compounds to be examined are carried inside the column with an inert gas, in this case argon. The compounds are adsorbed in the stationary phase with different rates, thus each one having a unique retention time. Each gaseous compound is recognized by its retention time. The specific micro-GC is a Varian CP-4900, nowadays branded as Agilent 490 micro-GC. In order to use the GC for the current research a method should be constructed in its software (Galaxie).

Essentially, the GC is calibrated for the gases expected to be present at the outlet of the reactor and for the range of concentrations that those will approximately be. In order to realize this, the reactor was filled with aluminum oxide pellets and flooded continuously with the 5 process gases of the set up (CO_2, H_2, CH_4, N_2, CO). The reactor was at room temperature and it was fed with 15 different fraction combinations of the 5 gases. Each combination was performed 5 times to increase the accuracy.

After the calibration process the reactor was heated at $300^\circ C$, known concentrations of the gases were led through, cooled down and measured again by the GC. The intention behind this process was to replicate the experimental procedure and test the accuracy of the method constructed (on the GC) for the experiments. The calibration procedure was proven successful.

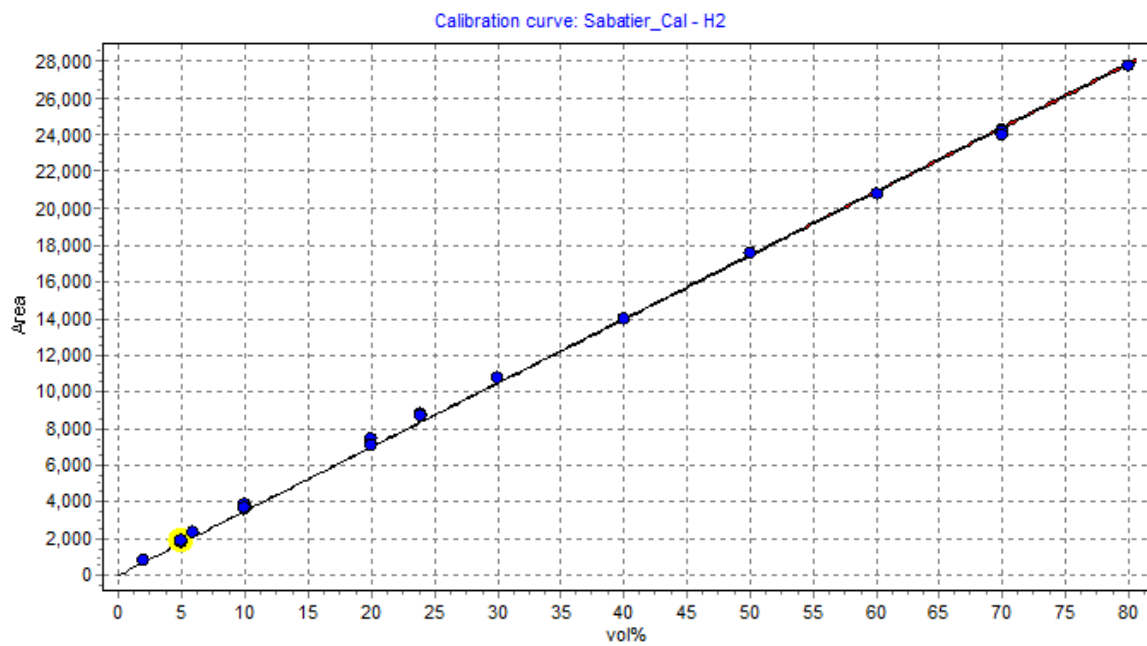
All 15 points used for the calibration of GC are enclosed in table 3.1.

The calibration performed for all of the gases gave a regression coefficient of more than 0,9993 for each one. The calibration curve of H_2 follows (figure 3.2), supporting the high regression coefficient.

The rest of the calibration curves for CO_2, CO, CH_4 and N_2 are included in the Appendix (chapter A.6).

Table 3.1: Calibration points:Gases fractions

points	1	2	3	4	5	6	7	8	9	10	11	12	13	14	15
H2	0.02	0.06	0.1	0.2	0.24	0.3	0.5	0.6	0.05	0.05	0.7	0.8	0.4	0.1	0.2
CO2	0.02	0.06	0.1	0.14	0.2	0.3	0.1	0.4	0.25	0.05	0.3	0.2	0.5	0.7	0.8
N2	0	0.04	0.1	0.2	0.16	0.3	0.4	0	0.7	0.9	0	0	0.1	0.2	0
CH4	0.94	0.8	0.6	0.4	0.2	0.1	0	0	0	0	0	0	0	0	0
CO	0.02	0.04	0.1	0.06	0.2	0	0	0	0	0	0	0	0	0	0
sum	1	1	1	1	1	1	1	1	1	1	1	1	1	1	1

Figure 3.3: Calibration line of H2, $R^2 = 0,9993$ (points in table 3.1)

3.2. Materials

The materials that the current work was based upon are introduced in this section. Those are a Nickel based catalyst, 2 different types of zeolites and aluminum oxide particles. All those are presented and examined in the next subsections.

3.2.1. Aluminum oxide pellets

The first material-component designated for the present experiments is Aluminum Oxide (Alumina). Namely, Alumina Balls, a product generously provided by "RVT Process Equipment GMBH". A German based company that focuses in equipment for mass and heat transfer for chemical, petrochemical, refinery and environmental applications.

Exactly that is the purpose of the Alumina Balls in the present research. To enhance gas mixing and heat transfer throughout the reactor and generally, perform a secondary, but non the less crucial role in the experiments. They are considered to be inert in the present reaction and appear no significant catalytic activity towards the methanation of CO_2 . In addition, they can withstand great temperatures, without thermal cracking, deformation or change in their composition. The usage of those is analyzed in length in the series of experiments developed onwards.

Regarding the specifications of this product. Its copyright trademark mark is "HiDur ©Balls Alumina". They are spherical pellets of 1/8 inch diameter (approximately 3,2 mm), with negligible variations on size. The bulk or packing density of those is 2000–2200 kg/m^3 , but calculated close to 2000 kg/m^3 . Water absorption at normal conditions is maximum 6% per weight. Lastly, its chemical composition is more than 99,5% aluminum oxide (Al_2O_3) with titanium dioxide (TiO_2), consisting also from traces of SiO_2 , Fe_2O_3 , MgO and NaO . The specific heat capacity is 880 $J/kg/K$ [1].

3.2.2. Catalyst

As it has been thoroughly examined in the literature review there are numerous options for the composition of the catalyst. It was decided for the present research to go with a nickel based catalyst. The reasons are that nickel demonstrates higher catalytic activity compared to other catalysts based on Magnesium (Mg), Iron (Fe), Manganese (Mn), Cobalt (Co) or Zinc (Zn) for example and, also, has a greater availability and abundance compared to the (more expensive) noble metals based catalysts. Those are Palladium (Pd), Rhodium (Rh) and Ruthenium (Ru).

The exact composition of the catalytic pellets is Ni/Al_2O_3 (referred to as Ni/Al hereafter). So the support is Aluminum Oxide, similar to the Alumina Balls used. Probably the most common support in nickel catalysts for methanation processes. It is widely researched in academia and has been commercially and industrially applied for similar processes in many occasions (methanation of both CO and CO_2). It reaches high activity values at the temperatures applied in the current research. Which implies that it can be a solid base to design a large scale (compared to previous researches [51][15]) sorption enhanced methanation process, with a physical mixture of the catalyst and zeolites.

Moving on with Ni/Al_2O_3 , as it has also been mentioned in the literature review, this binary mixture of Nickel can be impregnated with a third metal to enhance the activity.

So the end result would be a ternary mixture with Zirconia (Zr), Ceria (Ce), for example, or some noble metal as the third metal option. But, that would increase the cost of purchasing the catalyst and deviates from the main purpose of this research.

The catalyst was provided generously by "C&CS-catalysts & chemical specialties". A German company specialized in preparation of catalysts and adsorbents and it is dedicated in the specific market in Europe. The product's branded name is "METH ©134". It consists of spherical pellets of 3 – 6mm (considered to be close to 5mm, after examining them). The bulk or packing density is 800 – 1000kg/m³. From some basic (weight and volume) lab experimentations the density was calculated to be closer to 800kg/m³. The chemical composition as given by the manufacturer is 20 – 25% Nickel monoxide (NiO), 5 – 10% Calcium oxide (CaO), with the rest being Aluminum oxide (Al₂O₃). Based this composition the specific heat is calculated as 771J/kg/K. The product is inert upon arrival from the manufacturer, since it is in NiO form. The purpose for that is to be stable and easier to handle. So it should be activated (reduced) before usage. A process that is described onwards. To conclude this product is optimized for carbon monoxide and carbon dioxide methanation making a solid foundation for exploring the possibilities of sorption enhancement.

3.2.3. Sorbents

For the sorption of vapor formed from the reaction, it was decided to work with zeolites. A known group of microporous adsorbents in the industry, that come from crystalline metal aluminosilicates. They were favored over different types of physisorption materials due to their ability to adsorb vapor at high temperatures, without, also, thermal cracking or collapse of their structure.

Two different types of zeolites were used in the current research. Those are zeolite 3A and zeolite 4A. Below follow their specifications.

Molecular sieve 3A

The specific type of zeolites has a high affinity for water and ammonia. So it is suitable for desiccation of petroleum cracking gas and alkenes and purification of natural gas among others [8]. Thus it is considered to be a product dedicated for the present research.

The zeolite 3A-product used in this case consists of spherical pellets of an average diameter of 3,2mm. The bulk density is calculated close to 725kg/m³. The specific heat of this product is unknown, together with its specific composition.

Molecular sieve 4A

In the case of zeolite 4A it, also, has affinity towards carbon dioxide besides water. But, due to its hydrophilic nature (polarity of water is larger than CO₂) and the smaller kinetic diameter of H₂O to CO₂ (2,65Å to 3,3Å) the competitive adsorption between CO₂ and H₂O leans towards the later. Generally, it is also used for dehydrating liquid and gas streams, based on manufacturers reports [8]. In addition, in researches of molecular sieves 3A and 4A a similar adsorption capacity and selectivity to water has been recorded [10],[16]. This is observed as well in similar studies of sorption enhanced methanation reactions [51]. So, it can be safely assumed that the adsorption of H₂O on zeolite 4A will be successful.

The zeolite 4A-product used for the experimental work was purchased from "C&CS-catalysts & chemical specialties". It is in spherical form with a diameter of 1,6 – 2,5mm (on

Table 3.2: Composition of Molecular Sieve 4A. As given by manufacturer.

Magnesium Oxide	<5%
Aluminum Oxide	<30%
Sodium Oxide	<33%
Amorphous Silicon Dioxide	<50%

average it is considered to be $1,6\text{mm}$). The bulk density of the product is $700(\pm 50)\text{kg}/\text{m}^3$ and calculated also close to $725\text{kg}/\text{m}^3$. The melting temperature is below 1000°C as given from the manufacturer and can reach 600°C without any affections to its adsorbing ability. The composition as given from the manufacturer is included in table 3.2.

3.3. Experiments

The experiments performed in this research can be separated in two major groups. The first group refers to the experiments performed only with the catalyst and the Al_2O_3 pellets present in the reactor. In the second group of experiments, zeolites were included in the reactor's bed together with the catalytic pellets.

Before performing each series of experiments there is a procedure that must be followed. That procedure regards the activation of the catalyst, plus the regeneration of the zeolites for the second series of experiments. In addition, before each individual experiment a pretreatment of the catalytic bed is performed as well. All those steps are explained in detail in the following sections.

3.3.1. Experiments with catalyst

The 1st series of experiments is aimed in the characterization of the catalyst and specifically, in its activity. The goal is to determine its performance for different temperatures and in the same conditions that the catalysts-zeolite bed is evaluated.

Regarding the conditions mentioned. The goal of this research as it has been stated before is to evaluate the sorption enhancement of the methanation reaction with a physical mixture of zeolites and catalyst. In order to realize that there should be enough amount of zeolite present, compared to the pellets of catalyst to accommodate the vapor produced by the reaction. So it was decided to add 5 times more molecular sieves by mass compared to the $\text{Ni}/\text{Al}_2\text{O}_3$ particles. That corresponds to an approximately similar analogy per volume. Since the bulk densities of those products (catalyst and zeolites) are close. This analogy was calculated based on a minimum adsorption time of 10 minutes. Specifically, the amount of zeolite used was determined based on an average of $2\% \text{g}_{\text{H}_2\text{O}}/\text{g}_{\text{zeol}}$ capacity, on the amount of water produced (complete conversion of reactants) and on an adsorption time of 10 min (for the maximum experimental flow).

Hence, for the catalyst characterization experiments the catalytic bed was diluted with 5 times more Alumina balls per volume compared to Ni/Al , in order to assure a similar GHSV as in the experiments with $\text{Ni}/\text{Al} - \text{Zeolites}$.

Based on that volumetric analogy the catalytic bed was designed and its specifications are included in table 3.3.

Table 3.3: Catalyst/alumina oxide bed

	Mass(kg)	Bed	Height(m)	Diameter(m)	Volume(mL)
Catalyst	0,042		0,161	0,052	342
Aluminum oxide	0,580				

Table 3.4: Flow characteristics of 1st series of experiments

	Flow (L/min)	GHSV (total bed)(1/h)	GSHV (Ni/Al volume)(1/h)
N2	4	921	6000
H2	1		
CO2	0,25		

The reactor is split in three segments. The first one from the bottom to the top regards the tripod that supports the bed and it is 15cm. The second segment is the bed and it is approximately 16cm and the last part at the top is 14cm and is filled with Al_2O_3 balls. The two different spherical pellets inside the bed (catalyst and aluminum oxide) were physically mixed and poured inside with the aid of a funnel. Generally, material segregation isn't concerned an issue. Firstly, because the materials were handled cautiously. Secondly, nickel is embedded on alumina and prepared by the manufacturer to be used even in fluidized bed settings. So, an "escape" of nickel is considered non-existent.

Those alumina pellets define a major role in the physics of the flow and the reactor. The gases enter from the top of the reactor, so they pass through the pack of alumina balls first. That pack helps in mixing the gases, increases the length of the porous bed in order to achieve a plug flow (increase the ratio of length to diameter for securing plug flow) and last but not least enhances the preheating. Alumina oxide has a thermal conductivity of approximately $30W/(m * K)$, 60 times more than nitrogen in similar conditions. So, without them the gases would never reach and stabilize around the wanted experimental temperature in each run.

The composition of the reactor for the first series of experiments is depicted in figure 3.4.

Regarding the flow of gases, it was chosen 75% of the total volumetric flow to be composed of Nitrogen. The reasoning behind that was to constrain the temperature rise inside the reactor due to the heat release from the highly exothermic methanation of CO_2 . So the process could be considered relatively adiabatic.

The flow composition and Gas Hourly Space Velocity (GHSV), for the whole volume of the bed and the volume occupied only by the catalyst, are shown in table 3.4. The reason for using this composition was the maximum acceptable temperature rise inside the catalytic bed due to the exothermicity of the reaction. The calculation of the temperature rise (for that composition) can be seen in chapter 4.2.1.

The specific flow was applied for multiple temperatures in the range of 200–380°C with increments of 20°C. For each temperature the flow was continuous and stable for 40 minutes. Measurements were taken by the Gas Chromatography equipment every 4 minutes. At the 10th measurements the experiment stopped and the reactor was left with a flow of pure Nitrogen to clear out.

Prior to the experiments the catalyst must be activated. This process is analyzed be-

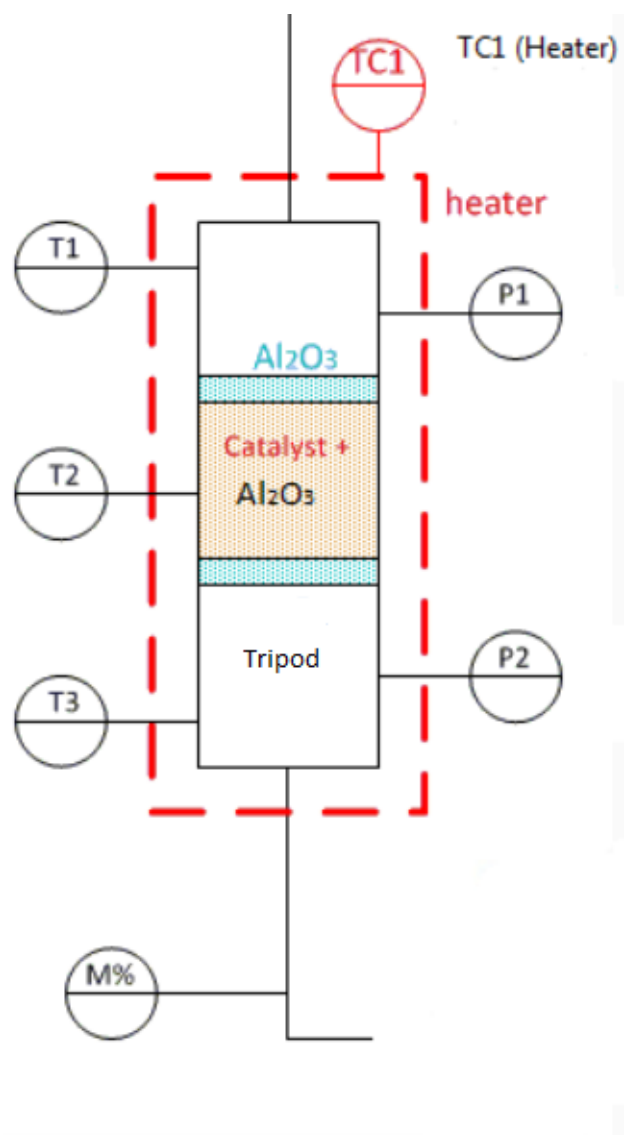


Figure 3.4: Reactor composition-1st series of experiments

low. After activation the catalyst performed without any reduction in its activity throughout each group of experiments.

Procedure of activating the catalyst

After loading the reactor with the combination of catalyst-alymina oxide, the bed has no activity, since the catalytic pellets are inert. That is because the catalyst is delivered by the company in a nickel oxide form (NiO/Al_2O_3). Oxygen must be removed and get activated Nickel (Ni/Al_2O_3).

In order to remove the molecule of oxygen from NiO, hydrogen must be provided in the system at elevated temperatures. The following reactions occurs and the process is named reduction of NiO to Ni:



Before passing hydrogen the reactor is left over night at $130^\circ C$ with a flow of $0,2L_n/min$ of N_2 to remove completely the humidity, oxygen and any other residue. After securing an inert and dehydrated environment inside the reactor, hydrogen starts to flow together with nitrogen and the temperature increases with a rate of $65^\circ C$ per hour. The gas flow consists of $5L_n/min N_2 - 0,2L/min H_2$ and the H_2 reaches gradually a maximum flow rate of $0,4L_n/min$. So, again, every one hour the temperature was increased together with the hydrogen content until the maximum limit is reached for both. So when the temperature inside the reactor gets up to $385^\circ C$, the process is kept steady for at least 2 hours to reassure the removal of all the bonded oxygen. After the reduction of the catalyst a stream of pure N_2 is passed through the reactor to dehydrate complete the catalytic bed.

3.3.2. Experiments with the combination catalyst/zeolites

After the 1st series of experiments and the characterization of the catalyst, followed the experimental sorption enhanced methanation of CO_2 .

As it has been stated before, the design of the bed was made with the principle of 5 times more zeolite than catalyst to accommodate the vapor produced by the reaction. Having that in mind the same procedure was followed as in the previous series of experiments, with the only difference that the catalyst was diluted in the bed with zeolite instead of aluminum oxide pellets. Thus, the same as before amount of catalyst was used and it was mixed physically with 5 times more (per volume) zeolites. Then this mixture was poured inside the reactor.

Hereby, follows the table (table 3.5) with the characteristics of the bed for the second series of experiments. It should be noted that the same amount of molecular sieve 3A and 4A was used during the two different experiments. Because the two products have essentially the same bulk densities. Also, another reason behind that was to have comparable results of their performance on this process.

The composition of the reactor for those experiments is depicted in figure 3.5.

Table 3.5: Catalyst/zeolites bed

	Mass(kg)	Bed	Height(m)	Diameter(m)	Volume(mL)
Catalyst	0,042		0,161	0,052	342
Zeolite 3A-4A	0,210				

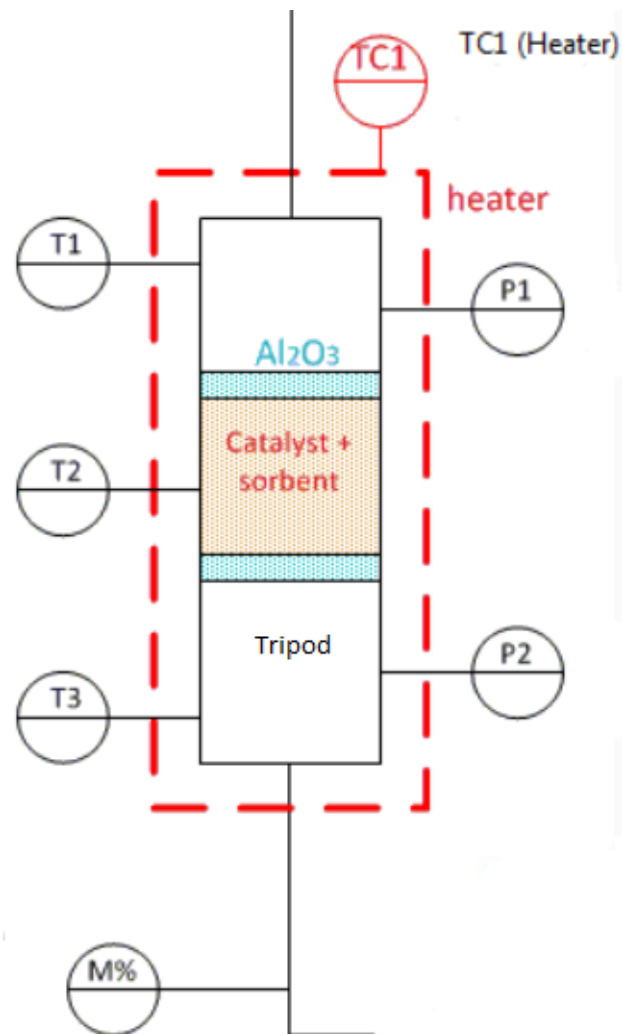


Figure 3.5: Reactor composition-2nd series of experiments

Activating catalyst and regenerating zeolites

After filling the reactor with a fresh amount of catalyst and zeolite (both for 3A and 4A), the same procedure is followed as before to activate the catalyst (see chapter 3.3.1). At the end of the reduction of the Ni/Al_2O_3 particles, the reactor is flooded with the same flow of Nitrogen (5 L/min) and hydrogen (0,4 L/min) for 4 hours, at the maximum temperature, in order to reassure the best possible dehydration of the molecular sieves. The maximum temperature for the case of catalyst/zeolites was recorded at $380^\circ C$, compared to the $385^\circ C$ of $Ni/Al_2O_3-Al_2O_3$. It is essential for the success of the experiments to have a completely activated and dried out catalyst/zeolite pair, since at elevated temperature the capacity of zeolites is already very low (1 – 4%). Compared to their capacity at room temperature (around 20%).

It should be mentioned, that for dehydrating zeolites one can either perform a pressure swing (reduce pressure below atmospheric, via vacuum) holding the temperature constant or increase the temperature high enough until complete dehydration. In this way full dehydration of zeolites is reassured. In both cases flow of a dry inert gas is necessary. Unfortunately there are not definite data of maximum temperatures at atmospheric conditions for the complete dehydration of zeolites. Also, no generally accepted procedure of regenerating zeolites 3A and 4A is available. In one study ([31]) the performance of 3A and 4A in dehydrating aliphatic alcohols is examined. It is mentioned in this study that for the regeneration of 3A and 4A temperatures of up to $400^\circ C$ and $500^\circ C$, respectively, are needed. But, no pressure condition is mentioned. Also, it could be that zeolite 4A had adsorbed a percentage of alcohols and, thereby, needed higher temperatures for its regeneration. In another study ([47]) for zeolite 3A (on fixed bed-near adiabatic reactors like the present study), a regeneration temperature of $240^\circ C$ was applied. But, at absolute pressure of less than 0,1 bar. In addition it was mentioned that above $270^\circ C$ the adsorption capacity of 3A is reduced. This statement conflicts with other researches that claim that only above $500^\circ C$ the adsorption capacity of zeolites is reduced. Other similar sorption enhanced studies ([51]) applied temperatures of up to $450^\circ C$ or even more ([13], [15]). Thus, in the present study complete dehydration of zeolites cannot be assumed, with the process followed and the maximum temperatures applied.

Molecular sieve 3A – Ni/Al_2O_3

The first experiments were performed with the combination of nickel-zeolite 3A. There are limited to none data in academia regarding the behavior of zeolites in elevated temperatures. So it was decided to perform the same cycle of experiments (similar temperatures and volumetric flow rates) as in the $Ni/Al_2O_3-Al_2O_3$ bed, performed prior. In that way it would be possible to detect the operational temperature limits of the zeolite and the level of enhancement it provides at each temperature.

So the 9 experiments were performed from $200-360^\circ C$ with increments of $20^\circ C$. At table 2.3 the flow composition can be seen together with the GHSV.

After those experiments it was decided to investigate the change in the conversion rates if one of the products of the reaction is included in the inlet stream. So one experiment was performed at $240^\circ C$ with the same GHSV as before and same H_2/CO_2 mass flow, but the majority of N_2 was exchanged for CH_4 . The flow values are enclosed in table 3.6.

Table 3.6: Experiment with presence of CH₄ as inlet, zeolite 3A

	Flow (L/min)	GHSV (total bed)(1/h)	GSHV (Ni volume)(1/h)
N ₂	1	921	6000
H ₂	1		
CO ₂	0,25		
CH ₄	3		

Table 3.7: Flow characteristics for the minimum volumetric flow rates

	Flow (L/min)	GHSV (total bed)(1/h)	GSHV (Ni volume)(1/h)
N ₂	1,6	368	2400
H ₂	0,4		
CO ₂	0,1		

With the previous set of experiments knowledge was gained regarding the performance of the pair nickel-zeolite 3A at each temperature. The next step was to apply the minimum GHSV the setup could handle (on the same catalytic bed) to observe the change in the conversion rates of the reactants. Explicitly, by reducing the flow of reactants the residence time is increased and the amount of vapor produced is decreased. This could lead to higher conversion rates than before.

In order to have relatable results with the ones at higher GHSV, the composition of the inlet gases was kept the same. Only the volumetric flow rates were reduced to the minimum.

The flow rates applied (together with the new GHSV) are included in table 3.7.

Molecular sieve 4A – Ni / Al₂O₃

After completion of the experiments with the pair catalyst-zeolite 3A, the reactor was emptied and loaded with a fresh amount of catalyst and zeolite 4A this time. Again the same procedure was followed for activating the catalyst and regenerating the zeolite.

To be able to compare the two different types of molecular sieves the same experiments should be performed in both. So 4 experiments were realized at 240, 260, 280, 300°C, with the same flows as in table 3.6.

Lastly, 2 experiments were realized at 260 and 280°C with the composition of CO₂ and H₂ kept the same and the addition of methane in the inlet. The flows applied are included in table 3.8..

As it can be noticed the same GHSV was chosen as the previous experiments. This is the minimum defined by the mass flow controllers capabilities. The purpose was to achieve

Table 3.8: Experiment with CH₄ as inlet and minimum flow rates, zeolite 4A

	Flow (L/min)	GHSV (total bed)(1/h)	GSHV (Ni volume)(1/h)
N ₂	0,5	368	2400
H ₂	0,4		
CO ₂	0,1		
CH ₄	1,1		

again the maximum conversion possible (for this combination of 4A-Ni) and have an immediate result for the influence of methane (as an inlet gas) in the performance of the process.

Molecular sieve 4A – Ni / Al₂O₃ 2,5mm in size

The next combination of materials that was utilized in the experimental procedure was again zeolite 4A and Ni pellets. But in this case the Ni pellets were reduced in size. The purpose was to increase the proximity of the catalytic sites to the adsorbents surface. The meaning and importance of proximity is analyzed in the following.

Catalysis occurs in a length scale of nm inside the catalyst's pores and the diffusion length of the molecule's gas to the catalytic sites. In order to have an estimation of the length scale of catalysis, we calculate the mean free path [6] of carbon dioxide for the present experimental conditions.

$$\lambda = \frac{RT}{2^{-2}\pi d^2 N_A P} \quad (3.2)$$

In equation 3.2, T refers to the temperature, R to the gas constant, d to the kinetic diameter of CO₂ (3,3 angstroms) and H₂O (2,65 angstroms), N_A to the Avogadro's number and P to the pressure. For 300°C and 1 bar the mean free path is 86nm for CO₂ and 133nm for H₂O. Hence, when the two material (Ni and zeolities) are physically mixed with each other, the length scale between them is constituted by their size, in this case mm . Thus only a small fraction of adsorbing surface is close to the catalytic sites of Ni to actually enhance the reaction. Essentially, this is proximity. The amount of the adsorbent's surface that is inside the diffusion length of the catalytic sites. By reducing in half the size of the catalyst and mixing them again in theory that amount should double.

So, a large amount of Nickel pellets was crushed in a mortar. The resulted Ni particles were sieved and the powder was removed keeping the rest of the material. From this material 42g were used for the new bed together with 210g of zeolite 4A. Amounts identical to the previous experiments. The average size of the Ni particle used were approximately half of the initial size of the pellets. So, close to 2,5mm. The technical difficulties in reducing the size of the catalyst is that the outcome is in amorphous shape and one can only so much reduce the size before resulting in a powder like material. A representation of the old and new Ni/Al₂O₃ particles (5mm and 2,5mm) can be seen in figure 3.6. The contact points between the catalyst and zeolites are increased due to the reduction of their size.

Four experiments were performed with this bed. Two at 260°C and two at 280°C. The flows chosen are same as before and are depicted in tables 3.7 and 3.8. The results are presented in chapter 5.

In this point it should be mentioned that all the necessary safety precautions were taken when handling toxic materials like nickel. Mask, safety glasses, disposable gloves and lab coat was used. Vacuum was used when crushing the particles so no nickel particles would be inhaled. Afterwards all the surfaces were sanitized.

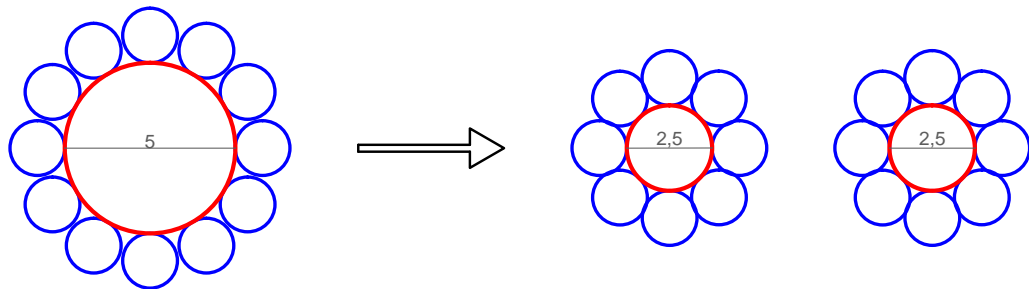


Figure 3.6: A representation of the old and new catalytic particles and their interaction with the zeolite pellets (numbers in mm)

Molecular sieve 4A – Ni/Al₂O₃ 1mm in size

With the purpose of exploring, furthermore, the possibilities from reducing the size of the catalytic pellets, a set of experiments with an even smaller particle size was performed. In this case the *Ni/Al₂O₃* particles were reduced in size with higher precision. A larger amount than before was smashed in a mortar. Onwards different sizes of sieves were applied on this mixture resulting in a more uniform group of amorphous particles with a minimum size of 0,71mm and maximum of 1,5mm. The average size of the resulted *Ni/Al₂O₃* was close to 1mm. On eye they were significantly smaller than the zeolite 4A which was paired with (1,6mm in diameter).

Once more 42g of the resulted catalyst and 210g of zeolite were weighted and combined to form the new bed. In this occasion though a problem was detected when combining the two material together in a glass volumetric container. Specifically, after stirring the mixture the bulk of *Ni/Al₂O₃* particles resulted at the bottom of the vessel, due to their smaller size and higher density compared to zeolite 4A particles. Regardless of the time put in mixing, when the pair was poured in the reactor spots of high concentration of *Ni/Al₂O₃* were created leading in a non uniform bed. Expecially, compared to the previous combination of 2,5mm *Ni/Al₂O₃*-Zeolite 4A, where uniformity was achieved. This phenomenon could possibly affect the conversion rate of the reactants, as it can be seen in the results (chapter 5).

To conclude, four pairs of zeolite-*Ni/Al₂O₃* were deployed. Those are zeolite 3A-*Ni/Al₂O₃*, zeolite 4A-*Ni/Al₂O₃*, zeolite 4A-2,5mm *Ni/Al₂O₃* and zeolite 4A-1mm *Ni/Al₂O₃*. The combinations can be seen in the following images (fig. 3.6, 3.7, 3.8 and 3.9).



Figure 3.7: Combination of zeolite 3A/Ni

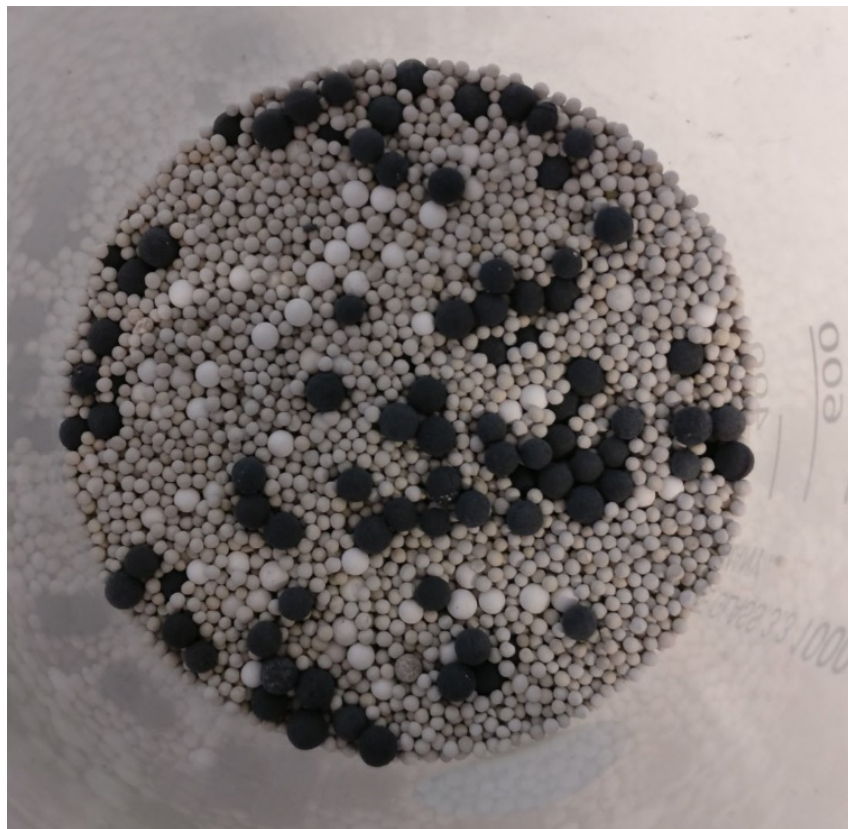


Figure 3.8: Combination of zeolite 4A/Ni



Figure 3.9: Combination of zeolite 4A/2,5mm Ni



Figure 3.10: Combination of zeolite 4A/1mm Ni

4

Modelling and calculations

This chapter is devoted in the calculations and modelling performed prior the experiments. The goal was to predict, based on thermodynamics, the progression of the present synergistic process and set the goal (partial pressure of water) for the optimum results. Also, approximate on hand the pressure drop and temperature rise inside the catalytic bed.

4.1. Pressure Drop in the Reactor

Upon designing the experimental procedure, the composition of the catalytic bed and the reactor in total, it should be reassured that the pressure drop would be in an acceptable range of values. An elevated pressure drop would affect the heat and mass transfer inside the reactor, leading in ill defined experimental conditions. But most importantly would influence significantly the performance of the catalysis and the sorption abilities of the pair of molecular sieves (3A and 4A). Because both processes (reaction and sorption) are favored by elevated pressure and affected negatively by pressures below the atmospheric. Since, the current research is performed in close to atmospheric conditions, pressure drops of more than 0,1 *bar* must be avoided.

In order to calculate the pressure drop for the present case study, Ergun's Equation for flow inside packed beds was deployed.

$$\frac{\Delta P}{L} = \frac{(150 * \mu * v)}{D_p^2} * \frac{(1 - \epsilon)^2}{\epsilon^3} + \frac{(1,75 * \rho * v^2)}{D_p} * \frac{(1 - \epsilon)}{\epsilon} \quad (4.1)$$

The section of the reactor examined was that between the two pressure sensors, which included the catalytic bed and part of the Al_2O_3 pellets. The length is approximately 20 *cm* and the fluid properties regard CO_2 at 1 *bar* and 300°C. The pressure drop was evaluated for porosities of 0.2, 0.3 and 0.4 and for the experimental volumetric flow rates of 2.1 and 5.25 *L/min*. The results are presented in figures 4.1(a), 4.1(b) and 4.1(c).

As it can be seen from the graphs, even in the worst case scenario the pressure drop is negligible.

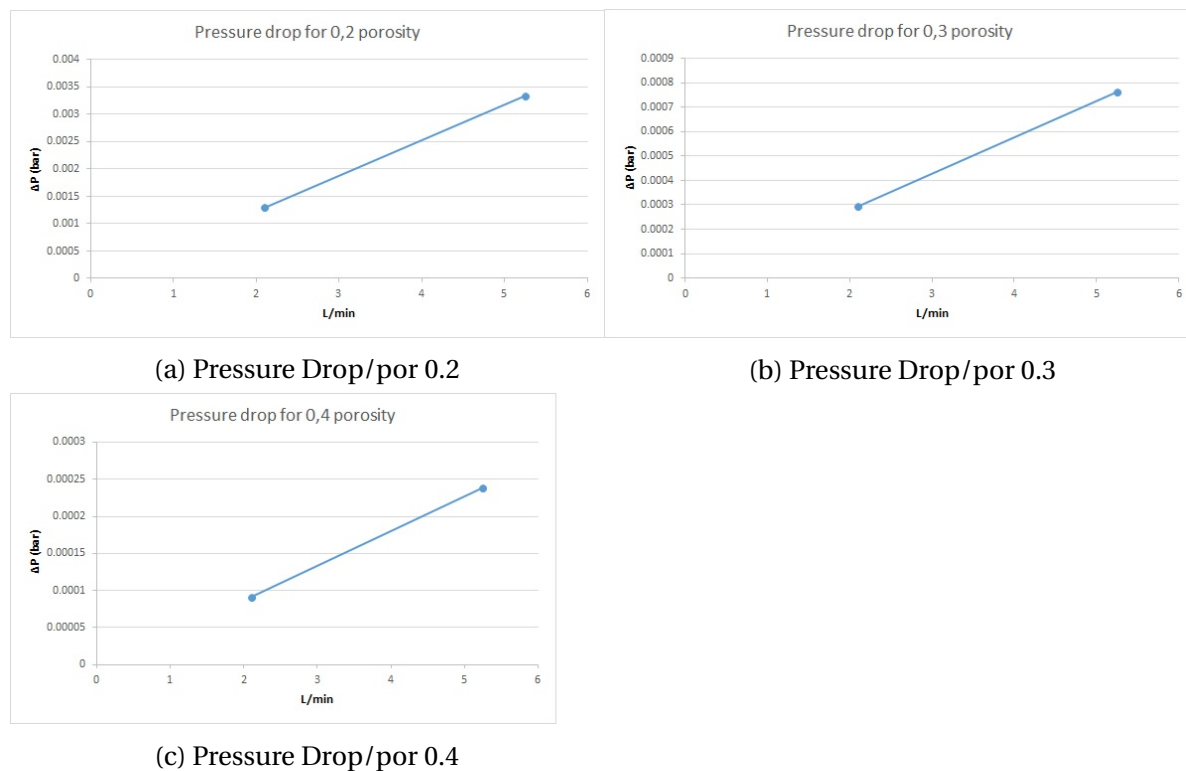


Figure 4.1: Pressure Drop for various porosities and flow rates. All pressures are in *bar*

Pressure difference results

The above mentioned calculations are consistent with the readings from the pressure sensors. Those sensors recorded pressures of up to 3 decimals of 1 bar and the readings showed maximum differences of 0.001 bar between them. That results are for the maximum flow rate of $5,25\text{ L/min}$. That number of pressure drop is even smaller than the uncertainty of the equipment so the pressure drop is negligible and the porosity is thus considered around 0.3-0.4.

4.2. Thermodynamics of the reaction

Moving on with the calculations regarding the progression of reaction with temperature at atmospheric pressure conditions. Due to lack of kinetics for the present Nickel catalyst, the conversion rate of the reactants will be calculated based on the thermodynamic equilibrium data of the reaction. In order to detect the actual activity (conversion rates of reactants) of the present Ni/Al_2O_3 catalyst a set of experiments was performed (analyzed in chapter 2.3.1).

4.2.1. Aspen model

For examining the reaction thermodynamically a model was constructed in the software *AspenPlus*. The model consists of a Gibbs Reactor module, as it can be seen in figure 4.2.

The reactor was designed based on the experimental conditions. So the pressure of the reactor was set at 1 bar and the composition of the inlet stream was $76,19\%N_2$, $19,05\%H_2$ and $4,76\%CO_2$.

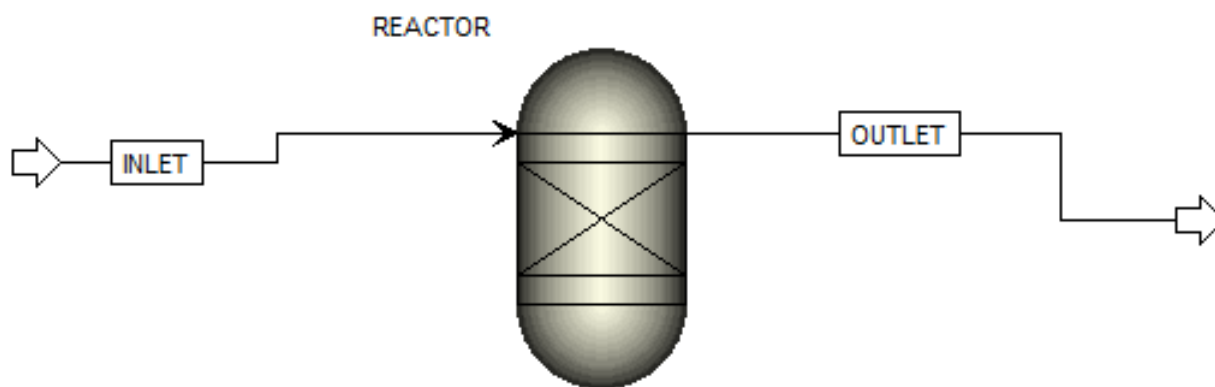


Figure 4.2: Gibbs Reactor model in AspenPlus

Based on the heat duty calculated from Aspen Plus the adiabatic temperature rise was calculated. For the gas phase of the reactor and the experimental composition of gases, this is $663K$ for one batch of gases at $300^{\circ}C$. But the reactor consists of 30% gases (based on a 0.3 porosity) and the rest consists of solid, packed pellets (Ni/Al_2O_3 , Al_2O_3 and zeolites). Taking into consideration the thermal capacity of alumina oxide, which is the lowest among the three (so the highest possible temperature rise), and for the highest experimental flow rates (GHSV=921), the temperature rise is no more than $22^{\circ}C$ for a continuous experimental operation of 1 hour. Which is an acceptable rise (inside the operating range of the reaction) and the process could be considered adiabatic. It should be mentioned that this calculation is an approximation of the worst case scenario. The expected rise should be less. The code regarding those calculations is included in the Appendix (chapter A.1).

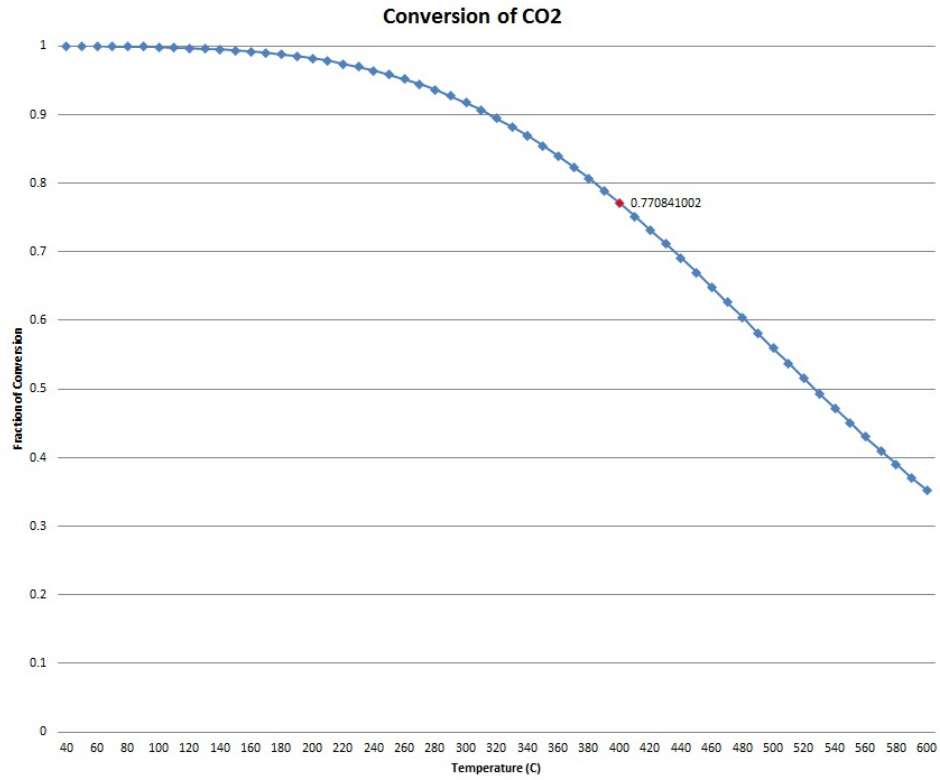
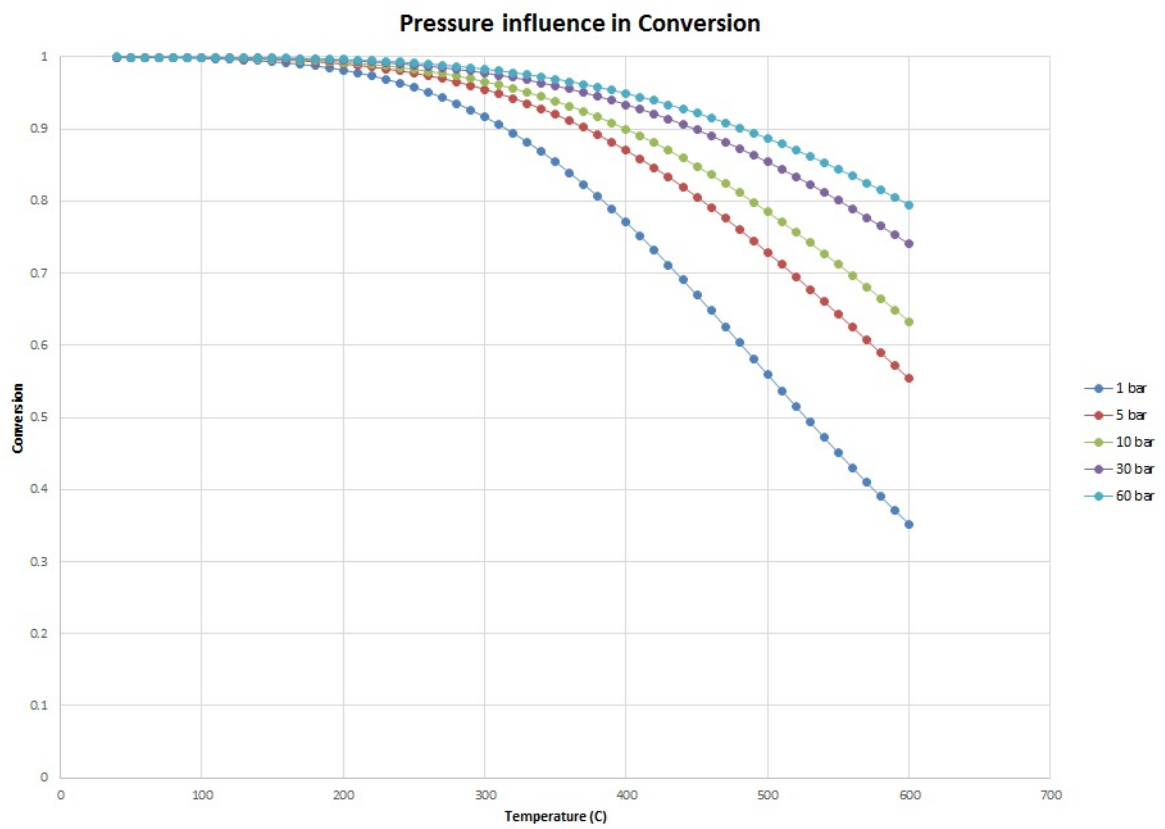
Indeed the temperature rise recorded by the sensors (during the experiments) was lower than the one predicted above. The maximum rise was recorded at the experiments with the zeolite 4A where the maximum of conversion was achieved (close to 100% conversion) and the rise was approximately $15^{\circ}C$.

Moving on with the conversion of the reactants as calculated via *Aspen Plus*. A sensitivity analysis was performed on the conversion of CO_2 , at 1 bar pressure of the reactor, for multiple temperatures and the previously mentioned composition of the reactants. The results are plotted in figure 4.3.

As it can be seen in that graph the conversion starts decreasing from $120^{\circ}C$ and onwards. The value of conversion at $400^{\circ}C$ is being marked on the graph (77,08%). The purpose of that is to have a direct comparison with the conversion as calculated in the next section (data from the software *Factsage*).

Moving on with the next sensitivity analysis. In this case the same variation of temperature occurred but for several different values of pressure of the reactor. Again, the composition of the inlet gases to the reactor was kept the same as in the experiments (always stoichiometric analogy between the reactants). The results are plotted in figure 4.4.

It can be easily noticed that pressure influence immensely the performance of reaction. For elevated pressures the conversion rises significantly. Hence, the reason why usually industrial applications for the methanation of CO and CO_2 take place at reactors of more than to 20bar of pressure [46], to ensure high conversion rates of reactants and high purity

Figure 4.3: Theoretical Conversion of CO₂Figure 4.4: Theoretical Conversion of CO₂, for different values of pressure, as calculated from *AspenPlus*

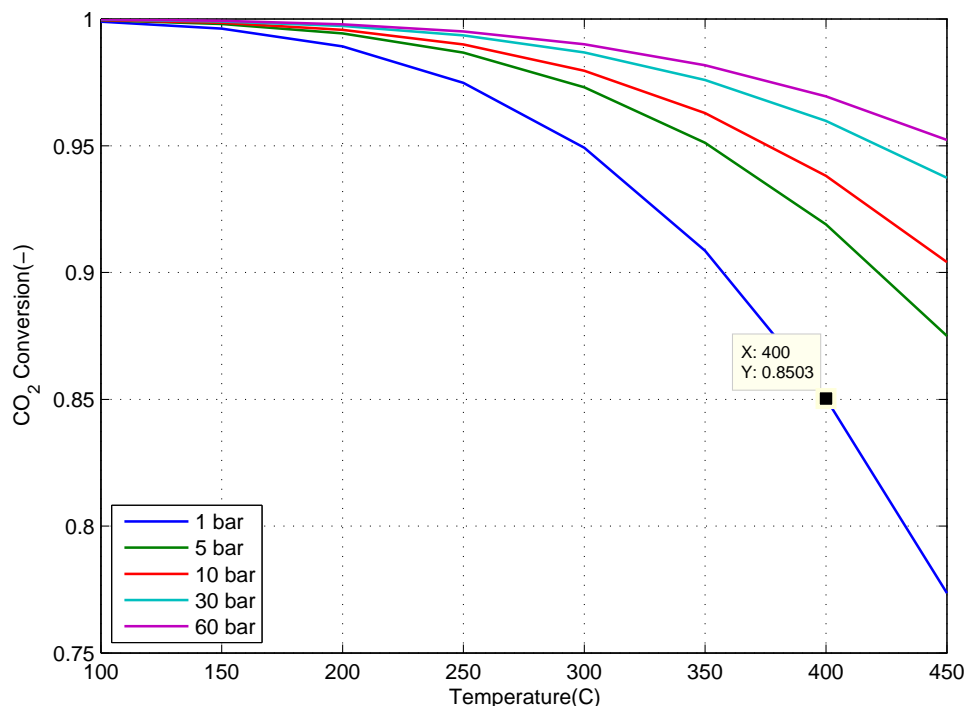


Figure 4.5: Theoretical Conversion of CO_2 , for different values of pressure, as calculated from *Factsage*

of methane.

4.2.2. Calculations based on *Factsage*

The equation of the chemical equilibrium constant of the Sabatier Reaction is the following:

$$K = \frac{4x^3(5-2x)^2}{(1-x)(4-4x)^4} \left(\frac{P_{tot}}{P_{ref}}\right)^{-2} \quad (4.2)$$

In equation 4.2, K refers to the equilibrium constant and x to the conversion of CO_2 . The derivation of this relation is presented in chapter A.2 of the Appendix.

Using this equation by applying the equilibrium constant's values for several temperatures and solving for x , the conversion again is calculated for 5 different reactor pressures. The K values were extracted from the software *Factsage* for the Sabatier Reaction. The results for all 5 pressure levels are included in one plot (fig 4.5) and the Matlab code for that is included in the Appendix (chapter A.3)

On figure 4.5 the conversion of CO_2 is marked for 1 bar of pressure at $400^\circ C$. This value is close to 86% and it is 9% higher compared to the one from figure 4.4 at the same conditions. The conversion rates calculated from the K values of *Factsage* are consistent with the ones given from literature [32]. The difference between the theoretical conversion from *AspenPlus* and from *Factsage* can be only attributed in their thermodynamic data. *Factsage* must have updated values of Gibbs free energy, different from those of *AspenPlus*. Therefore all of the following calculations and modelling are based on the K constants from *Factsage*.

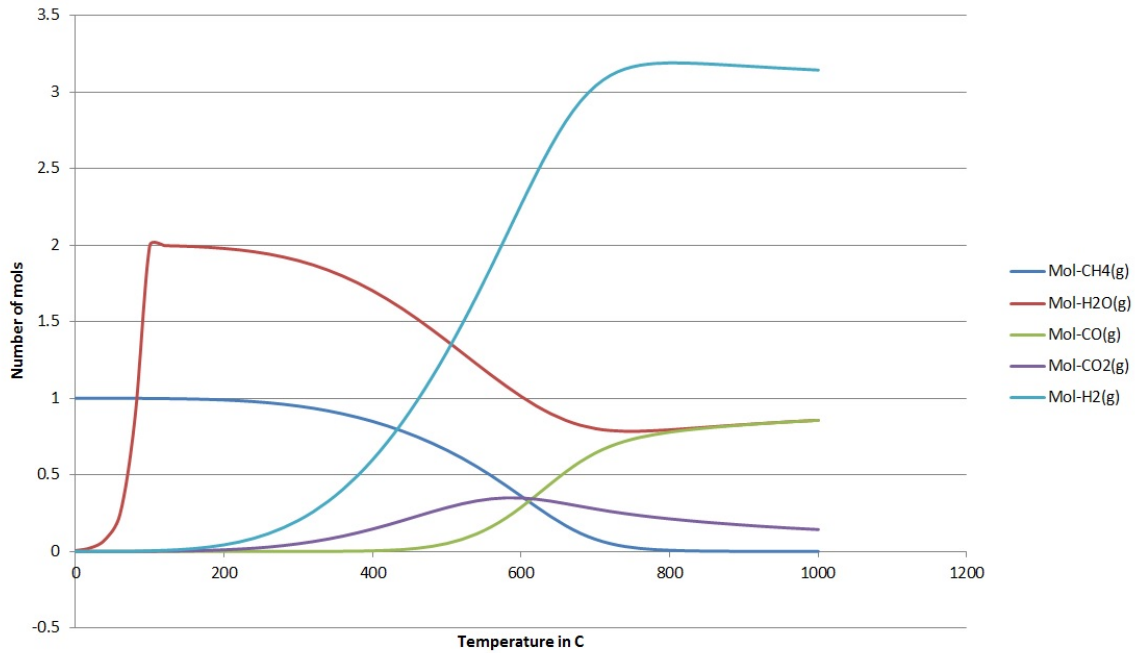


Figure 4.6: Gas composition in mols as a function of temperature

With the purpose of having an indication of the temperature range where carbon monoxide appears in the balance of compounds a sensitivity analysis was performed. An inlet of 1 mol CO_2 and 4 mol of H_2 was given in *Factsage* and the progression of mols was recorded for a range of temperatures. The results can be seen in figure 4.6.

It can be noticed that CO appears for temperatures well above the range applied in the experiments. Hence, it will be neglected in all the calculations applied and it isn't expected to be formed during the experimental procedure.

Last but not most important is the influence of the vapor (produced by the reaction) in the conversion of the reactants. As it has been mentioned previously the goal of this research is to investigate (via the Le Chatelier's principle) the influence of vapor on the reaction. Specifically, by removing vapor in situ enhances the conversion rate of the reaction. The way to quantify this phenomenon is via partial pressure of vapor. So by reducing the partial pressure of vapor the consumption of CO_2 and H_2 rises together with the production of CH_4 . The equation demonstrating this is the following.

$$K = \frac{x \left(\frac{P_{H_2O}}{P_{tot}} \right)^2 (5 - 4x)^4}{(1 - x)(4 - 4x)^4 \left(1 - \frac{P_{H_2O}}{P_{tot}} \right)^4} \left(\frac{P_{tot}}{P_{ref}} \right)^{-2} \quad (4.3)$$

It is the equation of the chemical equilibrium constant modified for the partial pressure of vapor. The derivation of this relation can be seen in chapter A.4 of the Appendix.

A sensitivity analysis is performed using equation 4.3. By inserting the values of K as taken from *Factsage* for different temperatures and for different partial pressures of water the conversion rates of H_2 are plotted (the overall pressure of the reaction is held at 1bar). The Matlab code for the following (fig 4.7) is enclosed in chapter A.5 of the Appendix.

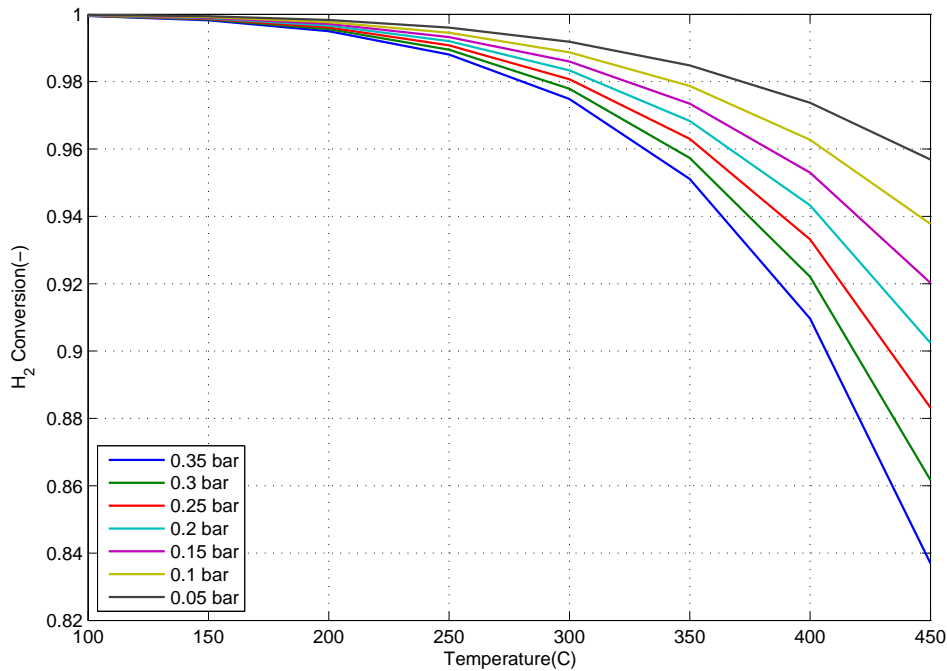


Figure 4.7: Influence of P_{H_2O} in conversion of H_2

It can be seen, from figure 4.7, that if the partial pressure of vapor is reduced enough, close to 100% conversion of the reactants can be achieved. Without having to increase the overall pressure more than the atmospheric. Hence, keeping the costs of the process down.

Based on the Natural Gas Grid specifications of Netherlands [9] the maximum acceptable content of CO_2 and H_2 in natural gas for commercial use is $3\%mol$ and $0,03\%mol$, respectively. So the limiting compound in this case is the Hydrogen content.

For 99,7% conversion of H_2 the partial pressure of water at $260^\circ C$ and $280^\circ C$ is around $0,055bar$ and $0,045bar$ respectively. Based on equation 4.3.

4.3. Thermodynamics of Sorption

After modelling the thermodynamics of the reaction and setting the goal for the desired conversion rates of H_2 , we continue with the thermodynamics of the sorption part of the process.

The link between the main two phenomena that occur inside the reactor (catalysis and adsorption of vapor on the zeolites) is the partial pressure of vapor. Zeolites adsorb vapor inside their large internal surface area, thus reducing the partial pressure of vapor on the reactor and on the catalytic sites of Ni/Al_2O_3 particles and drive the reaction to the right side (of the products).

Physisorption, in contrast to chemisorption, is a dynamic process. In chemical adsorption for a specific temperature and pressure, sorption of H_2O is a steady state process with a certain equilibrium constant (similar to a chemical reaction). In physical adsorption, keeping the temperature constant the partial pressure of the vapor increases as the capacity of the adsorbent reduces. Moreover the capacity of zeolites to water depends on temperature.

At elevated temperatures the available capacity reduces, until zeolites lose their ability to adsorb water above a maximum value of temperature. The reason behind this is that physisorption is constituted by Van de Waals forces, as it was mentioned in chapter 2.3. Van de Waals forces change constantly for different temperatures, pressure and water content inside the zeolites.

The way to link in this case the partial pressure of water with temperature is through a Van't Hoff relation [35].

$$\ln\left(\frac{P_{H_2O}}{P_{tot}}\right) = -\frac{\Delta H}{R} * \frac{1}{T} + \frac{\Delta S}{R} \quad (4.4)$$

On the left side of the relation (eq. 4.4) is the partial pressure of vapor. In a Van't Hoff equation normally inside the natural logarithm is the equilibrium constant. But because in this case occurs only the adsorption of vapor, the equilibrium constant is equal to the partial pressure of vapor (eq. 4.5). Equation 4.5 refers to an ideal gas behavior of water vapor. If non ideal behavior was considered then the pressure must be exchanged with activities, making the calculation of K_{eq} more intriguing.

It should be mentioned that the adsorption of CO_2 on the zeolites is neglected. The reason is that the competitive adsorption of CO_2 and water vapor on zeolites leans completely towards the latter. The zeolite is fully capacitated with water before adsorbing any CO_2 . This is been research with zeolite 13X in Joos et al. [36].

$$K = \frac{P_{H_2O}}{P_{tot}} \quad (4.5)$$

The right hand side of equation 4.4 includes the enthalpy and entropy change together with temperature. The term of entropy can be considered constant since entropy is linked to the nature of water. But the change of enthalpy isn't constant. The heat of adsorption (which is represented by the enthalpy difference) changes with a variation of the capacity of zeolites. Thus, linear relations of constant capacity can be formed between $\ln\left(\frac{P_{H_2O}}{P_{tot}}\right)$ and $\frac{1}{T}$. These lines are called isosteres and are used to predict the temperature or pressure for different capacities of the zeolites.

In order to obtain these isosteres, experiments should be performed for each type of different zeolites. The reason is that there are limited to none data regarding the capacity of zeolites for the elevated temperature range that this research is focused upon. Only a few data were obtained by prior research and are included the in graphs presented in the current section.

Zeolite 3A

For the case of zeolite 3A data from two different sources were used. One academic research of Gabrus et al [31]. and one product report of a molecular sieve manufacturer and distributor (Grace 2010 [24]). The isosteres plotted from those data are enclosed in the figures 4.8 and 4.9.

In the first graph (figure 4.8) the isosteres of 1% and close to 0% calculated based on data extrapolated from the isosteres of higher capacity.

The dotted vertical lines in both graphs replicate the operational lines of the present process. Explicitly, they are the range of acceptable partial pressures of vapor (values for

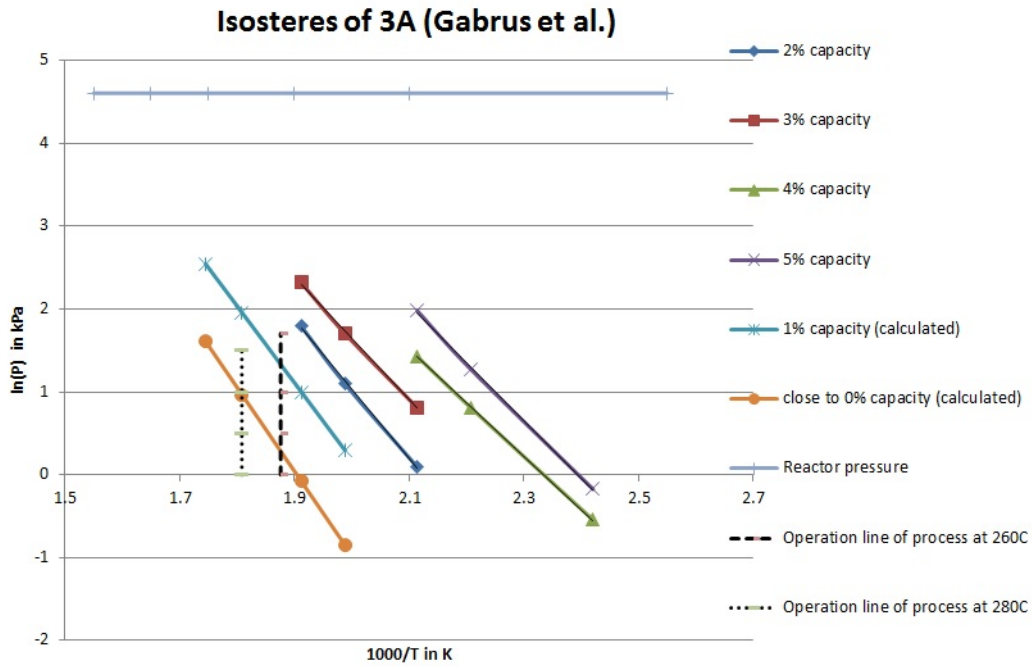


Figure 4.8: Isosteres of 3A and operational lines of the present process

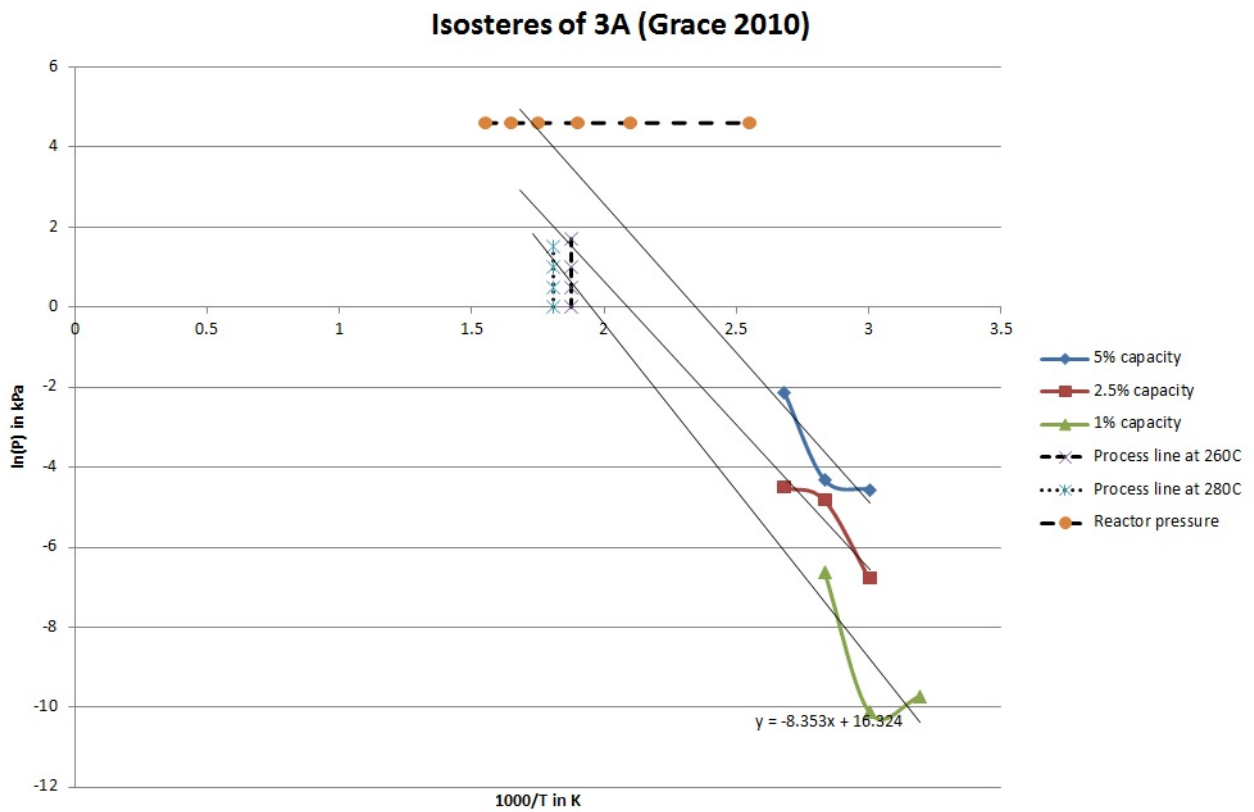


Figure 4.9: Isosteres of 3A and operational lines of the present process

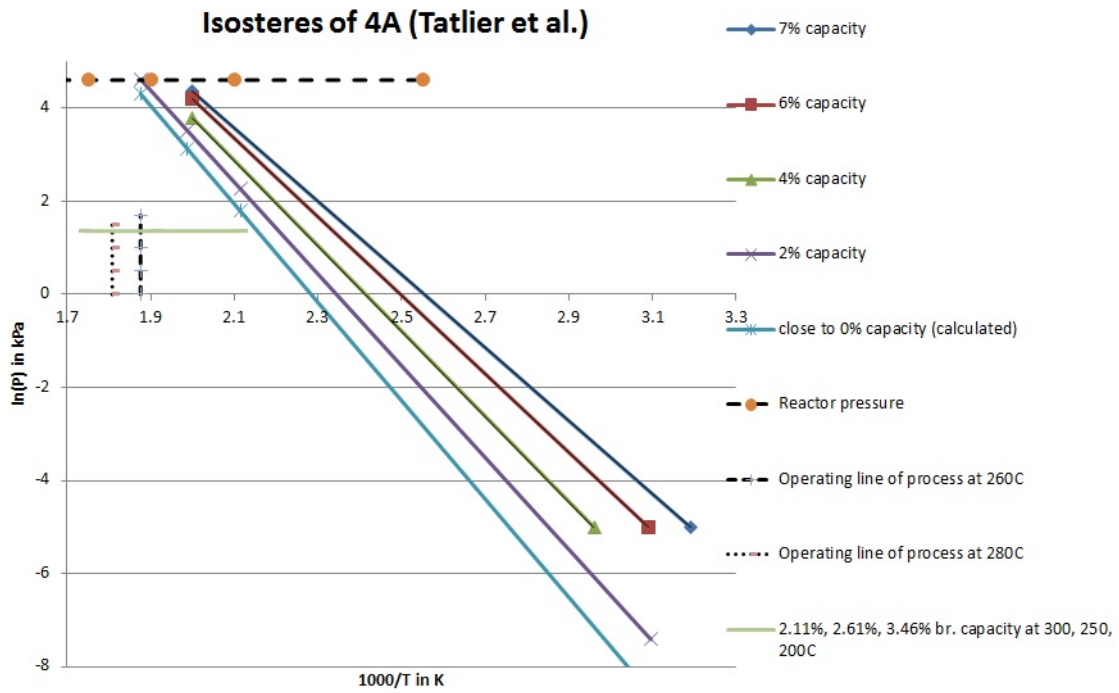


Figure 4.10: Isosteres of 4A and operational lines of the present process

which the hydrogen content in the outlet will be less than $0,03\%mol$. Their upper limit is $\ln(P_{H_2O}) = 1,70475$ (in kPa) for $260^\circ C$ and $\ln(P_{H_2O}) = 1,50408$ (in kPa) for $280^\circ C$. Those are the $0,055bar$ and $0,045bar$ limits calculated in the previous chapter. Thus, the experimental process should initiate when the zeolites are fully dehydrated and stop when the capacity, that corresponds to the acceptable limits of partial pressure of vapor, is reached.

The data from those two sources can be considered relatively consistent with each other and prove that the process can be theoretically viable (with zeolite 3A) in the temperature range that this research is focused on.

Zeolite 4A

Next follow the isosteres of zeolite 4A. Plotted from data extracted from two sources. An academic research on the use of zeolites on heat pumps (Tatlier et al. [48]) and the same report (as in zeolites 3A) of the manufacturer of molecular sieves (Grace 2010 [24]).

The horizontal straight line in both cases (figures 4.10 and 4.11) refers to the experiments performed by Walspurger et al. Specifically for a constant pressure of $0,039bar$ (below the upper operating limits of the present work) the capacity of zeolite 4A was measured, at $200^\circ C$, $250^\circ C$ and $300^\circ C$. In all three cases the capacity was well above 2% of g_{H_2O}/g_{4A} . Unfortunately the data of Tatlier et al. contradict with that and demonstrate no capacity at all at $260^\circ C$ and $280^\circ C$. On the other hand the data from Grace 2010 go along with the capacities as measured by Walspurger but the isosteres exhibit a wrong pattern. All three isosteres diverge from each other (as the temperature increases) whilst they should converge in order to be consistent with the theory [35].

Despite the fact that the data from literature in the case of zeolite 4A are conflicted, they provide an indication of the capacity of 4A at the desired temperature range. The process should be viable in the case of zeolite 4A as in the case of 3A.

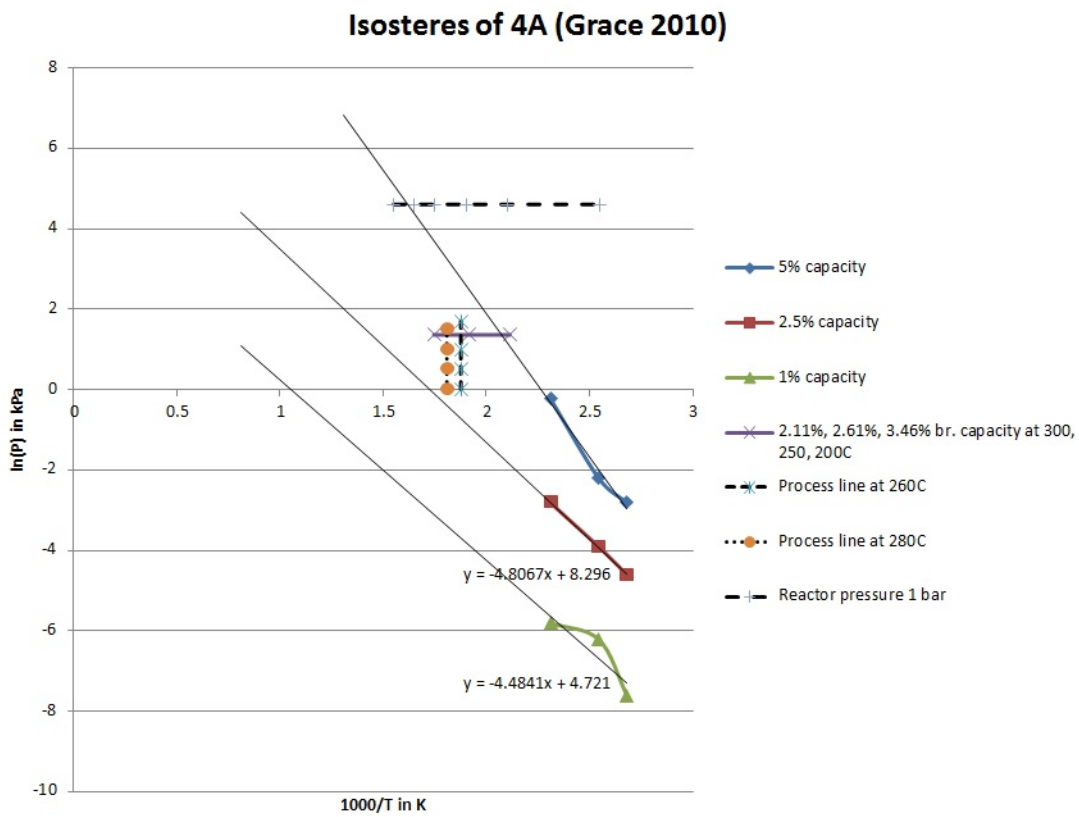


Figure 4.11: Isotherms of 4A and operational lines of the present process

5

Results of experiments

This chapter presents the experimental results along with their interpretation. Firstly, the series of experiments with the combination $Ni/Al_2O_3 - Al_2O_3$ were performed to determine the activity of the present catalyst for a range of temperatures at atmospheric pressure. Subsequently, the experiments with the combination $Ni-Al/Z$ eolites followed. Initially, the pair $Ni/Al_2O_3 - 3A$ was tested, followed by $Ni - Al/4A$. Lastly, the two combinations of grained Ni/Al_2O_3 (2,5mm and 1mm average sizes) paired with zeolite 4A were tested.

Before introducing the results of the experimental work it should be mentioned that those focus on the conversion rates of CO_2 and H_2 . Selectivity towards methane is not presented since it is in every case 100%. The only possible by-products from this process would be carbon monoxide and formation of solid carbon on the catalyst. Regarding carbon deposition it occurs in temperatures above $600^\circ C$ [21] and it wasn't formed, also, in similar experimental studies with the same temperature range applied [51], [15]. Regarding CO , as it can be seen in chapter 4.2.2 (figure 4.6), it is favored thermodynamically above $400^\circ C$ and none of the GC measurements detected CO .

In order to verify that methane is the only compound formed from this process (together with H_2O), the fraction yield of CH_4 was calculated (actual yield/theoretical yield). The graphs of yield of methane can be seen in Appendix A.7. Those graphs match the conversion rates of H_2 as calculated for the same experiments. Meaning that CH_4 is the only compound formed from CO_2 .

5.1. Experiments with $Ni/Al_2O_3 - Al_2O_3$

The first series of experiments was performed with the pair of $Ni/Al_2O_3 - Al_2O_3$. As it has been mentioned previously the goal was to determine the activity of the catalytic pellets provided by "C&CS-catalysts & chemical specialties", in the same conditions that the pair catalyst/zeolites would be tested. Thus, the Ni/Al_2O_3 spherical pellets were diluted with Al_2O_3 balls to form the final bed. This bed was tested at the temperature range of $200 - 380^\circ C$ with increments of approximately $20^\circ C$. The results can be seen in figures 5.1 and 5.2 for the conversion of CO_2 and H_2 , respectively.

Uncertainties of results

As it has been stated in *Chapter 3* the temperature inside the reactor cannot be regulated with high precision and the readings of the thermocouples vary constantly in a range of 4 –

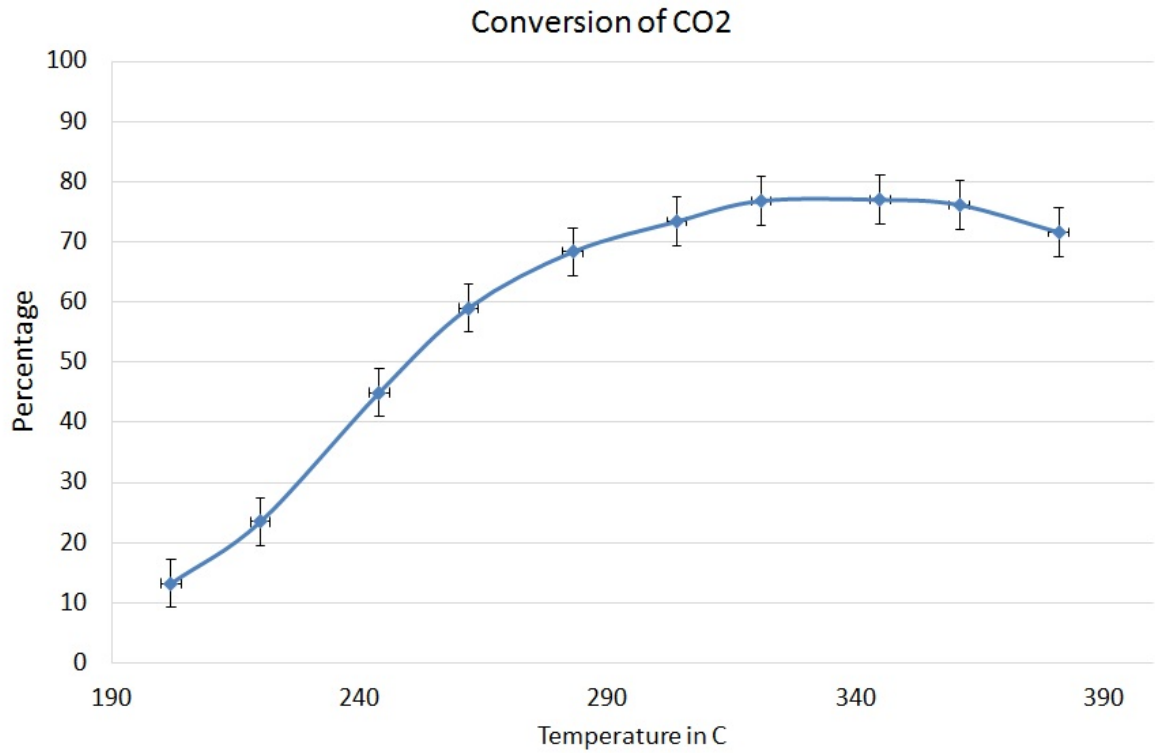


Figure 5.1: Conversion of CO₂, Ni/Al₂O₃ – Al₂O₃ (temperature range 200 – 380°C), (GHSV=6000, table 3.4)

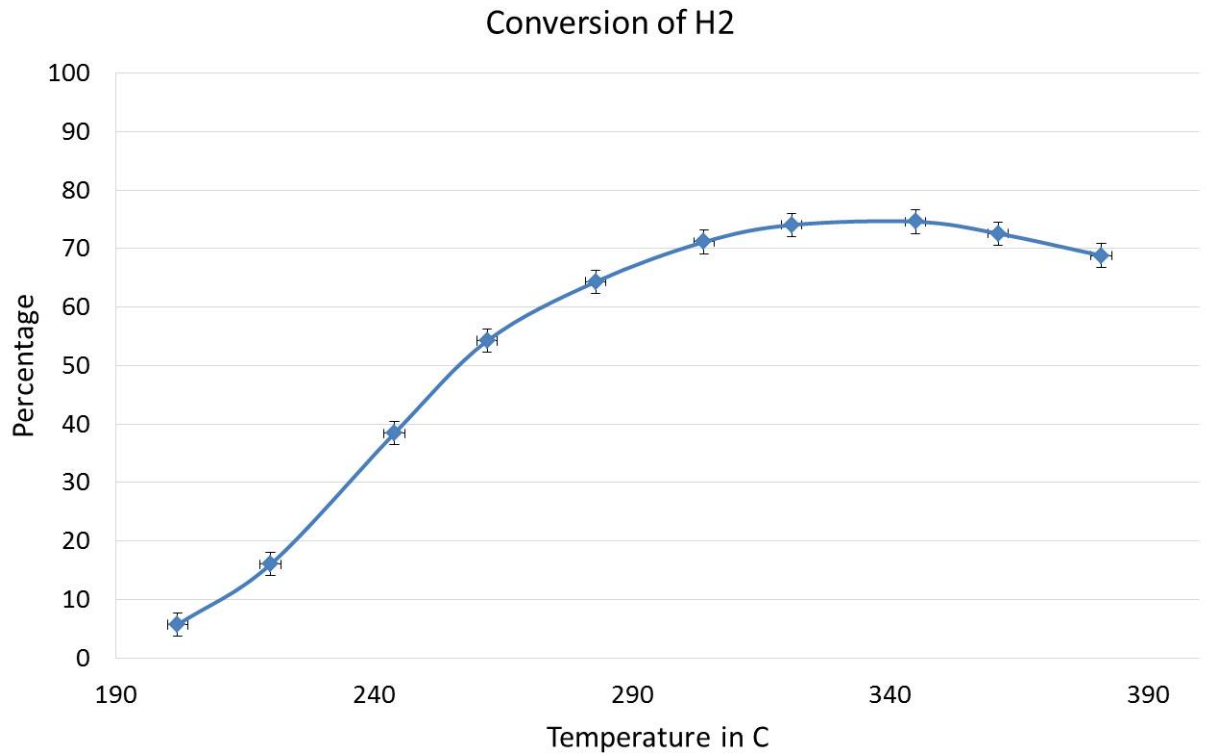


Figure 5.2: Conversion of H₂, Ni/Al₂O₃ – Al₂O₃ (temperature range 200 – 380°C), (GHSV=6000, table 3.4)

5°C. Hence, the horizontal uncertainty in the figures, which is 2%. The vertical uncertainty of the figures is 4% in the case of CO_2 and 2% in the case of H_2 . The first one has a higher uncertainty than the latter. The reasons are twofold. One is the fact that CO_2 is soluble in water and it can be absorbed in the condensed vapor inside the second vessel. Due to that solubility factor, the conversion rate can increase up to 0,5%. The second reason is the relatively big deviation of the readings of CO_2 (taken from the GC), from the average value of experiment. This difference can be up to 1% of the conversion rate. The rest 2% (of the vertical error bar) for both hydrogen and carbon dioxide is the uncertainties from the overall equipments of the set up.

Moving on with results of those experiments. The maximum conversion of the reactants is at 344°C. For CO_2 is 77% and for H_2 is 74,6%. At 321°C the conversion is 76,8% and 74% respectively. The pattern followed by the conversion rates with temperature is the expected one and the conversion rates are similar to those of other studies (with similar Ni/Al_2O_3 catalysts)[51], [33], [42]. The conversion rates of carbon dioxide and hydrogen should match precisely, since they flow inside the reactor in stoichiometry. But, they diverge due to the uncertainties analyzed above.

5.2. Experiments with Ni/Al_2O_3 -zeolite 3A

The next series of experiments were performed with the combination of catalyst-zeolite 3A. Two different GHSV were applied on this bed and the results are presented in the following sections.

5.2.1. 6000 GHSV

The first experiments were performed with the same flows (GHSV of 6000) applied in the combination $Ni/Al_2O_3 - Al_2O_3$. The temperature range was again 200 – 360°C, with increments of 20%. The temperature of 380°C was rejected, because it was too high to observe any influence of zeolites in the reaction. The purpose was to discover the range of temperatures at which zeolite 3A influences positively the conversion. The exact experimental temperatures may differ by a few degrees Celsius (up to 4°C) compared to the ones of the experiments with catalyst/alumina. The reason is the difficulty in regulating with precision the temperature inside the reactor. Nevertheless, the comparison between the two experiments provides a solid indication of the enhancement the sorption of vapor has on the catalysis. This comparison is depicted in figure 5.5. Figures 5.3 and 5.4 include the conversion of CO_2 and H_2 respectively.

One can clearly see an increase in the conversion rates at the range of 200–300°C. Those conversion values and their differences are enclosed in table 5.1. The 1% uncertainty in the column with the differences is added due to the small variation between the temperatures of two series of experiments.

One more experiment was performed with this combination of Ni/Al_2O_3 -Zeolite 3A and the same GHSV of 6000. The flow composition of reactants was kept constant but the composition of N_2 was reduced and CH_4 was added instead. The flow's details can be seen in table 3.6 (chapter 3). The reason of this experiment was to detect the difference in conversion due to the addition of one of the products in the inlet. So in essence apply the reverse Le Chatelier's principle compared to the one this research aims for with the sorption

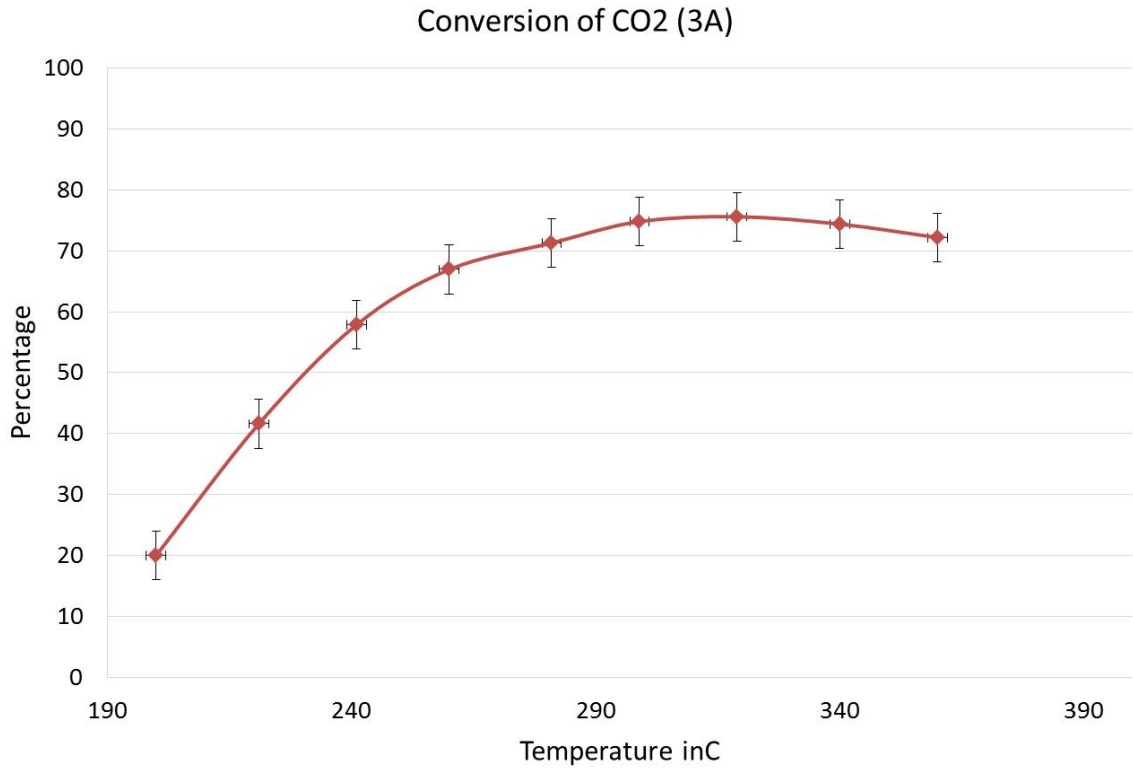


Figure 5.3: Conversion of CO₂, Ni/Al₂O₃ – 3A, (temperature range 200 – 360°C), (GHSV=6000, table 3.4)

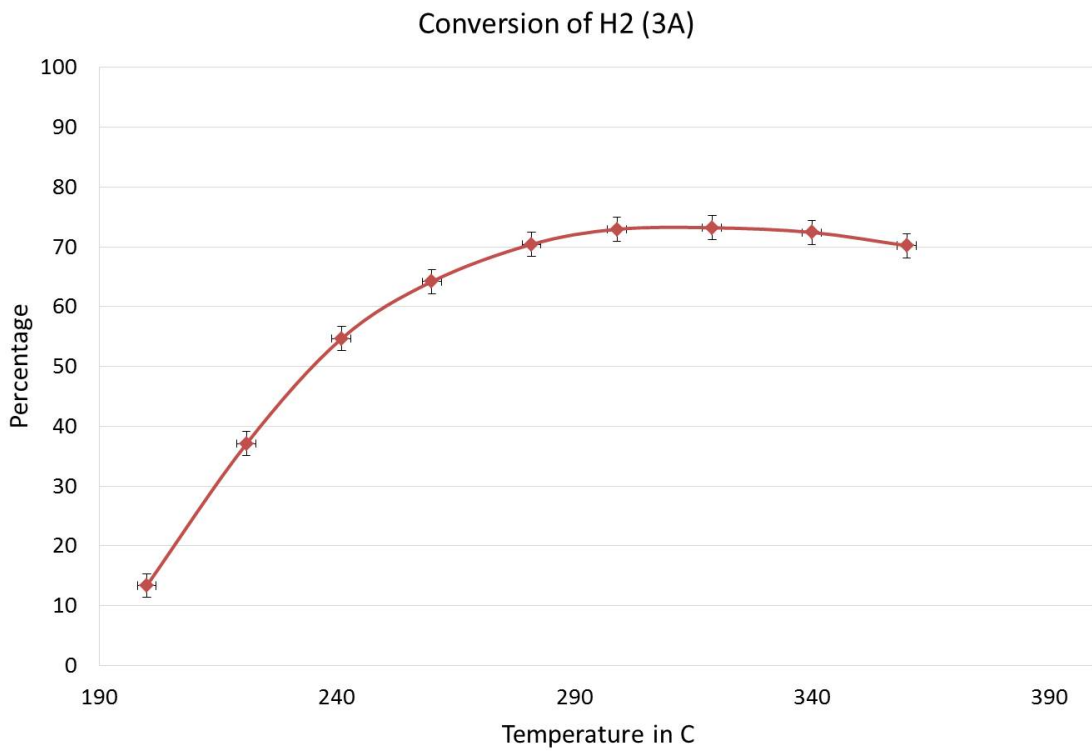


Figure 5.4: Conversion of H₂, Ni/Al₂O₃ – 3A, (temperature range 200 – 360°C), (GHSV=6000, table 3.4)

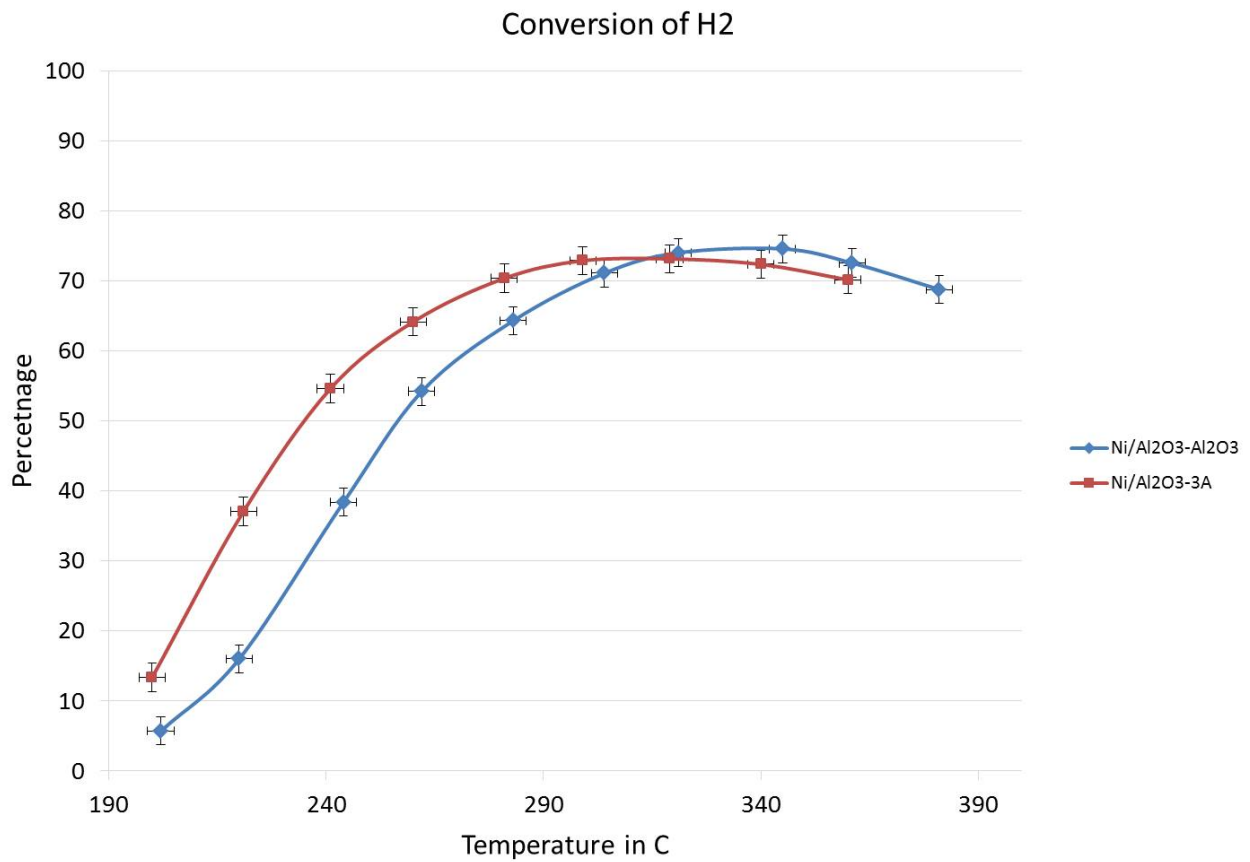


Figure 5.5: Conversion of H₂, comparison between pure Ni/Al_2O_3 and $Ni/Al_2O_3 - 3A$, (GHSV=6000, table 3.4)

Table 5.1: Corvesion of H₂ for experiments with catalyst-alumina and catalyst-zeolite 3A

Temperature (in C)	Conversion rates of H ₂ (in %)		
	$Ni/Al_2O_3 - Al_2O_3$	$Ni/Al_2O_3/3A$	Difference
200	5,72	13,18	+8 ±1
220	16,01	37,10	+21 ±1
240	38,42	54,66	+16 ±1
260	54,26	64,19	+10 ±1
280	64,35	70,41	+6 ±1
300	71,15	72,93	+2 ±1
320	74,06	73,19	-1 ±1
340	74,62	72,41	-2 ±1
360	72,60	70,19	-2 ±1

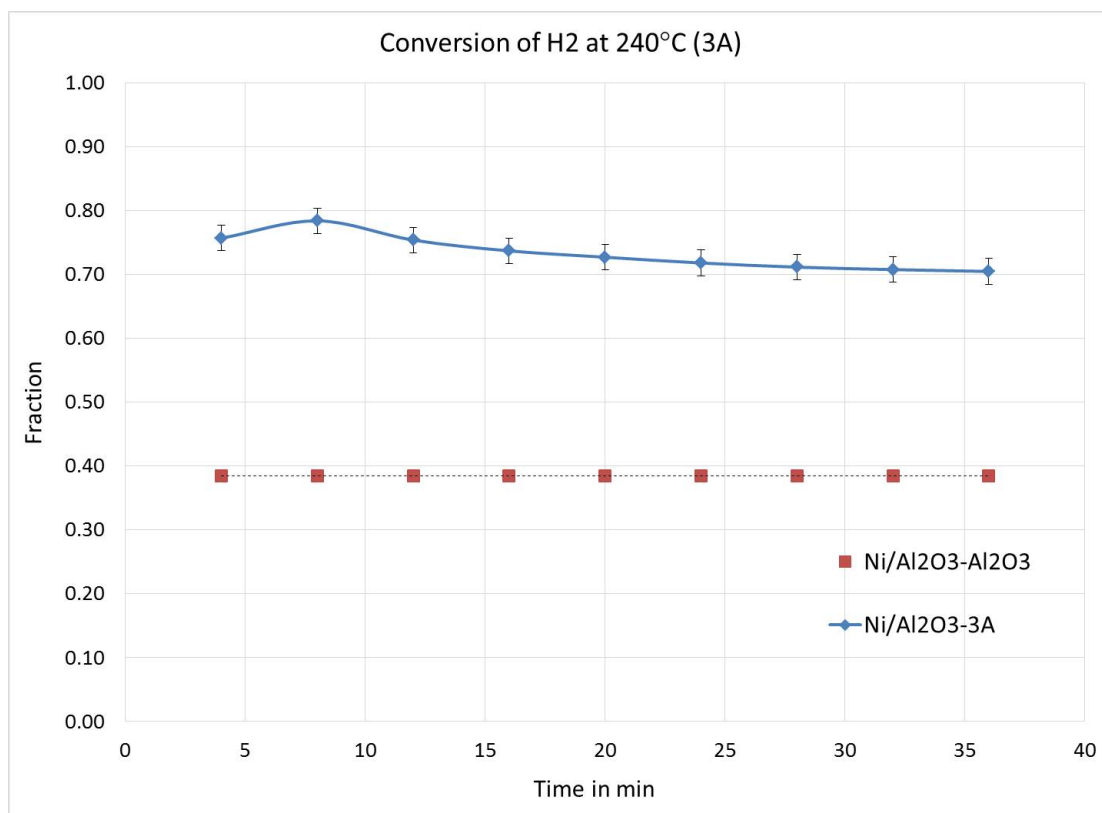


Figure 5.6: Conversion of H_2 , $Ni/Al_2O_3 - 3A$ (temperature $240^\circ C$), (GHSV=2400, table 3.7)

of water.

The experimental temperature was approximately $242^\circ C$ and the hydrogen conversion was 45%, whilst in the same experimental conditions with no methane as inlet the conversion of hydrogen was 54,7%. As it was expected by adding CH_4 the conversion of reactants reduces. In this case by 9%.

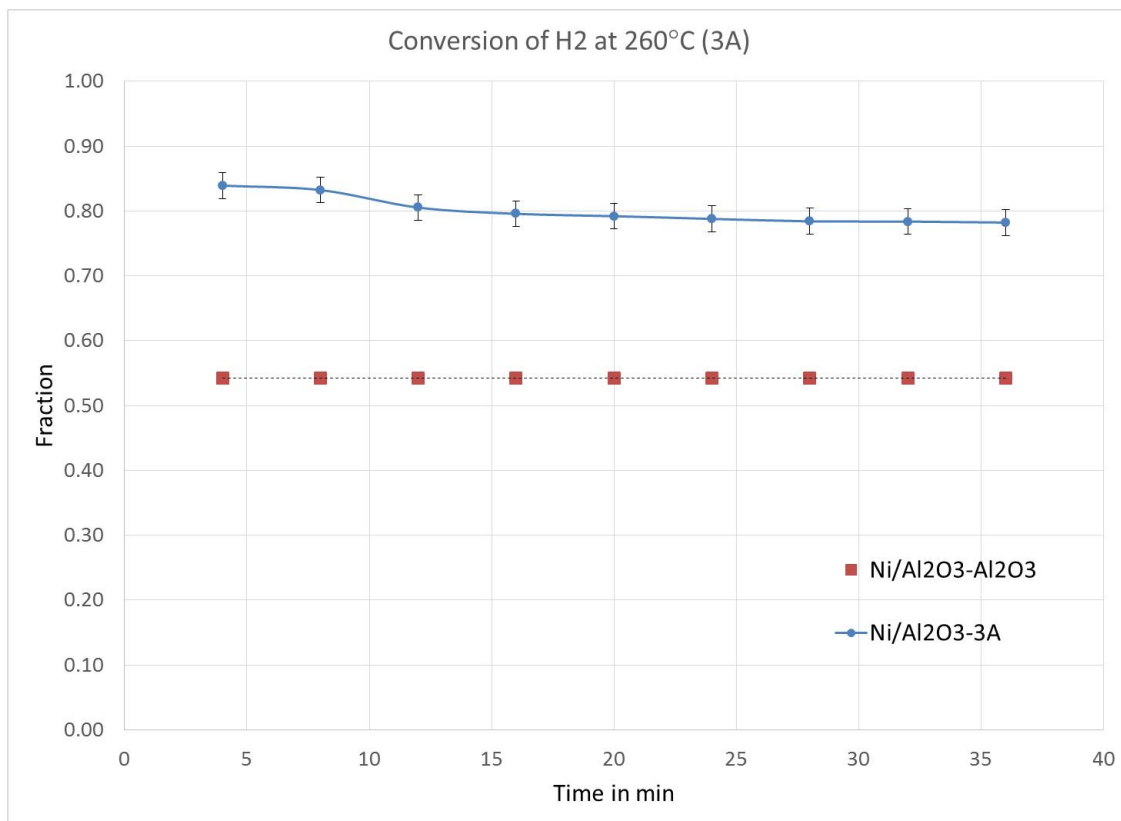
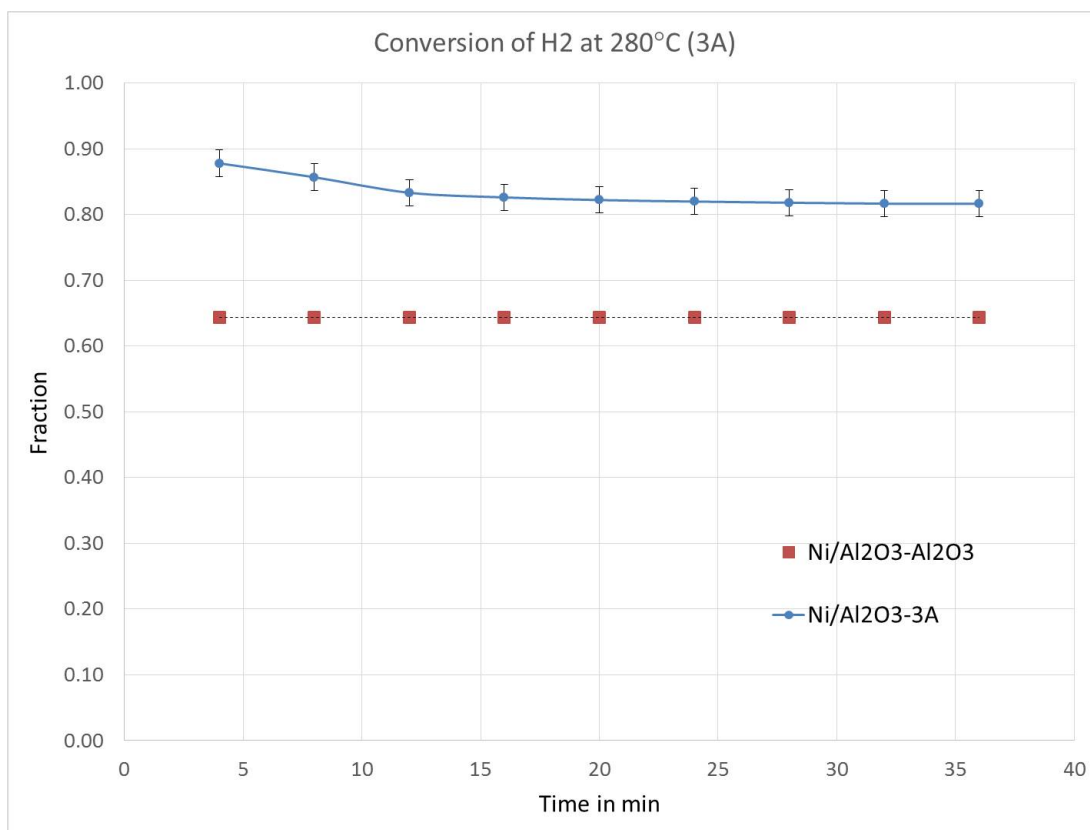
5.2.2. 2400 GHSV

The next experiments, with the combination of catalyst-zeolite, 3A were performed under lower volumetric flow rates than before. Specifically, a GHSV of 2400. That GHSV corresponds to the lower possible flows that the mass flow controllers can regulate, whilst keeping the composition of gases constant. By reducing the GHSV one can expect the conversion rates to rise. This results from the increase of the residence time (more time for the two phenomena to evolve) and from the reduced amount of vapor needed to be adsorbed by the zeolites. The details of this flow of gases can be seen in table 3.7.

Generally, thereafter all the remaining experiments are performed under the minimum GHSV of 2400.

Three experiments were performed at the temperatures of $241^\circ C$, $259^\circ C$ and 280° . The results can be seen in graphs 5.6, 5.7 and 5.8 respectively.

The graphs represent the progression of hydrogen's conversion with time. The experiment started at time zero and every 4 minutes GC was recording measurements (as explained in chapter 3). The first measurement at time zero is rejected because the GC's inlet is contaminated with gases from the previous measurements, thus it produces false results.

Figure 5.7: Conversion of H₂, Ni/Al₂O₃ – 3A (temperature 260°C),(GHSV=2400, table 3.7)Figure 5.8: Conversion of H₂, Ni/Al₂O₃ – 3A (temperature 280°C),(GHSV=2400, table 3.7)

The dotted line in every graph represents the conversion of hydrogen, at the same temperature, as calculated from the experiments with the combination $Ni/Al_2O_3 - Al_2O_3$. It is placed there as a visual indication of the enhancement of catalysis due to the sorption of vapor.

The maximum values for every experiment is 78,4%, 83,9% and 87,8% for the 241, 259 and 280°C respectively. From the graph of 241°C one can notice that the conversion initially rises until it reaches the maximum of conversion and subsequently it decreases gradually. The decrease can possibly be attributed in the reduce of the capacity of zeolite 3A, as the experiment proceeds. This increase in conversion would possibly be noticed also in the experiments with 259°C and 280°C, if the GC could provide measurements in smaller time increments or if the first measurement (time zero) was valid.

5.3. Experiments with Ni/Al_2O_3 -zeolite 4A

The experiments with catalyst and zeolite 3A where followed by the series of experiments with the combination catalyst/zeolite 4A (Ni/Al_2O_3-4A). Those experiments were divided into two groups. The ones with N_2, H_2 and CO_2 in the inlet stream of the reactor and the ones with N_2, H_2, CO_2 and CH_4 as an input to the reactor.

5.3.1. Experiments without CH_4 as an inlet gas

First group of experiments was the one without methane in the inlet mixture of gases. It was decided that the combination of catalyst-zeolite 4A should be tested in the same temperatures as the pair catalyst/3A, to record its optimum operational range. Thus, four experiments were performed at the temperatures of 239, 261, 279 and 300°C (GHSV of 2400, table 3.7). The results are plotted in figures 5.9, 5.10, 5.11 and 5.12 respectively. As before, each graph encloses the conversion rate of the pure Nickel catalyst at the same temperature. Those are the dotted line in each graph.

In the case of the combination $Ni/Al_2O_3 - 4A$ a steeper pattern can be noticed compared to the same graphs of $Ni/Al_2O_3 - 3A$. Specifically, a longer and steeper delay is noticed until the conversion rate reaches it's maximum value. In the graphs of 3A the maximum is reached at the second measurements, in the graphs of 4A the maximum is achieved at the third measurement. Also, one can notice that the first value of conversion for each temperature (with 4A) corresponds to the conversion rate calculated from the experiments with $Ni/Al_2O_3 - Al_2O_3$. For example, at 240°C the conversion with $Ni/Al_2O_3 - 4A$ is 35,7% and with $Ni/Al_2O_3 - Al_2O_3$ is 38,4%. At 260°C is 54,6% and 54,2% respectively. This can be interpreted as a delay in the initiation of vapor adsorption on 4A or, as a slower rate of water adsorption by 4A compared to 3A. Although in the literature no apparent difference (regarding adsorption rates) could be found between zeolites 3A and 4A.

After the maximum value of conversion in the graphs, the slope of reduction is also significantly bigger compared to the slope in the pair $Ni/Al_2O_3 - 3A$. The main reason behind this steeper reduction of conversion (in time) is the smaller available capacity of zeolite 4A compared to zeolite 3A. But, as it can be seen in chapter 4.3 there is no apparent difference in the capacity of the two zeolites at those temperature ranges. One can only attribute this difference in the regeneration process. The temperature for the case of zeolite 4A wasn't high enough to be fully regenerated. Verifying in this the way the founding of study ([31]) (mentioned in chapter 3.3.2), that zeolite 4A needs higher temperatures than

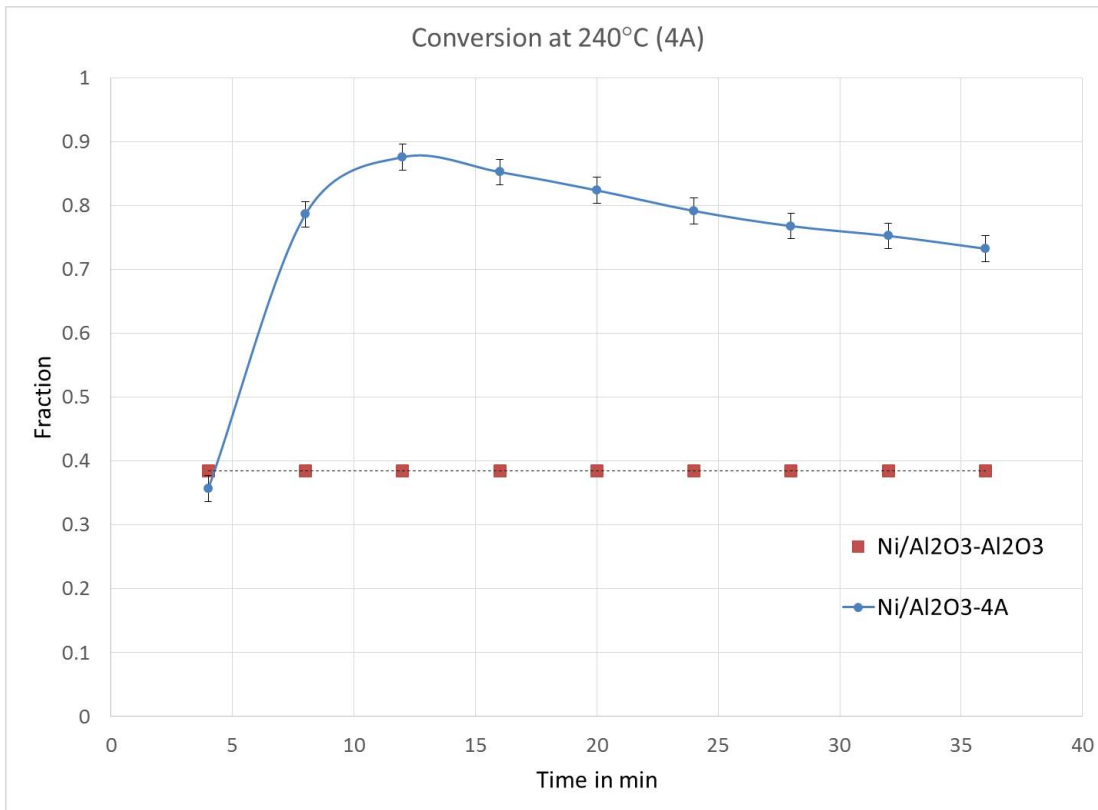


Figure 5.9: Conversion of H_2 , $Ni/Al_2O_3 - 4A$ (temperature 240°C), (GHSV=2400, table 3.7)

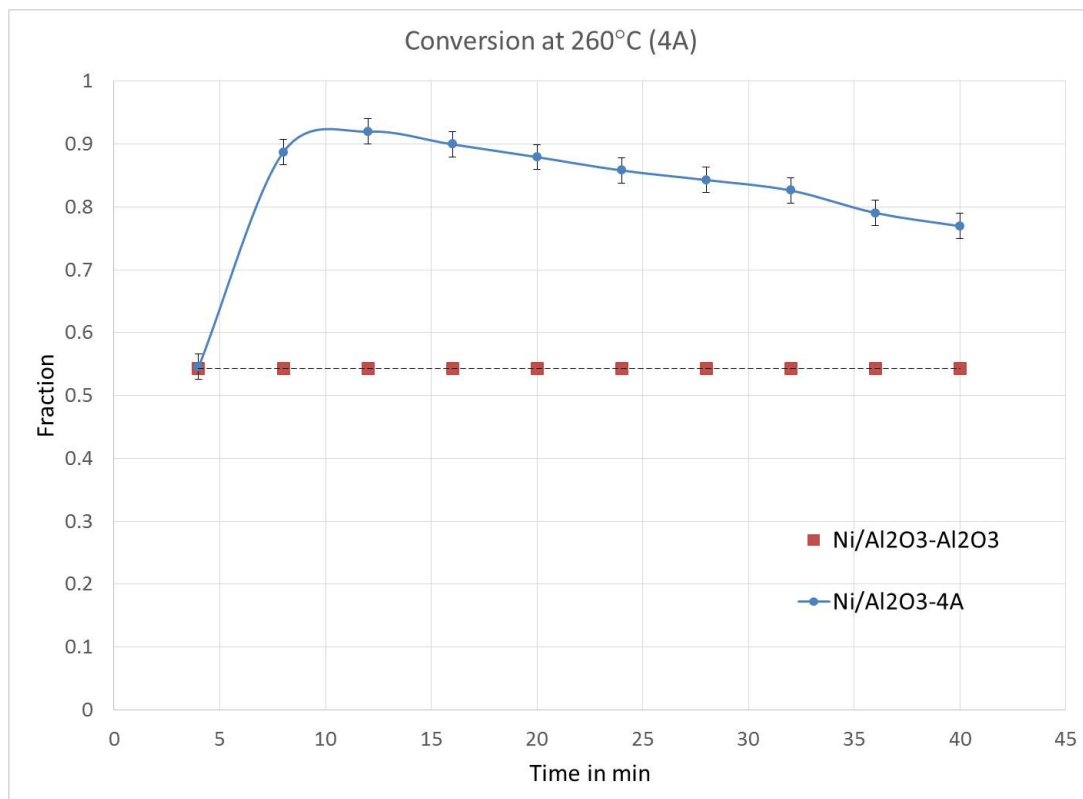


Figure 5.10: Conversion of H_2 , $Ni/Al_2O_3 - 4A$ (temperature 260°C), (GHSV=2400, table 3.7)

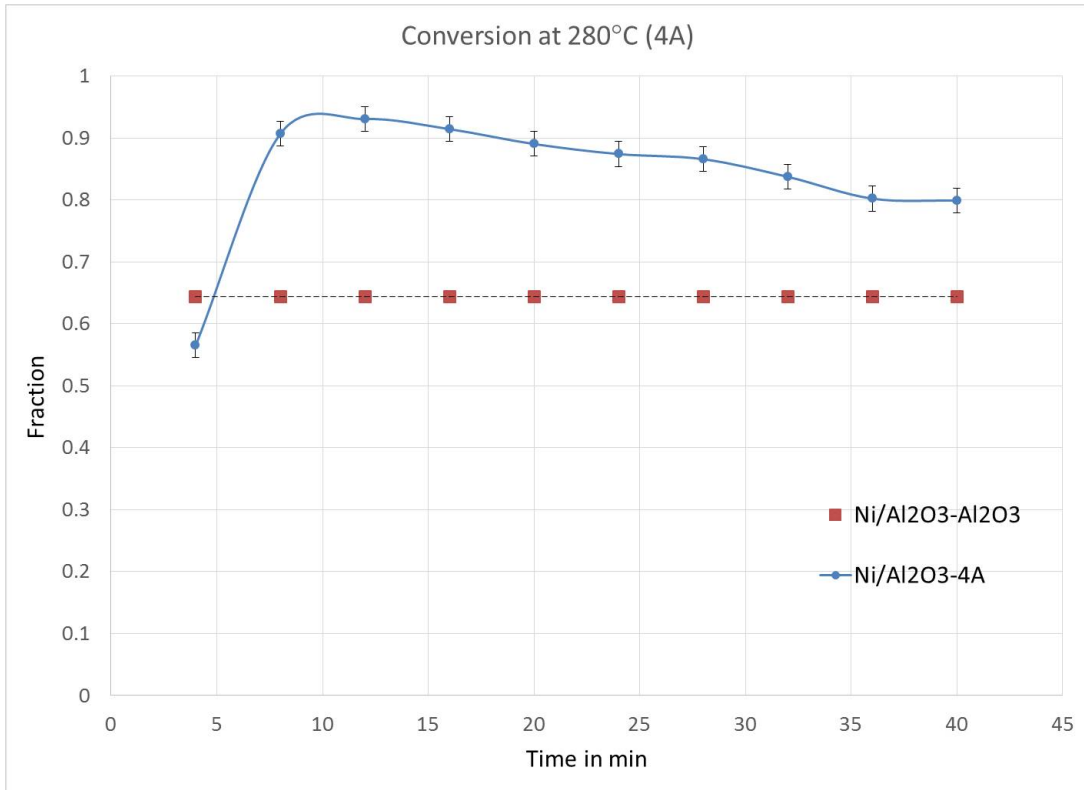


Figure 5.11: Conversion of H_2 , $Ni/Al_2O_3 - 4A$ (temperature 280°C), (GHSV=2400, table 3.7)

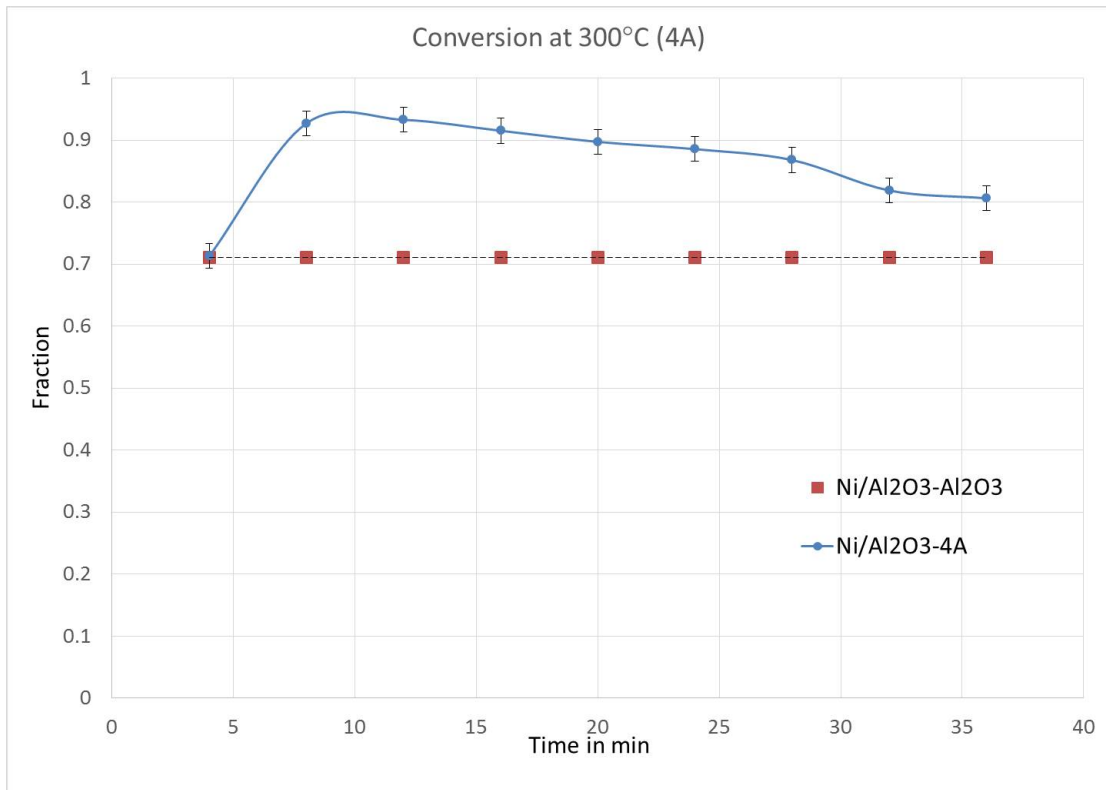


Figure 5.12: Conversion of H_2 , $Ni/Al_2O_3 - 4A$ (temperature 300°C), (GHSV=2400, able 3.7)

3A to be fully regenerated.

Nevertheless, the conversion (in the case of 4A) gets to much higher values. Those are 87,6%, 92%, 93,1% and 93% for 239, 261, 279 and 300°C, respectively.

The differences in maximum conversion between zeolites 3A and 4A are up to 9,2% in the case of around 240°C. This difference is unexpected, since both types of zeolites are hydrophilic and have recorded capacities of water of at least 2% in that temperature range (see chapter 4.3). Moreover zeolites 3A and 4A are both used in the industry for drying light hydrocarbons and more specifically natural gas [24], [2].

Thus, this difference can only be attributed to their particle sizes. Zeolite 4A is half in size (diameter of 1,6mm) compared to zeolite 3A (diameter of 3mm). By decreasing the size of the zeolites the proximity between the surface of the adsorbent and the catalytic sites increases (referred to this topic in chapter 3.3.2). Which means that larger surface of zeolites participate in the enhancement of the reaction. Hence, the higher conversion rates.

5.3.2. Experiments with CH₄ in the inlet stream

The pair of catalyst-zeolite 4A was also tested for its performance under the same GHSV of 2400 but with a product as inlet (CH_4). The experimental temperatures applied were 262°C and 281°C. The flows chosen can be seen in table 3.8. The results of the two experiments are depicted in figures 5.13 and 5.14.

Generally, from the experiments with the current combinations (of catalyst-zeolite 3A and catalyst-zeolite 4A) it has been found that the optimum operational range is 260 – 280°C, close to the experimental temperatures of similar studies [15], [51], [13].

The conversion rates for the two experiments exhibit exactly the same pattern as before but for lower values of conversion rates. The maximum conversion at 262°C and 281°C are 80,8% and 89,8% respectively.

5.4. Experiments with ground Ni/Al_2O_3 (2,5mm in size) and zeolite 4A

After realizing the importance and influence the particle's sizes have on the conversion rates of the reactants, it was decided to reduce the size of the Ni/Al_2O_3 pellets.

As it has been referred to in chapter 3.3.2, using a mortar the nickel/alumina particles are reduced to half their original size (on average 2,5mm). Those were paired with zeolite 4A to form the new catalytic bed. Zeolite 4A was chosen over zeolite 3A, due to its smaller diameter and subsequently the higher conversion rates it succeeded when combined with Ni/Al_2O_3 .

The experiments are again grouped in two parts. The ones without methane as inlet and the ones with methane in the inlet mixture of gases. Their results are presented in the following sections.

5.4.1. Experiments without CH₄ as an inlet gas

The experiments without CH_4 were performed first. The exact temperatures were 261°C and 280°C. The flows applied are enclosed in table 3.7. Figures 5.15 and 5.16 depict the progression of these experiments and enclose (as before) the conversion of the pure catalyst at the same temperatures.

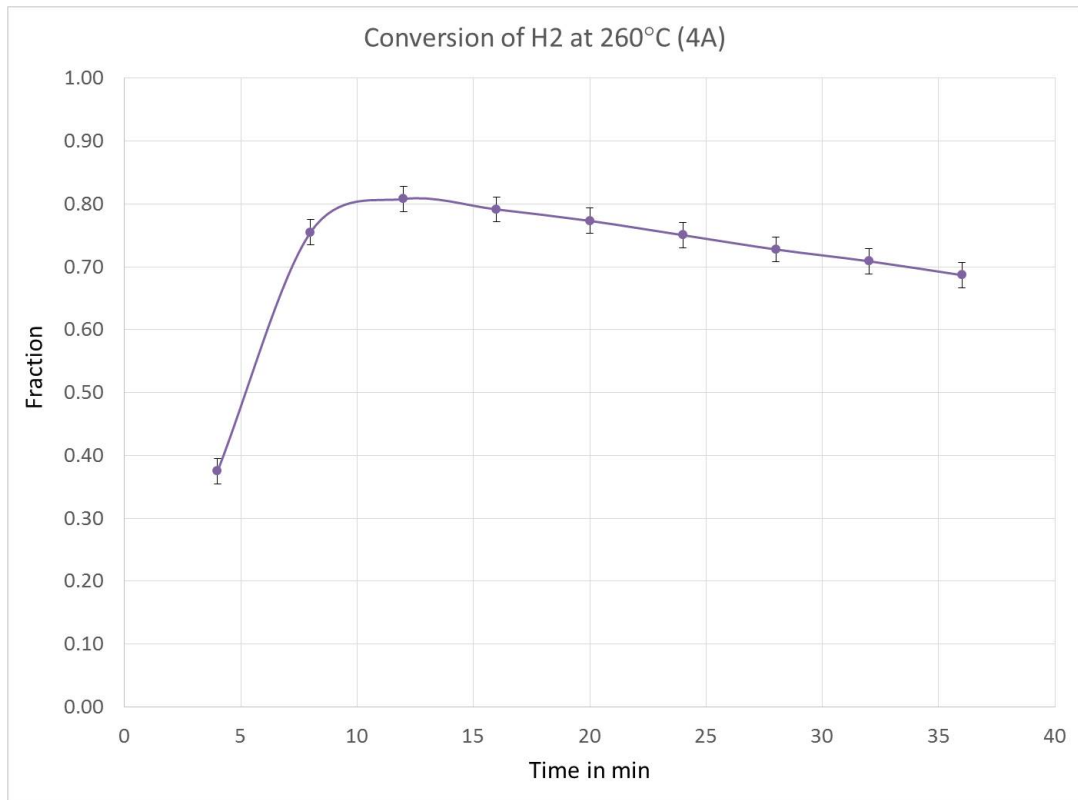


Figure 5.13: Conversion of H₂, Ni/Al₂O₃ – 4A (temperature 260°C and CH₄ in inlet),(GHSV=2400, table 3.8)

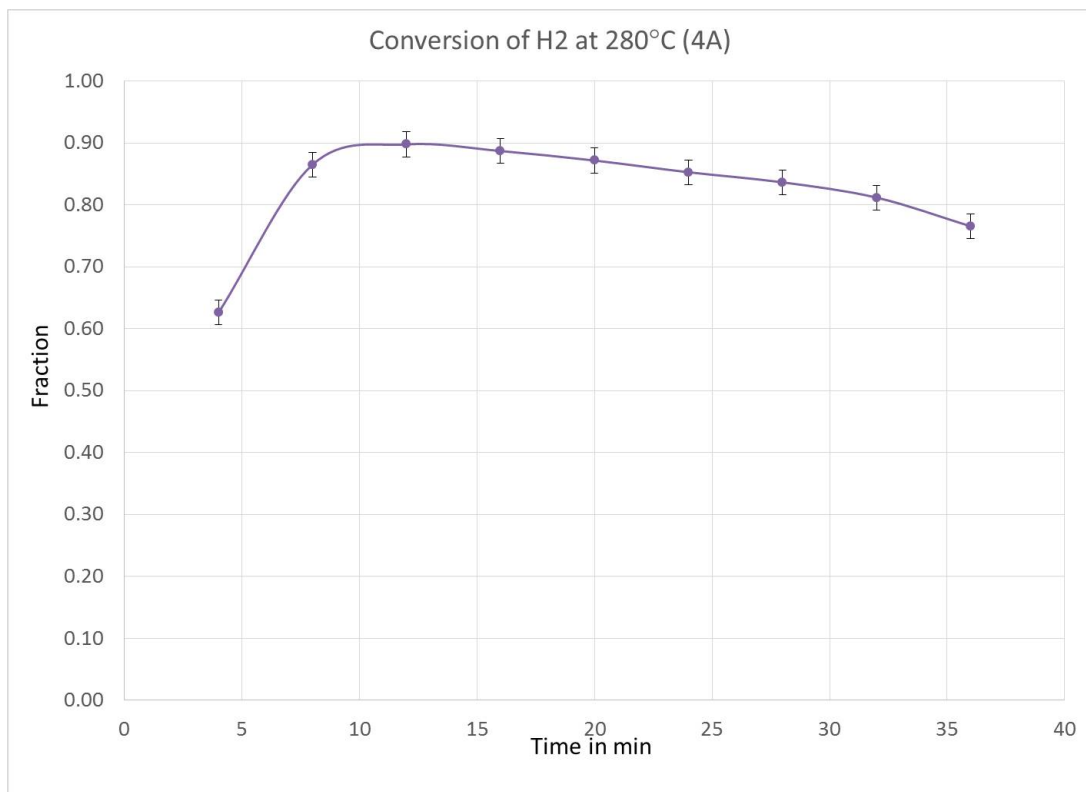
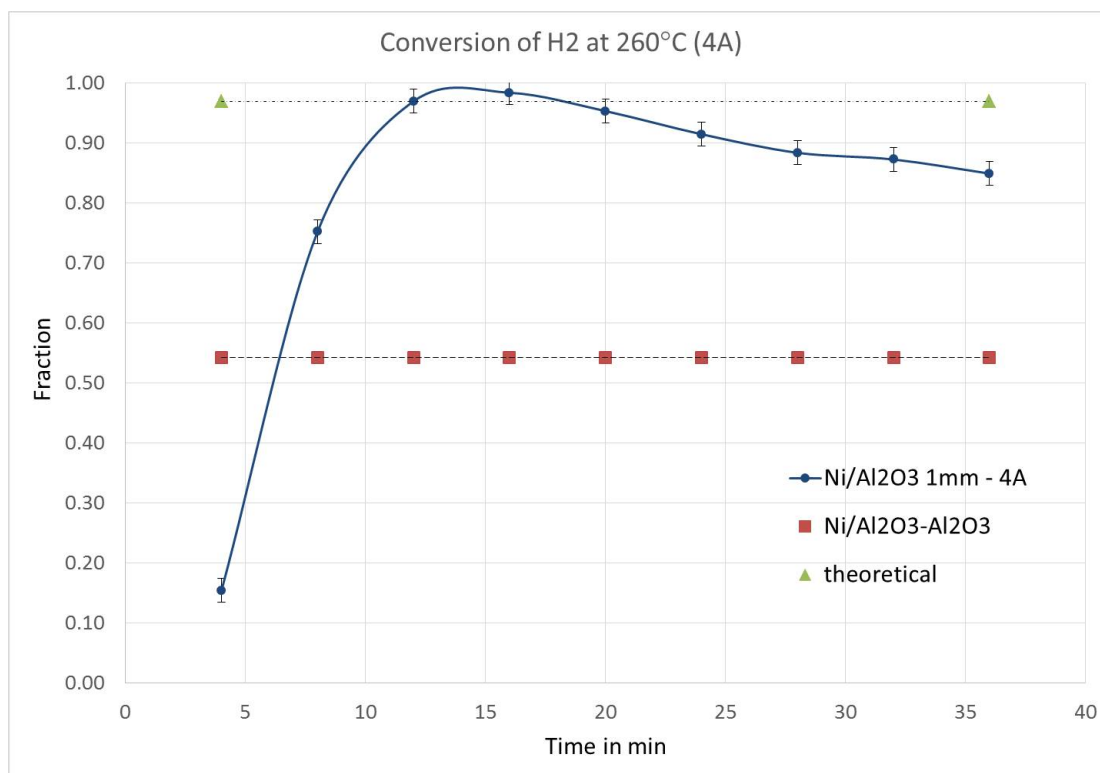
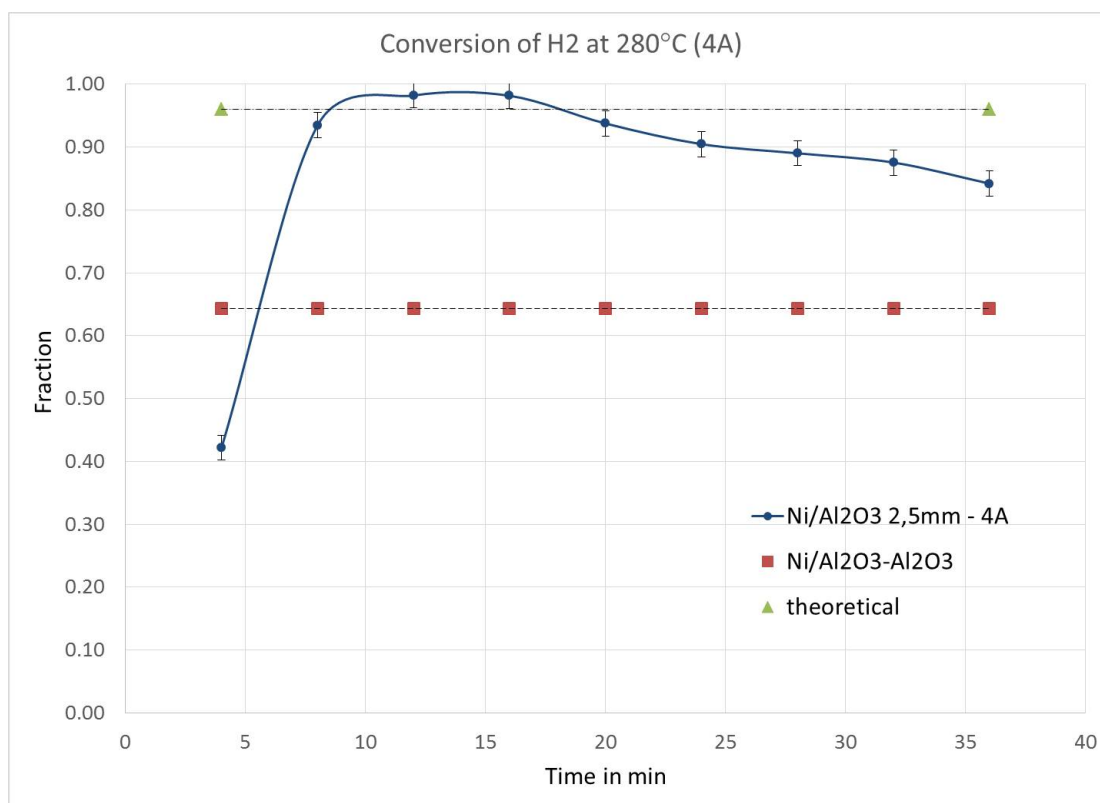


Figure 5.14: Conversion of H₂, Ni/Al₂O₃ – 4A (temperature 280°C and CH₄ in inlet),(GHSV=2400, table 3.8)

Figure 5.15: Conversion of H₂, Ni/Al₂O₃ 2,5mm – 4A (temperature 260°C),(GHSV=2400, table 3.7)Figure 5.16: Conversion of H₂, Ni/Al₂O₃ 2,5mm – 4A (temperature 280°C),(GHSV=2400, table 3.7)

Useful conclusions can be extracted from the experiments. First and foremost the high increase in the maximum conversion rates compared to the previous experiments (intact catalyst/zeolite 4A). The conversion of hydrogen reached values of 97% at 262°C and 98,2% (constant for two consecutive measurements of 8 mins) at 281°C. The reduction of the conversion rates after those maxima had a similar slope as the experiments with the combination intact catalyst-zeolite 4A.

The conversion predicted by thermodynamics (as calculated in chapter 4.2.2) at 260°C and at 280°C is 97% and 96%, respectively. Those values are depicted by the upper dotted lines in both figures 5.15, 5.16 Which means, that with the sorption enhancement one can reach and even break the barrier as set by thermodynamics. Also, this fact verifies the predictions made in chapter 4.2.2, for the influence of sorption of vapor, in the conversion of reactants.

Another difference (compared to the previous experiments with 4A) appeared in the initial part of the experiment, before reaching the maximum conversion. The slope is significantly steeper and the first recorded measurements correspond to lower conversion values than before. One interpretation of this phenomenon could be the reduced catalytic activity. After smashing the catalyst into smaller particles, it's catalytic activity is possibly reduced to lower values. Leaving the catalytic pellets intact was one of the contra-indications of the manufacturer (in order to maintain the optimum activity of the Ni/Al_2O_3 pellets). This can also be verified based on the justification used before. That the first measurements in figures 5.10 and 5.11 correspond to the conversion rates of the $Ni/Al_2O_3 - Al_2O_3$ combination. Subsequently, the first measurements in those graphs (fig. 5.15, 5.16) could correspond to the activity of the smashed nickel catalyst. Another reason could be that the nickel particles were covered with impurities like dust.

Moving on with the comparison of the maximum conversion rates between the experiments with 2,5mm $Ni/Al_2O_3 - 4A$ and with intact $Ni/Al_2O_3 - 4A$. The difference of those values can be seen in figure 5.17.

Only by reducing the catalyst from 5mm to 2,5mm the conversion increases by 6% in one case and 5% in the other. This linear correlation can be used as a rough approximation and show that below 1,5 – 2mm 100% conversion could possibly be achieved.

5.4.2. Experiments with CH₄ in the inlet stream

The experiments with methane as inlet followed. The flow rates applied are enclosed in table 3.8 and the experimental temperatures were 262°C and 281°C. The results are plotted in figures 5.18 and 5.19.

The graphs are similar to the ones without methane as inlet. There curves are simply shifted to lower values of conversion. The maximum values are 95,6% and 97,1% for 262°C and 281°C respectively. Also, a comparison has been done (as before) between the two set the experiments. The differences are plotted in figure 5.20.

The rise of the conversion in this case is even higher, being 7% and 15%. Again, a rough prediction can be made via those linear correlations. So, for a particle diameter smaller than 1,5mm 100% can be achieved for this flow rates.

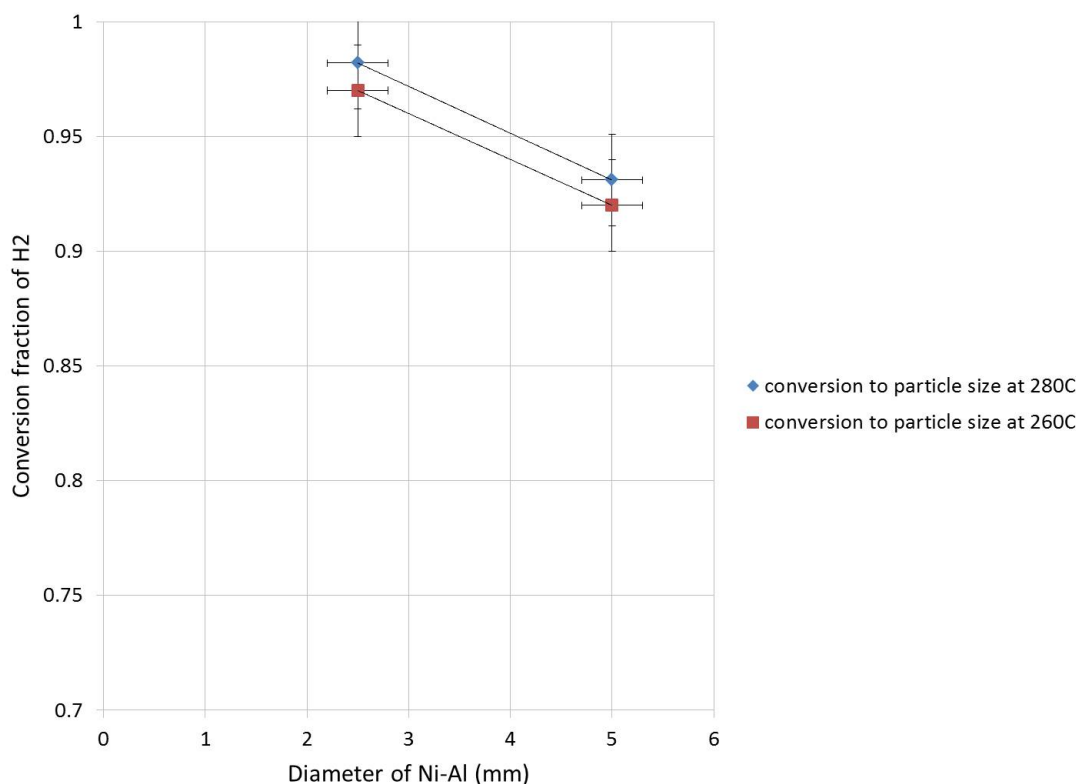


Figure 5.17: Conversion of H_2 , comparison between Ni/Al_2O_3 2,5mm-4A and Ni/Al_2O_3 -4A, (GHSV=2400, table 3.7)

5.5. Experiments with ground Ni/Al_2O_3 (1mm in size) and zeolite 4A

A last set of experiments was performed with the combination of zeolite 4A and catalyst. In this case the catalytic pellets of Ni/Al_2O_3 were reduced to even smaller particle sizes than before. The purpose was to evaluate the previously introduced linear correlation between catalytic particle size and maximum conversion rates.

The average size of Ni/Al_2O_3 pellets was 1mm. This mixture was tested under the same experimental conditions as before and the results are presented in the following sections.

5.5.1. Experiments without CH_4 as an inlet gas

Firstly, the experiments without CH_4 in the inlet composition are presented. The flow characteristics can be seen in table 3.7. The temperatures, at which the catalytic bed was tested, were $259^\circ C$ and $279^\circ C$. The results are plotted in figures 5.21 and 5.22, together with the conversion of pure nickel at those temperatures.

Useful information can be deduced by those graphs. To begin with the conversion rate didn't reach 100% as it was expected. The possible reasons for that are two. First, the lack of uniformity in the bed, due to spots of high concentration of Ni/Al_2O_3 inside the bed with zeolite 4A. This matter is been analyzed in chapter 3.3.2. The second reason is that, the relation between maximum conversion rates and Ni/Al_2O_3 size, possibly is not be linear as proposed previously.

So the maximum conversion rate is 98,5% at $259^\circ C$ and 97.6% at $279^\circ C$. Those values

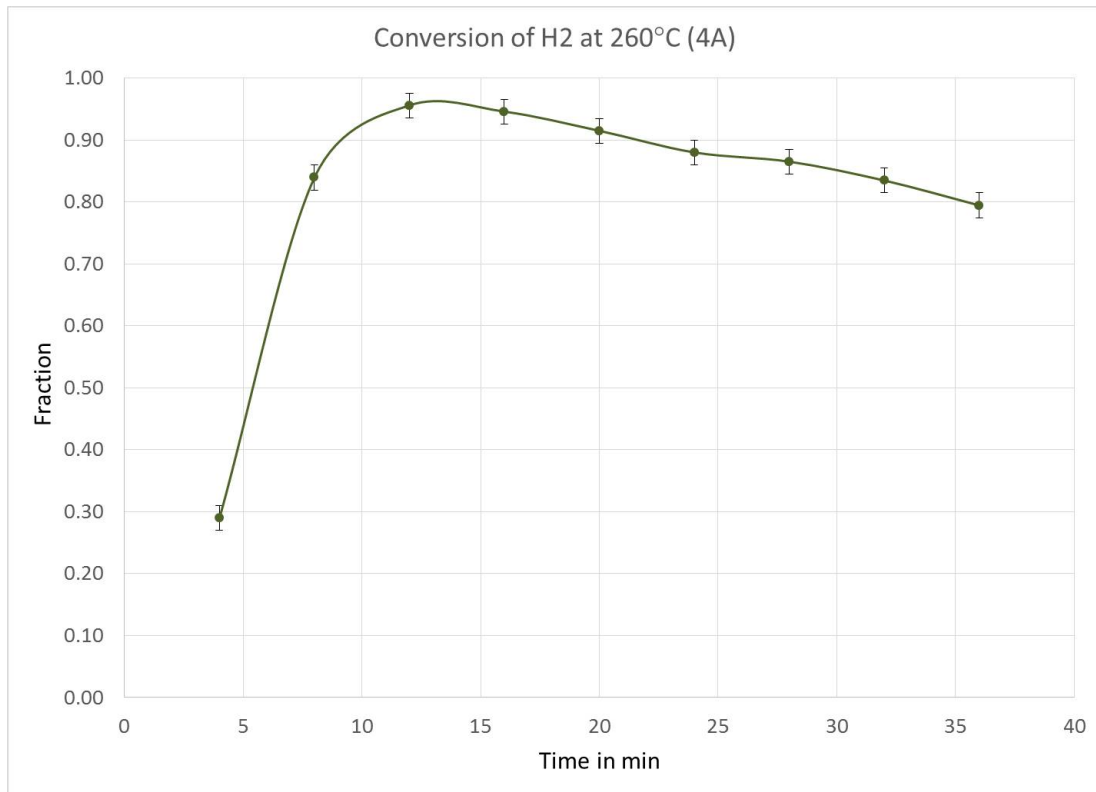


Figure 5.18: Conversion of H₂, Ni/Al₂O₃ 2,5mm – 4A (temperature 260°C and CH₄ in inlet),(GHSV=2400, table 3.8)

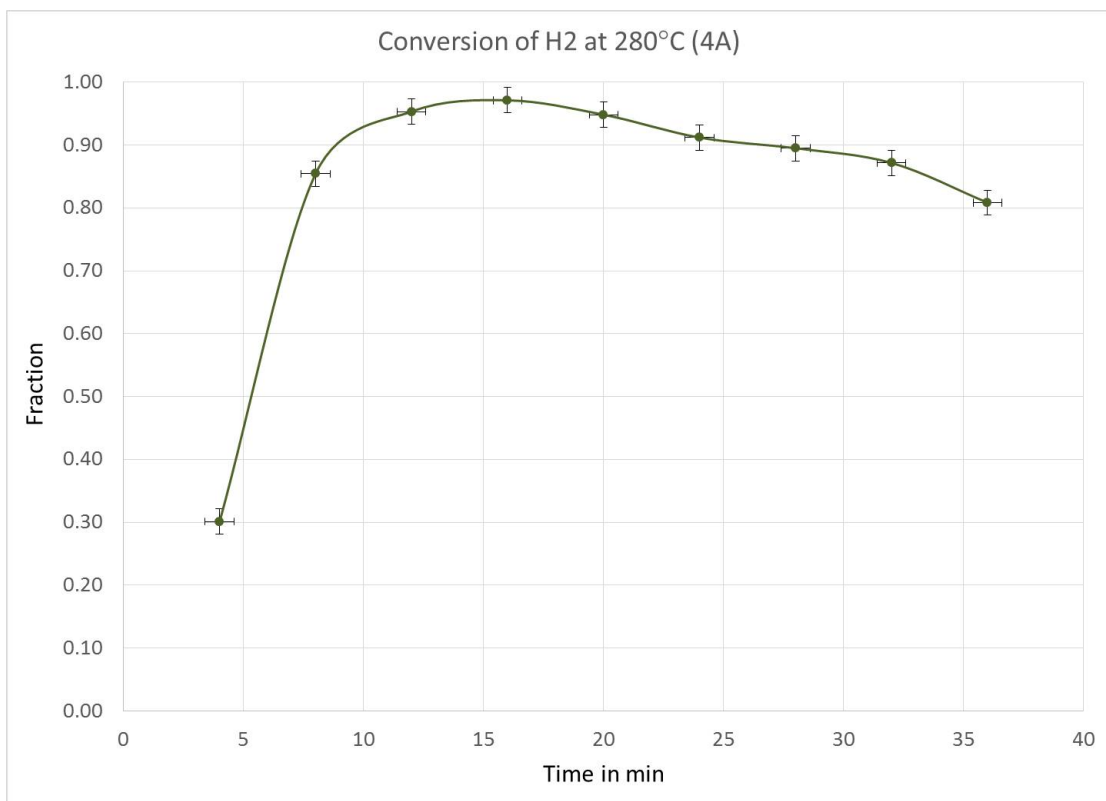


Figure 5.19: Conversion of H₂, Ni/Al₂O₃ 2,5mm – 4A (temperature 280°C and CH₄ in inlet),(GHSV=2400, table 3.8)

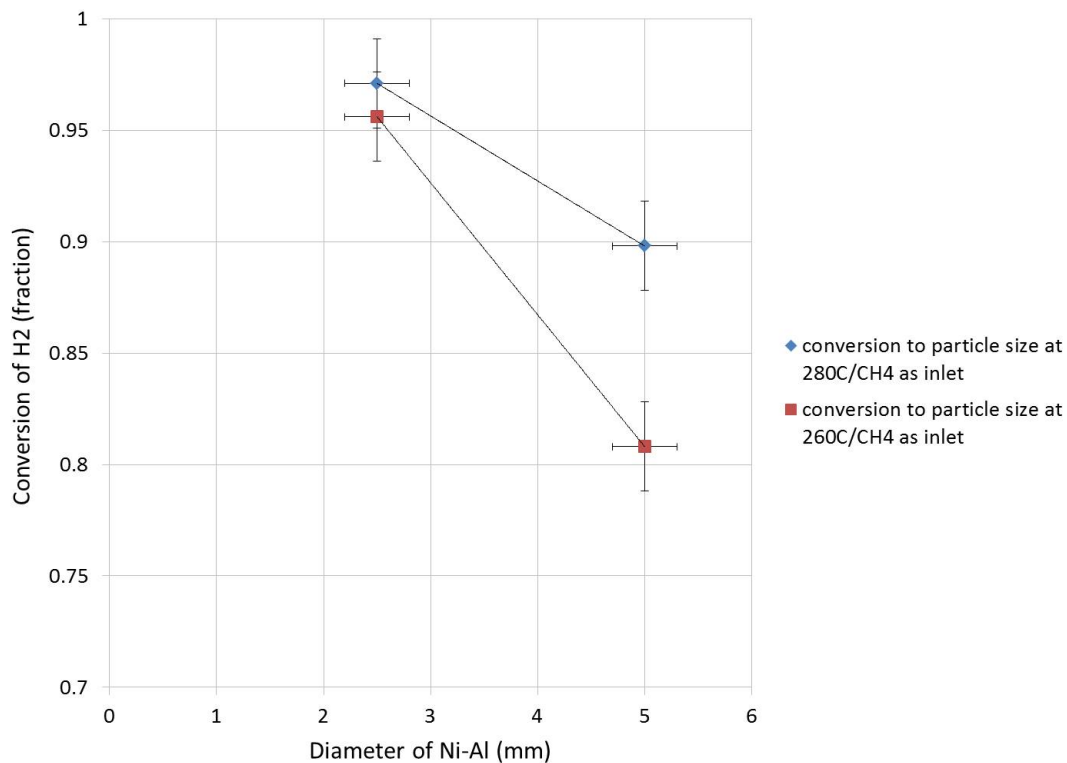


Figure 5.20: Conversion of H_2 , comparison between Ni/Al_2O_3 2,5mm – 4A and Ni/Al_2O_3 – 4A, with ch₄ as inlet, (GHSV=2400, table 3.8)

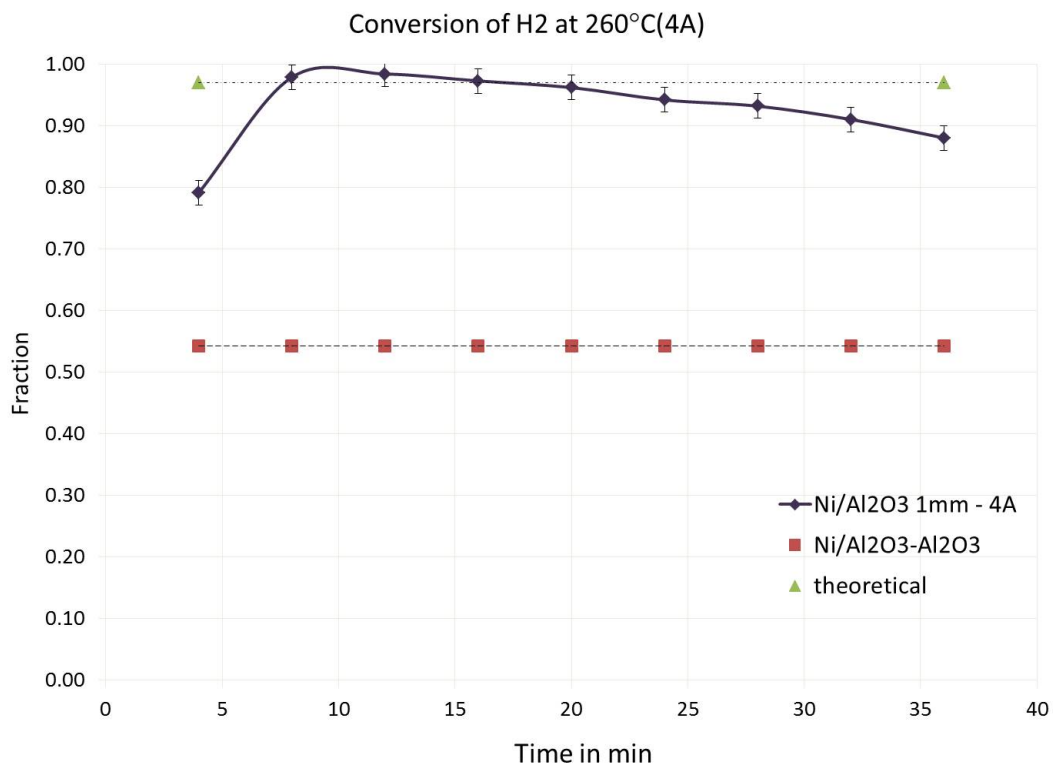


Figure 5.21: Conversion of H_2 , Ni/Al_2O_3 1mm – 4A (temperature 260°C),(GHSV=2400, table 3.7)

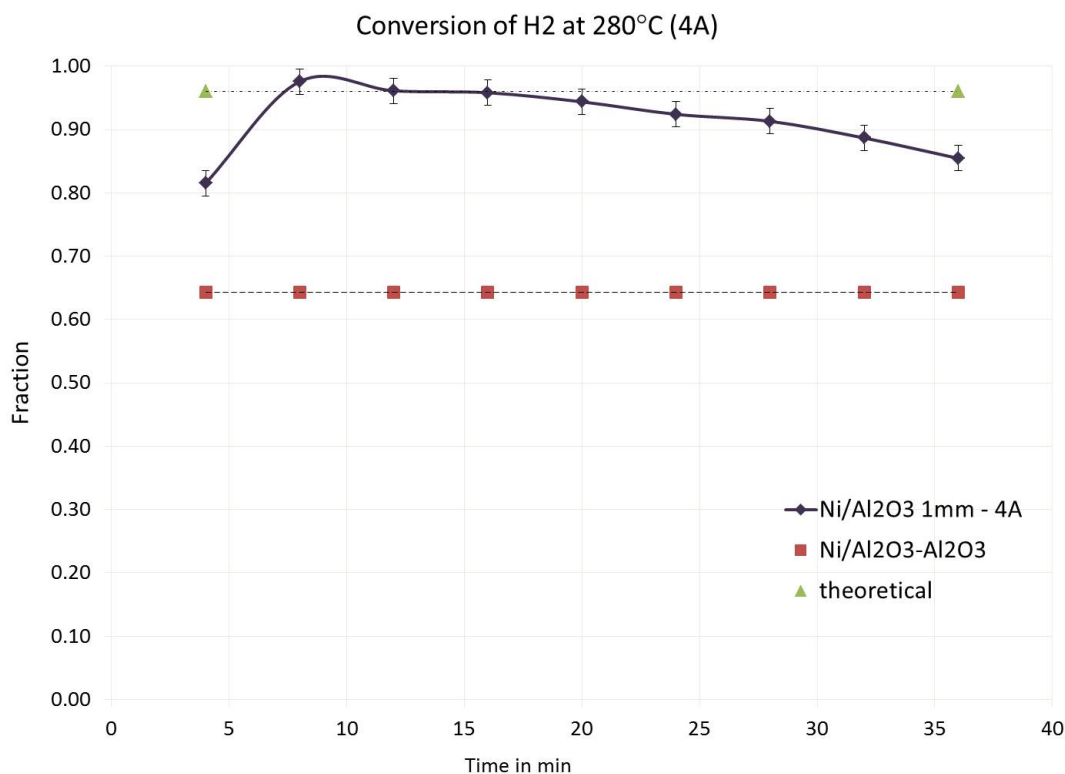


Figure 5.22: Conversion of H_2 , Ni/Al_2O_3 1mm – 4A (temperature 280°C),(GHSV=2400, table 3.7)

of conversion are similar to the ones from the experiment with 2,5mm Ni/Al_2O_3 – 4A. A small difference is that, previously, the maximum conversion was higher at 280°C than at 260°C, on average by 1%. In this occasion, the opposite can be observed.

Nonetheless, improvement can be noticed in that set of experiments compared to the previous ones. First the enhancement of the catalysis (sorption of vapor) initiates faster. So the maximum is been achieved at the second measurement instead of the third and the first recorded measurement corresponds already to more than 80% conversion. Secondly, the slope of conversion is less steep. The conversion curve remains above 91% for 30 minutes at 260°C and above 90% for 25 minutes at 280°C. The last measurement in both temperatures is above 85%.

This phenomenon can be attributed indeed in the reduction of the size of the catalytic pellets. Because, an increased amount of zeolite's 4A surface was actually involved in the enhancement of the catalysis of reactants, thus leading to an increased capacity for vapor and finally to higher conversion rates for a longer time span.

A final comparison can be done between conversion and particle size of the Ni/Al_2O_3 pellets. Since the addition of the experiments with 1mm particles of Ni/Al_2O_3 a non linear correlation can be deduced between particle size and conversion. This is visible in figure 5.23.

5.5.2. Experiments with CH₄ in the inlet stream

The last experiments performed with the bed of 1mm Ni/Al_2O_3 -Zeolite4A were at 261°C and 280°C and the inlet mixture of gases was composed by H_2 , CO_2 , CH_4 and N_2 . The re-

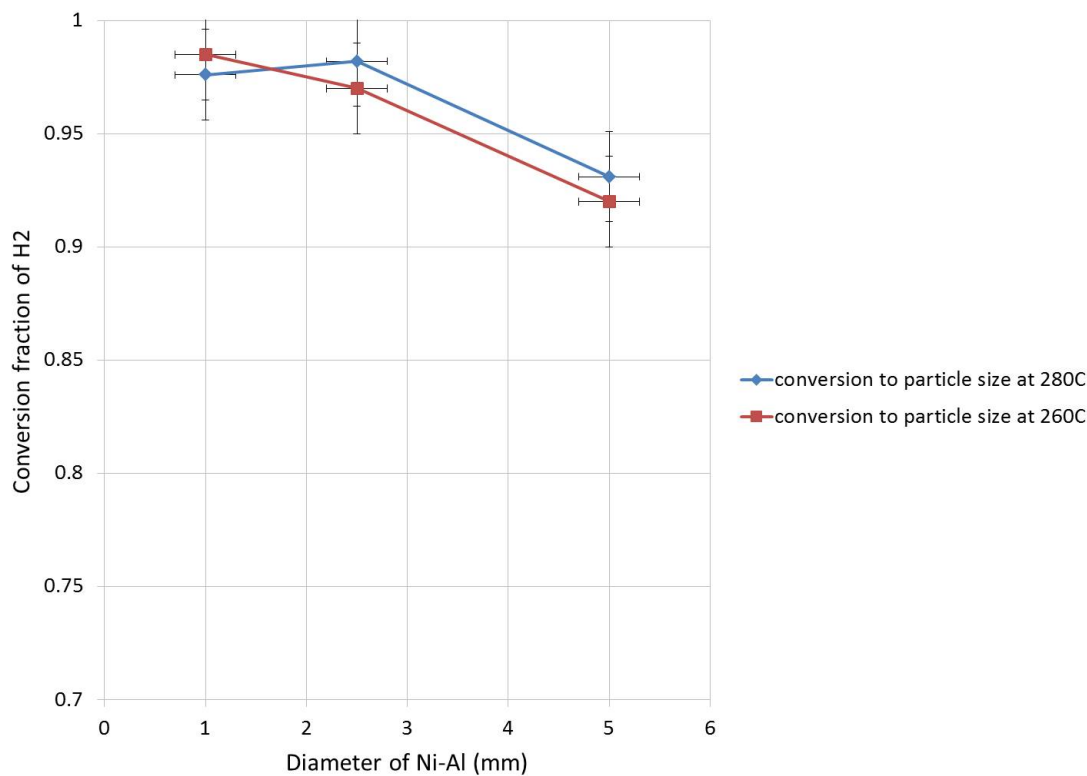


Figure 5.23: Conversion of H_2 , comparison between Ni/Al_2O_3 2,5mm – 4A, Ni/Al_2O_3 – 4A and Ni/Al_2O_3 1mm – 4A, (GHSV=2400, table 3.7)

sults are plotted in figures 5.23 and 5.24.

The graphs of those two experiments exhibit exactly the same patterns as the experiments without methane in the inlet composition. The only difference is that the conversion curves are displaced by 1 – 2% to lower values. The maxima in those cases are 97,1% and 96,1% at 261°C and 280°C respectively.

The same comparison (as in the experiments without methane as inlet) takes place between particle size and conversion rate of H_2 . The results are plotted in figure 5.26.

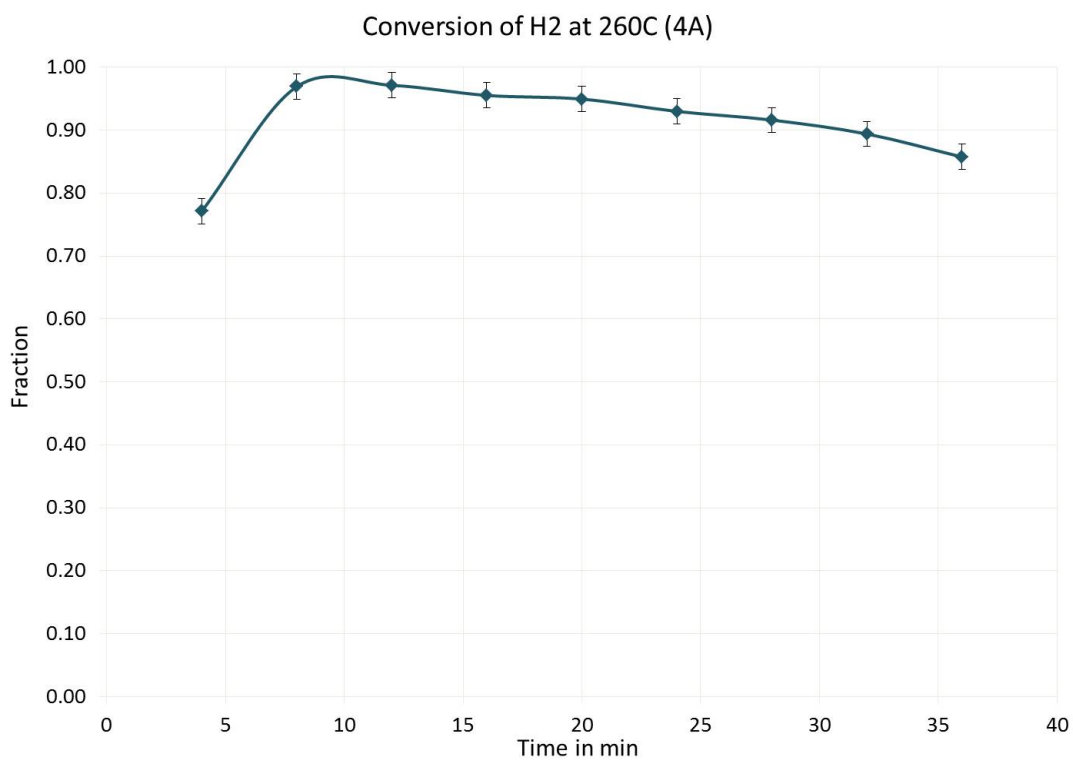


Figure 5.24: Conversion of H₂, Ni/Al₂O₃ 1mm-4A (temperature 260°C and CH₄ in inlet), (GHSV=2400, table 3.8)

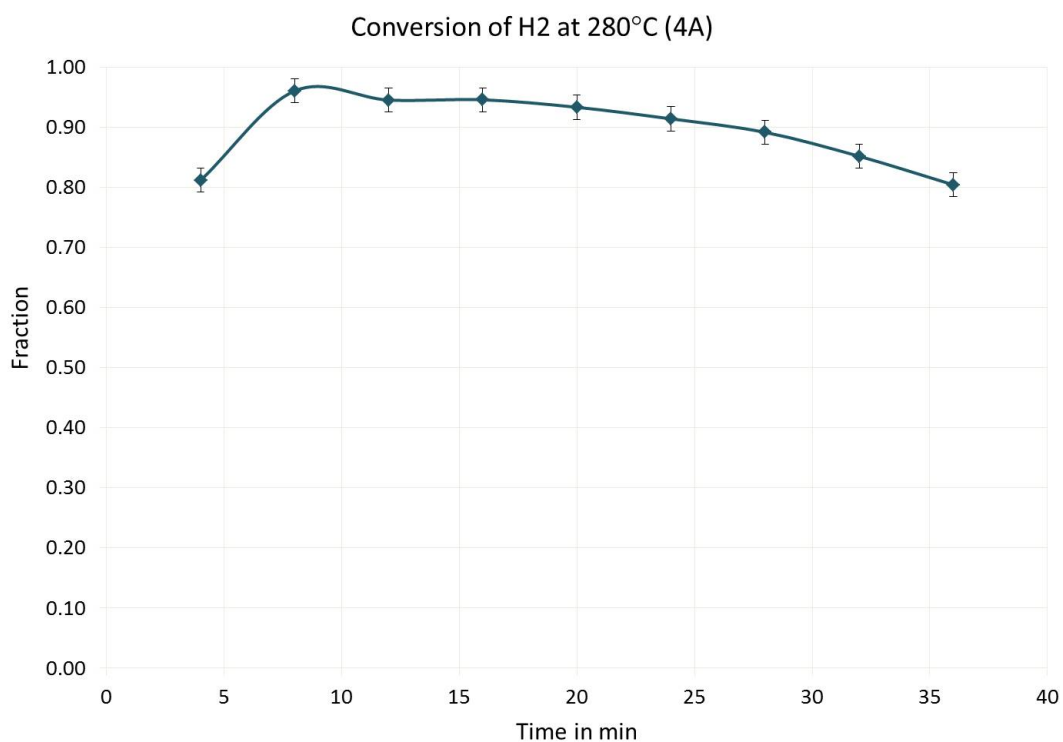


Figure 5.25: Conversion of H₂, Ni/Al₂O₃ 1mm-4A (temperature 280°C and CH₄ in inlet), (GHSV=2400, table 3.8)

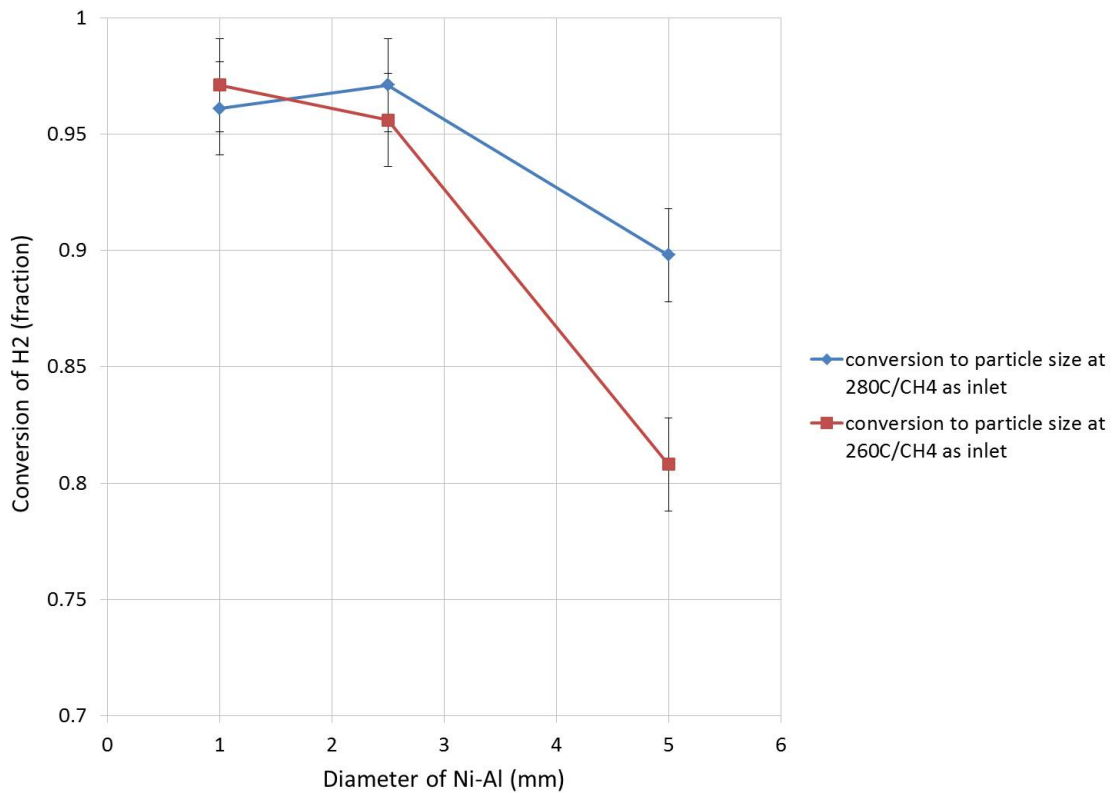


Figure 5.26: Conversion of H_2 , comparison between Ni/Al_2O_3 2,5mm – 4A, Ni/Al_2O_3 – 4A and Ni/Al_2O_3 1mm – 4A, with ch₄ as inlet, (GHSV=2400, table 3.8)

6

Concluding remarks

The conclusions, drawn from this work, are discussed in this chapter. Also, recommendations for future work in this field are provided.

6.1. Conclusions

In the current thesis work the separation enhanced methanation of CO_2 was experimentally examined. A catalytic bed was formed from the physical mixture of the nickel catalyst and the zeolites and it was placed in an (in-house designed) fixed-bed reactor. Different combinations of those materials were applied for different flows rates and flow compositions.

Useful conclusions can be drawn. First and foremost, the phenomenon of adsorption of vapor on zeolites enhances the catalytic conversion of the reactants. It doesn't only exceeded the conversion values as set by the Ni/Al_2O_3 catalyst but, also, shifted the thermodynamic equilibrium towards higher conversion values of H_2 and CO_2 . Reaching almost the purity of methane as specified for the natural gas distribution network (see chapter A.7, graphs of fraction yield of CH_4). Secondly, the main factors that influence the performance of the process the most are twofold. The first one is the proximity between the surfaces of nickel catalyst and zeolites. It was proven experimentally that by reducing the average size of the pellets, which form the catalytic bed, the conversion values increase and stabilize at higher values for longer time frames. So, zeolite 4A exhibited higher conversion values than zeolite 3A, due to its smaller particle diameter. Subsequently, by reducing the size of Ni/Al_2O_3 (combined with 4A) higher values of conversion were recorded and for a longer time frame. In the last set of experiments more than 91% of conversion was obtained for 30min of continuous process, at $260^\circ C$. In the case of Walspurger et al. [51] the maximum proximity was achieved by using a sieve fraction from pressurized pellets containing a combination of zeolite 4A and Ni/Al_2O_3 catalyst. In this was a conversion of 100% was achieved for more than 5 min of continuous process. Thus, indeed a conversion of 100% can be achieved from a physical mixture of catalyst-zeolite.

The second factor that influences the efficiency of the synergistic effect is the regeneration process of the zeolite particles. At the temperature range that this process occurs the available capacity of zeolites is very low, hence a complete regeneration of those is required. The result that led to this statement is the comparison between the experiments

with $Ni/Al_2O_3 - 3A$ and $Ni/Al_2O_3 - 4A$. In the first ones even though the maximum conversion value was smaller, the conversion values remained stable for 30 min whilst the conversion values of the latter dropped continuously. Another, useful conclusion obtained was the relatively large temperature range that the sorption enhanced methanation can realize. At the temperature range of $220^\circ C - 280^\circ C$ the enhancement occurs. This means that in an optimized Ni/Al_2O_3 -zeolites bed the temperature rise can be up to $40^\circ C$ without influencing negatively the conversion of reactants. In addition, the pair Ni/Al_2O_3 -zeolites exhibits its maximum performance (98,5% at $260 - 280^\circ C$) at lower temperatures, than the sole catalyst bed (74,5% at $340^\circ C$), and for a wider temperature range. This $\Delta T = 80^\circ C$ shows the potential of a significant cost savings in heat duties for a large scale process.

To end, the enhancement effect can overpasses the presence of methane in the inlet and exhibit high conversion rates (maximum of 97,1% at $280^\circ C$). This fact is promising for the design concept of 2-3 adiabatic reactors in a row, with the last one being the sorption enhanced methanation one.

6.2. Recommendations

Having approached the end of this study, a number of ideas rose for continuing the present topic. Firstly, the same experiments can be performed for a bigger variety of flow rates to compare those with the minimum GHSV applied in this research. Secondly, perform experiment with an even smaller average diameter of particles in the bed. This can be achieved by purchasing smaller zeolites. It would be wise to continue the research with zeolite 3A, since it produced a more stable conversion of reactants with time. This was attributed to its regeneration (as mentioned also in conclusions). But in order to accommodate smaller particles technical solutions must be found to support this bed inside the tubular reactor. Thirdly, the sorption enhanced methanation of carbon monoxide can be researched. The set up can accommodate CO (GC and a mass flow controller are calibrated for CO) and the nickel catalyst provided by the company is optimized for the co-methanation of CO_2 and CO . Hence, using the same catalytic beds as before and applying the same flow rates (keeping the new stoichiometry), one can generate comparable results with the previous set of experiments. Furthermore, experiments with a typical composition of a syngas can be performed. Thus, the future of this process and its applications can be researched. All the above-mentioned recommendations can be tested without any changes in the current set up.

Based on the conclusions drawn from the current study some more intriguing projects can be realized. The main idea is to design and create a uniformal particle of zeolites and nickel. So, impregnate chemically the nickel on zeolites. The end results will be a nickel catalyst supported on a type of zeolite. In this way one can obtain the maximum out of the synergistic effect, as it has been proved by other recent studies [25], [13], [15]. In addition, using that particle to form the bed, different reactor designs can be researched, like fluidized bed. Because in the case of a pressurized combination of nickel-zeolites, the end result would decompose under friction and collisions. Finally, due to the lack of information in literature regarding the exact capacity of zeolites in elevated temperatures, experiments should be designed to address this issue. This can be realized with some alterations in the current set up. Mainly, to dehydrate zeolites at specific temperatures and subsequently, measure its water content. So, isosteres could be obtained for the capacity of zeolites in the

temperature range that this process operates in. The same isosteres would be very useful for the case of a Ni/zeolite catalyst.

Bibliography

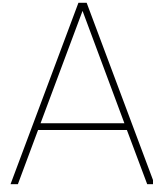
- [1] <http://accuratus.com/alumox.html>. 2013.
- [2] <https://www.deltaadsorbents.com>. 2015.
- [3] <https://yearbook.enerdata.net/CO2-emissions-data-from-fuel-combustion.html>. 2017.
- [4] <https://yearbook.enerdata.net/>. 2017.
- [5] <http://fischer-tropsch.org/>. 2017.
- [6] <http://hyperphysics.phy-astr.gsu.edu/hbase/Kinetic/menfrevis.html>. 2016.
- [7] <https://en.wikipedia.org/wiki/Sabatier-reaction>. 2017.
- [8] <http://www.sigmaaldrich.com/chemistry/chemical-synthesis/learning-center/technical-bulletins/al-1430/molecular-sieves.html>. 2017.
- [9] <http://wetten.overheid.nl/BWBR0035367/2016-04-01>. 2016-04-01.
- [10] M Abdillahi, M Gharami, and M Siddiqui. Characterization of synthesized a-zeolite: Simultaneous thermal analysis, x-ray diffraction, scanning electron microscopy and icp-chemical analysis. *Journal of Thermal Analysis and Calorimetry*, 42(6):1275–1284, 1994.
- [11] M Agnelli, M Kolb, and C Mirodatos. Co hydrogenation on a nickel catalyst.: 1. kinetics and modeling of a low-temperature sintering process. *Journal of Catalysis*, 148(1):9–21, 1994.
- [12] Michele Aresta. *Carbon dioxide recovery and utilization*. Springer Science & Business Media, 2013.
- [13] MC Bacariza, I Graça, A Westermann, MF Ribeiro, JM Lopes, and C Henriques. Co2 hydrogenation over ni-based zeolites: Effect of catalysts preparation and pre-reduction conditions on methanation performance. *Topics in Catalysis*, 59(2-4):314–325, 2016.
- [14] V Barbarossa and G Vanga. Methanation of carbon dioxide. In *XXXIV Meeting of the Italian section of the Combustion Institute–Roma*, 2011.
- [15] Andreas Borgschulte, Noris Gallandat, Benjamin Probst, Riccardo Suter, Elsa Callini, Davide Ferri, Yadira Arroyo, Rolf Erni, Hans Geerlings, and Andreas Züttel. Sorption enhanced co 2 methanation. *Physical Chemistry Chemical Physics*, 15(24):9620–9625, 2013.

- [16] DW Breck, WG Eversole, RM Milton, TB Reed, and TL Thomas. Crystalline zeolites. i. the properties of a new synthetic zeolite, type a. *Journal of the American chemical society*, 78(23):5963–5972, 1956.
- [17] BT Carvill, JR Hufton, M Anand, and S Sircar. Sorption-enhanced reaction process. *AIChE Journal*, 42(10):2765–2772, 1996.
- [18] Gabriele Centi and Siglinda Perathoner. Opportunities and prospects in the chemical recycling of carbon dioxide to fuels. *Catalysis Today*, 148(3):191–205, 2009.
- [19] Feg-Wen Chang, Ming-Tseh Tsay, and Maw-Suey Kuo. Effect of thermal treatments on catalyst reducibility and activity in nickel supported on rha-al₂o₃ systems. *Thermochimica acta*, 386(2):161–172, 2002.
- [20] Feg-Wen Chang, Maw-Suey Kuo, Ming-Tseh Tsay, and Ming-Chung Hsieh. Hydrogenation of co₂ over nickel catalysts on rice husk ash-alumina prepared by incipient wetness impregnation. *Applied Catalysis A: General*, 247(2):309–320, 2003.
- [21] Tao Chen, Wei Guo Wang, He Miao, Tingshuai Li, and Cheng Xu. Evaluation of carbon deposition behavior on the nickel/yttrium-stabilized zirconia anode-supported fuel cell fueled with simulated syngas. *Journal of Power Sources*, 196(5):2461–2468, 2011.
- [22] PD Cobden, P Van Beurden, H Th J Reijers, GD Elzinga, SCA Kluiters, JW Dijkstra, D Jansen, and RW Van Den Brink. Sorption-enhanced hydrogen production for pre-combustion co₂ capture: thermodynamic analysis and experimental results. *International journal of greenhouse gas control*, 1(2):170–179, 2007.
- [23] AF Cunha, Y-J Wu, JC Santos, and AE Rodrigues. Sorption enhanced steam reforming of ethanol on hydrotalcite-like compounds impregnated with active copper. *Chemical Engineering Research and Design*, 91(3):581–592, 2013.
- [24] Grace Davison. Sylobead-adsorbents for process applications. *WR Grace, Columbia, MD*, 2010.
- [25] R Delmelle, RB Duarte, T Franken, D Burnat, L Holzer, A Borgschulte, and A Heel. Development of improved nickel catalysts for sorption enhanced co₂ methanation. *International Journal of Hydrogen Energy*, 41(44):20185–20191, 2016.
- [26] Shuguang Deng. Sorbent technology. *Encyclopedia of Chemical Processing*, pages 2825–2845, 2006.
- [27] UN DeSA. World population prospects: the 2015 revision. *Population Division of the Department of Economic and Social Affairs of the United Nations Secretariat, New York*, 2016.
- [28] Guoan Du, Sangyun Lim, Yanhui Yang, Chuan Wang, Lisa Pfefferle, and Gary L Haller. Methanation of carbon dioxide on ni-incorporated mcm-41 catalysts: The influence of catalyst pretreatment and study of steady-state reaction. *Journal of catalysis*, 249(2):370–379, 2007.

- [29] S Fujita, H Terunuma, H Kobayashi, and N Takezawa. Methanation of carbon monoxide and carbon dioxide over nickel catalyst under the transient state. *Reaction Kinetics and Catalysis Letters*, 33(1):179–184, 1987.
- [30] Hiroyasu Furukawa, Kyle E Cordova, Michael O’Keeffe, and Omar M Yaghi. The chemistry and applications of metal-organic frameworks. *Science*, 341(6149):1230444, 2013.
- [31] Elżbieta Gabruś, Józef Nastaj, Piotr Tabero, and Tomasz Aleksandrak. Experimental studies on 3a and 4a zeolite molecular sieves regeneration in tsa process: Aliphatic alcohols dewatering–water desorption. *Chemical Engineering Journal*, 259:232–242, 2015.
- [32] Jiajian Gao, Yingli Wang, Yuan Ping, Dacheng Hu, Guangwen Xu, Fangna Gu, and Fabing Su. A thermodynamic analysis of methanation reactions of carbon oxides for the production of synthetic natural gas. *RSC Advances*, 2(6):2358–2368, 2012.
- [33] Gabriella Garbarino, Paola Riani, Loredana Magistri, and Guido Busca. A study of the methanation of carbon dioxide on ni/al 2 o 3 catalysts at atmospheric pressure. *International journal of hydrogen energy*, 39(22):11557–11565, 2014.
- [34] Wim Haije and Hans Geerlings. Efficient production of solar fuel using existing large scale production technologies. *Environmental Science and Technology-Columbus*, 45(20):8609, 2011.
- [35] M.M. Abbott J.M. Smith, H.C. Van Ness. *Introduction to chemical engineering thermodynamics*. Mc Graw, 2005.
- [36] Lennart Joos, Joseph A Swisher, Berend Smit, et al. Molecular simulation study of the competitive adsorption of h₂o and co₂ in zeolite 13x. *Langmuir*, 29(51):15936–15942, 2013.
- [37] Christian Junaedi, Kyle Hawley, Dennis Walsh, Subir Roychoudhury, Morgan Abney, and Jay Perry. Compact and lightweight sabatier reactor for carbon dioxide reduction. In *41st International Conference on Environmental Systems*, page 5033, 2011.
- [38] Jan Kopyscinski, Tilman J Schildhauer, and Serge MA Biollaz. Production of synthetic natural gas (sng) from coal and dry biomass—a technology review from 1950 to 2009. *Fuel*, 89(8):1763–1783, 2010.
- [39] Zbigniew Kowalczyk, Kazimierz Stolecki, Wioletta Rarog-Pilecka, Elzbieta Miskiewicz, Ewa Wilczkowska, and Zbigniew Karpinski. Supported ruthenium catalysts for selective methanation of carbon oxides at very low cox/h₂ ratios. *Applied Catalysis A: General*, 342(1):35–39, 2008.
- [40] AL Kustov, Anne Mette Frey, Kasper Emil Larsen, Tue Johannessen, Jens Kehlet Nørskov, and Claus H Christensen. Co methanation over supported bimetallic ni–fe catalysts: from computational studies towards catalyst optimization. *Applied Catalysis A: General*, 320:98–104, 2007.

- [41] Gun Dae Lee, Myung Jun Moon, Jeong Hwan Park, Seong Soo Park, and Seong Soo Hong. Raney ni catalysts derived from different alloy precursors part ii. co and co₂ methanation activity. *Korean Journal of Chemical Engineering*, 22(4):541–546, 2005.
- [42] Hezhi Liu, Xiujing Zou, Xueguang Wang, Xionggang Lu, and Weizhong Ding. Effect of ceo₂ addition on ni-al₂o₃ catalysts for the methanation of carbon dioxide with hydrogen. *Journal of Natural Gas Chemistry*, 21:703–707, 2012.
- [43] Bert Metz, Ogunlade Davidson, Heleen de Coninck, Manuela Loos, Leo Meyer, Working Group III of the Intergovernmental Panel on Climate Change, et al. Carbon dioxide capture and storage, 2005.
- [44] Jos GI Olivier, Jeroen AHW Peters, and Greet Janssens-Maenhout. Trends in global co₂ emissions 2016 report. 2016.
- [45] S Sane, JM Bonnier, JP Damon, and J Masson. Raney metal catalysts: I. comparative properties of raney nickel proceeding from ni-al intermetallic phases. *Applied catalysis*, 9(1):69–83, 1984.
- [46] Schuster Markus Roman Rothenfluh Tobias Orth Andreas Schaaf Tanja, Grunig Jochen. Methanation of co₂-storage of renewable energy in a gas distribution system. *Energy, Sustainability and Society*, 4(1):2, 2014.
- [47] Marian Simo, Siddharth Sivashanmugam, Christopher J Brown, Vladimir Hlavacek, et al. Adsorption/desorption of water and ethanol on 3a zeolite in near-adiabatic fixed bed. *Industrial and Engineering Chemistry Research*, 48(20):9247, 2009.
- [48] Melkon Tathier, Birgül Tantekin-Ersolmaz, and Ayşe Erdem-Şenatalar. A novel approach to enhance heat and mass transfer in adsorption heat pumps using the zeolite–water pair. *Microporous and Mesoporous Materials*, 27(1):1–10, 1999.
- [49] M.V. Twigg. *Catalyst Handbook, second edition*. Manson Publishing Ltd., 1996.
- [50] M van Sint Annaland. Pre-combustion co₂ capture by sorption-enhanced water-gas shift (sewgs): Modelling from molecules to. 2013.
- [51] Stéphane Walspurger, Gerard D Elzinga, Jan Wilco Dijkstra, Marija Sarić, and Wim G Haije. Sorption enhanced methanation for substitute natural gas production: Experimental results and thermodynamic considerations. *Chemical Engineering Journal*, 242:379–386, 2014.
- [52] Gordon D Weatherbee and Calvin H Bartholomew. Hydrogenation of co₂ on group viii metals: I. specific activity of ni/sio₂. *Journal of Catalysis*, 68(1):67–76, 1981.
- [53] Gordon D Weatherbee and Calvin H Bartholomew. Hydrogenation of co₂ on group viii metals: II. kinetics and mechanism of co₂ hydrogenation on nickel. *Journal of Catalysis*, 77(2):460–472, 1982.
- [54] Wang Wei and Gong Jinlong. Methanation of carbon dioxide: an overview. *Frontiers of Chemical Science and Engineering*, 5(1):2–10, 2011.

-
- [55] Tao Zhu, Seil Yang, Dae Ki Choi, and Kyung Ho Row. Adsorption of carbon dioxide using polyethyleneimine modified silica gel. *Korean Journal of Chemical Engineering*, 27(6):1910–1915, 2010.



Appendix

A.1.

```
D=5.25*10(-3);  
h=16.1*10(-3);  
por=0.3;
```

```
V_cat=pi*(D/2)2*h; %volume of the catalytic bed side  
V_gases=V_cat*por; %volume of the gases in the catalytic bed  
V_al=V_cat*(1-por); %volume of alumina pellets
```

```
%Thermodynamic data
```

```
T=573; %Temperature of catalytic bed in Kelvin  
DH_reac=107287; %enthalpy of reaction in j/mol  
rho_co2=24.110; %density of co2 at T in mol/m3 NIST  
rho_h2=24.100; %density of h2 at T in mol/m3 NIST  
den_al=2; %density of Al2O3 at T in g/cm3 NIST  
mol_m_al=102; %molar mass of alumina in g/mol  
rho_al=den_al/(mol_m_al*10(-6)); %density of Al2O3 at T in mol/m3  
cp_co2=44.700; %cp of co2 at T in j/mol/K  
cp_h2=29.256; %cp of h2 at T in j/mol/K  
cp_al=110; %cp of Al2O3 at T in j/mol/K  
cp_n2=29.58; %cp of N2 at T in j/mol/K  
%Number of mols in a batch of the reactor  
mol_co2=rho_co2*V_gases*0.0476; %mols of co2 in cat bed stoich.  
mol_h2=rho_h2*V_gases*0.1905; %mols of h2 in cat bed stoich.  
mol_al=rho_al*V_al; %mols of alumina in the catalytic bed
```

```
%Adiabatic temperature rise for full conversion of one batch
```

```
Q_reac=DH_reac*mol_co2; %heat released from full conversion of CO2  
DT_ad_al=Q_reac/(cp_al*mol_al); %adiabatic temperature rise
```

% due to reaction on the alumina side

DT_ad=Q_reac / (cp_co2*mol_co2+cp_h2*mol_h2+cp_al*mol_al); %adiabatic temperature

% rise due to reaction on the gases and alumina combined

DT_ad_gases=Q_reac / ((cp_co2*mol_co2+cp_h2*mol_h2));

DT_ad_hr=DT_ad*0.6667*921;

A.2.

Table A.1: Mols reacted based on stoichiometry

	CO_2	$4H_2$	\leftrightarrow	CH_4	$2H_2O$	
mols	1	4		1	2	Total
mols	1-x	4-4x		x	2x	5-2x

The general equation of the chemical equilibrium is the following.

$$K_{eq} = \frac{y_{CH_4} y_{H_2O}^2}{y_{CO_2} y_{CH_4}^4} * \left(\frac{P_{tot}}{P_{ref}}\right)^{-2} = \frac{\frac{x}{5-2x} \left(\frac{2x}{5-2x}\right)^2}{\frac{1-x}{5-2x} \left(\frac{4-4x}{5-2x}\right)^4} * \left(\frac{P_{tot}}{P_{ref}}\right)^{-2} = \frac{4x^3(5-2x)^2}{(1-x)(4-4x)^4} \left(\frac{P_{tot}}{P_{ref}}\right)^{-2} \quad (A.1)$$

A.3.

%Influence of total pressure in the conversion of CO2

%Similar file to the other with K, but with the extra total pressure term
%K values from Factsage

K=[1.06e14 1.64e11 9.21e8 1.32e7 3.79e5 1.86e4 1.39e3 1.45e2];

T=[100 150 200 250 300 350 400 450];

Conversion = zeros(5,8);

P=[1 5 10 30 60];

for j=1:5

for i=1:8

eqn=@(x) K(i)*(1-x)*(4-4*x)^4-4*x^3*(5-2*x)^2*P(j)^(-2)

Conversion(j,i)=fzero(eqn,1);

end

end

plot(T,Conversion,'LineWidth',1.2)

grid on

% y axis

```

ylabel('CO_{2} Conversion (-)');
% x axis
xlabel('Temperature(C)');
% legend
legend('1 bar', '5 bar', '10 bar', '30 bar', '60 bar', 'Location', 'SouthWest')

```

A.4.

In the equation of the equilibrium constant with vapor's partial pressure, the term y_{H_2O} is not substituted by the mol concentration as before ($\frac{2x}{5-2x}$) but by the partial pressure $\frac{P_{H_2O}}{P_{tot}}$.

Also the total amount of mols is $5 - 4x$ but corrected for the amount of vapor that hasn't been adsorbed by the zeolite pellets. So it becomes $\frac{5-4x}{1-\frac{P_{H_2O}}{P_{tot}}}$.

The equilibrium constant will be:

$$K_{eq} = \frac{\frac{x}{5-4x} \left(\frac{2x}{5-4x}\right)^2 \frac{1-\frac{P_{H_2O}}{P_{tot}}}{1-\frac{P_{H_2O}}{P_{tot}}}}{\frac{1-x}{5-4x} \left(\frac{4-4x}{5-4x}\right)^4 \frac{1-\frac{P_{H_2O}}{P_{tot}}}{1-\frac{P_{H_2O}}{P_{tot}}}} * \left(\frac{P_{tot}}{P_{ref}}\right)^{-2} = \frac{x \left(\frac{P_{H_2O}}{P_{tot}}\right)^2 (5-4x)^4}{(1-x)(4-4x)^4 \left(1-\frac{P_{H_2O}}{P_{tot}}\right)^4} \left(\frac{P_{tot}}{P_{ref}}\right)^{-2} \quad (A.2)$$

A.5.

%H2O partial pressure influence in the conversion

%Using the K equation for different water partial pressures, the theoretical CO2 conversion curved is calculated

```

K=[1.06e14 1.64e11 9.21e8 1.32e7 3.79e5 1.86e4 1.39e3 1.45e2];
T=[100 150 200 250 300 350 400 450];
Ptot=1;
P=[0.35 0.3 0.25 0.2 0.15 0.1 0.05];

Conversion = zeros(7,8);

for j=1:7
for i=1:8
eqn=@(x) K(i)*(1-x)*(1-P(j)/Ptot)^4*(4-4*x)^4-x*(5-4*x)^4*(P(j)/Ptot)^2;
Conversion(j,i)=fzero(eqn,1);
end
end

plot(T,Conversion, 'LineWidth', 1.2)
grid on

% y axis
ylabel('H_{2} Conversion (-)');

```

```
% x axis  
xlabel('Temperature(C)');
```

```
% legend  
legend('0.35 bar', '0.3 bar', '0.25 bar', '0.2 bar', '0.15 bar', '0.1 bar',  
'0.05 bar', 'Location', 'SouthWest')
```

A.6.

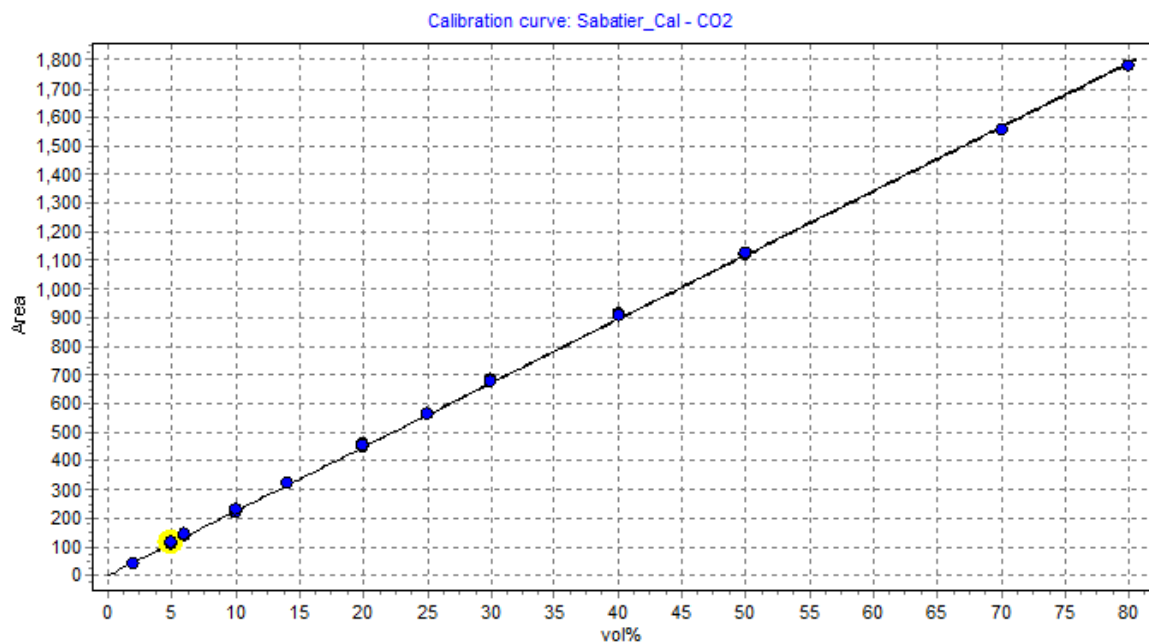


Figure A.1: Calibration line of CO2

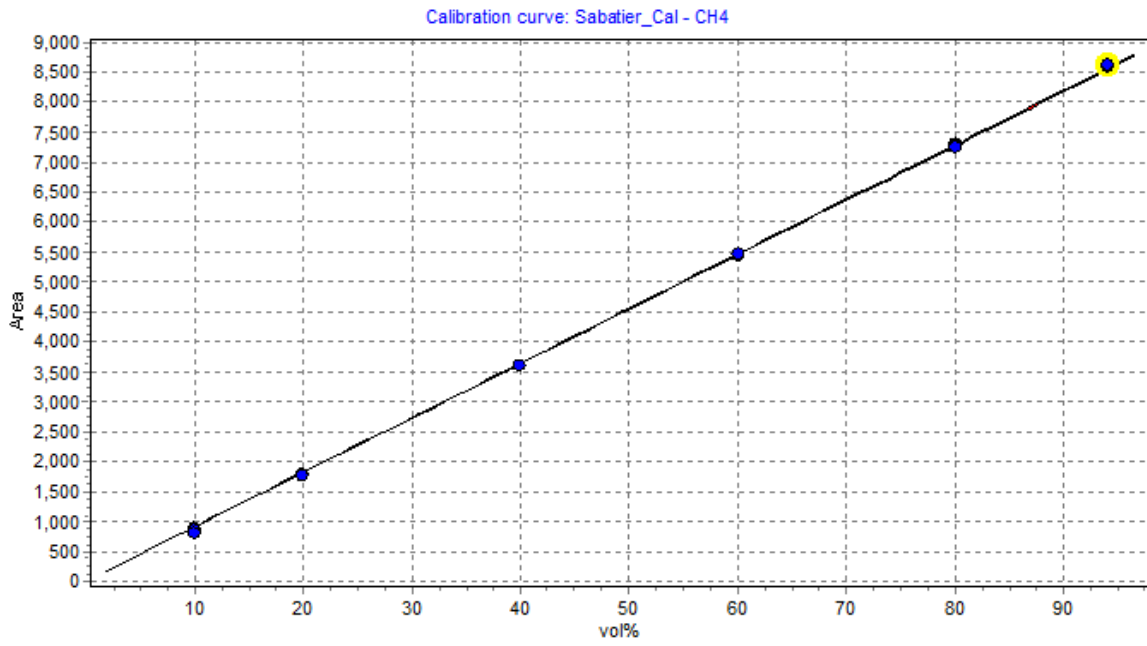


Figure A.2: Calibration line of CH4

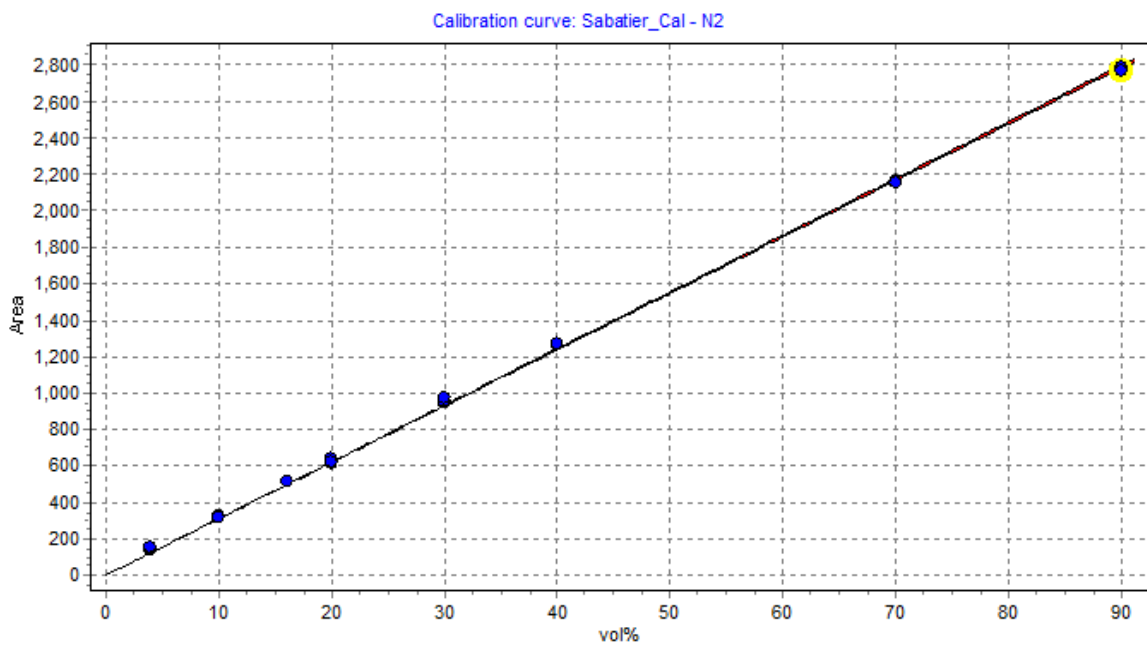


Figure A.3: Calibration line of N2

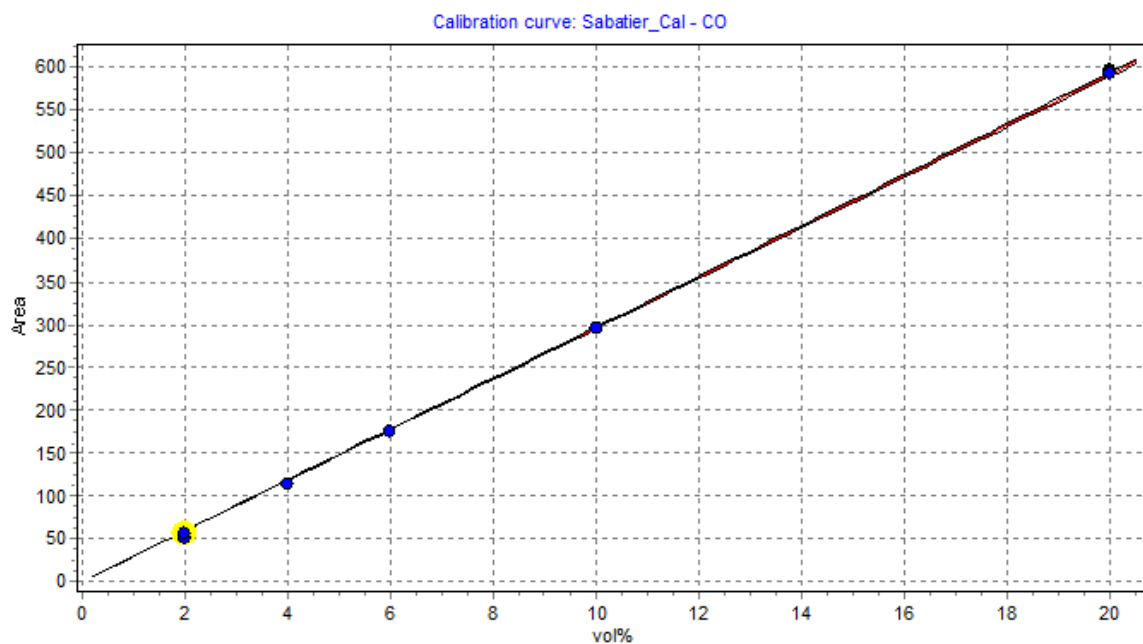


Figure A.4: Calibration line of CO

A.7.

This section contains the graphs of fraction yield of methane. Four graphs were obtained from the experiments with $2,5\text{mm Ni/Al}_2\text{O}_3\text{-4A}$ and $1\text{mm Ni/Al}_2\text{O}_3\text{-4A}$ (at 260°C and 280°C). Figures A.5 and A.6 refer to the experiments with $2,5\text{mm Ni/Al}_2\text{O}_3\text{-4A}$ at 260°C and 280°C , respectively. Those graphs match with the ones of conversion of H_2 at the same experimental conditions (figures 5.15, 5.16), verifying the 100% selectivity towards methane. The same holds for figures A.7 and A.8, which match with figures 5.21, 5.22 (conversion of hydrogen at the same experimental conditions).

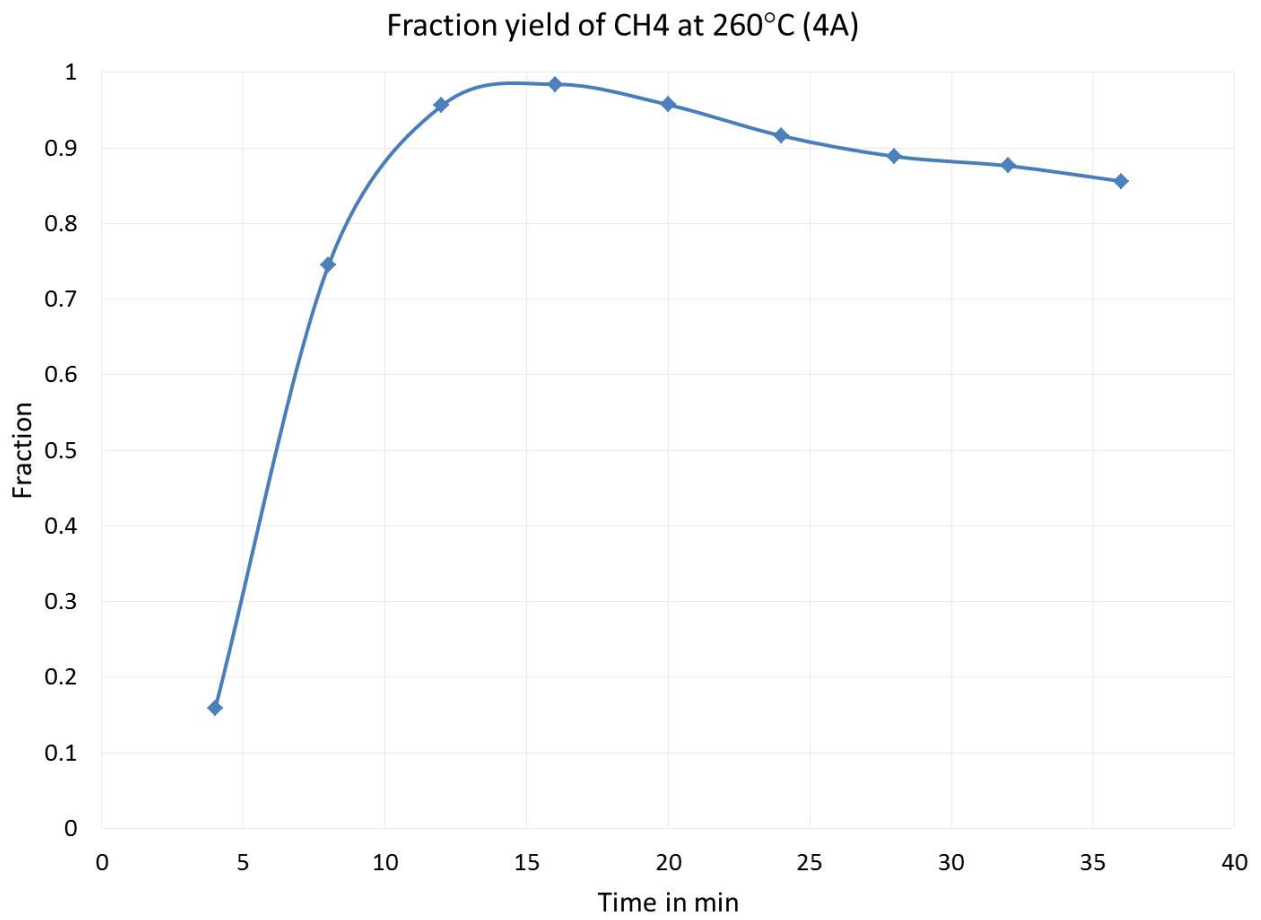


Figure A.5: Fraction yield of CH₄, Ni/Al₂O₃ 2,5mm-4A, (at 260°C),(GHSV=2400, table 3.7)

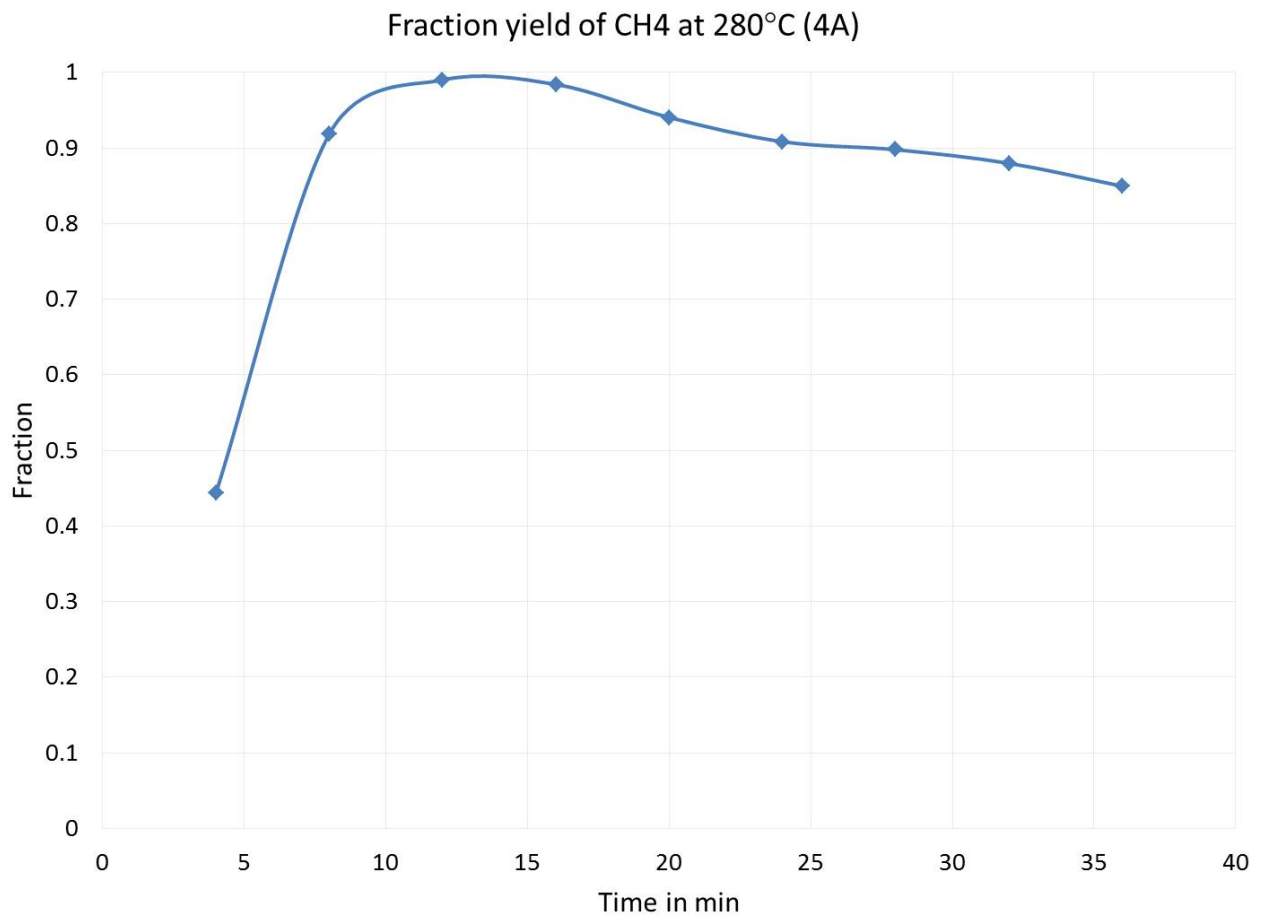


Figure A.6: Fraction yield of CH₄, Ni/Al₂O₃ 2,5mm-4A, (at 280°C),(GHSV=2400, table 3.7)

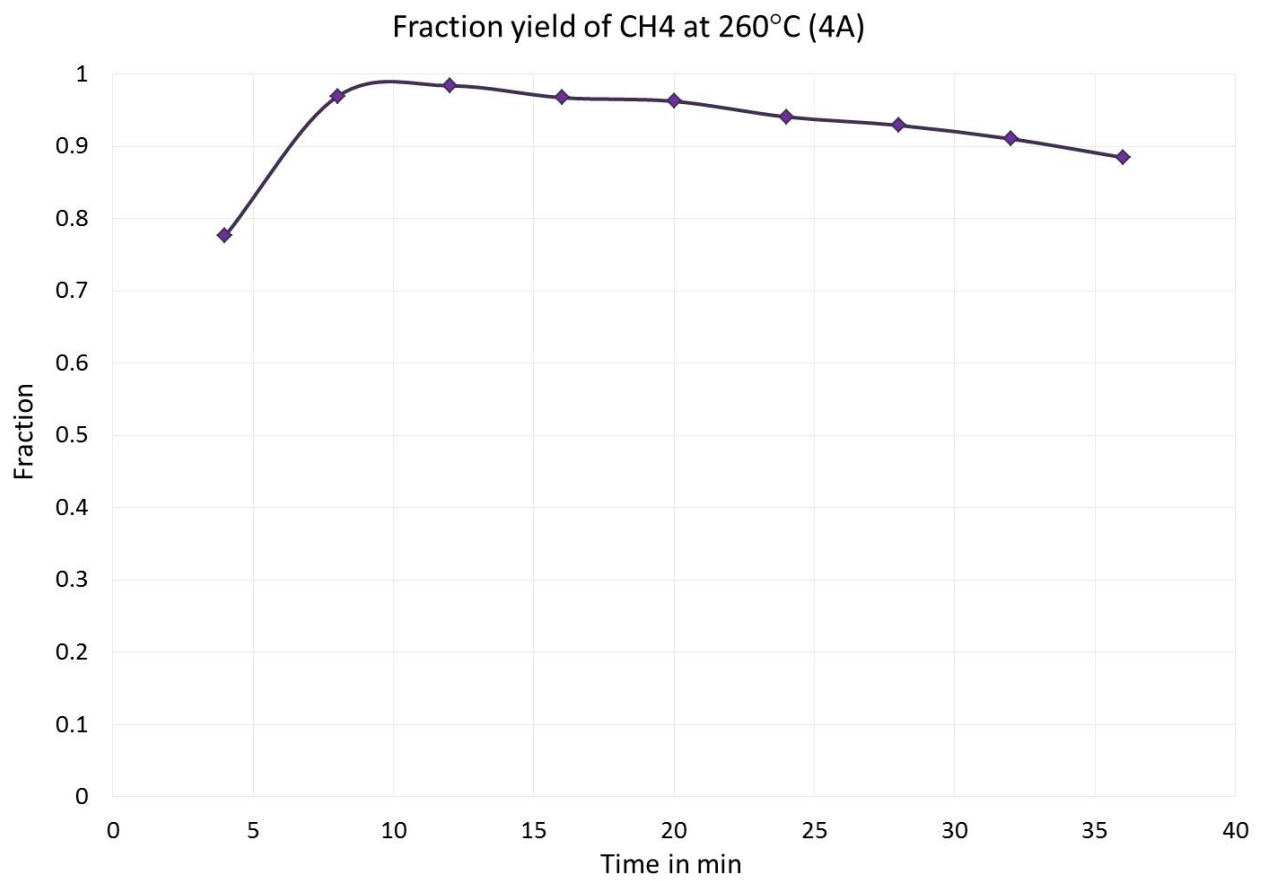


Figure A.7: Fraction yield of CH₄, Ni/Al₂O₃ 1mm-4A, (at 260°C),(GHSV=2400, table 3.7)

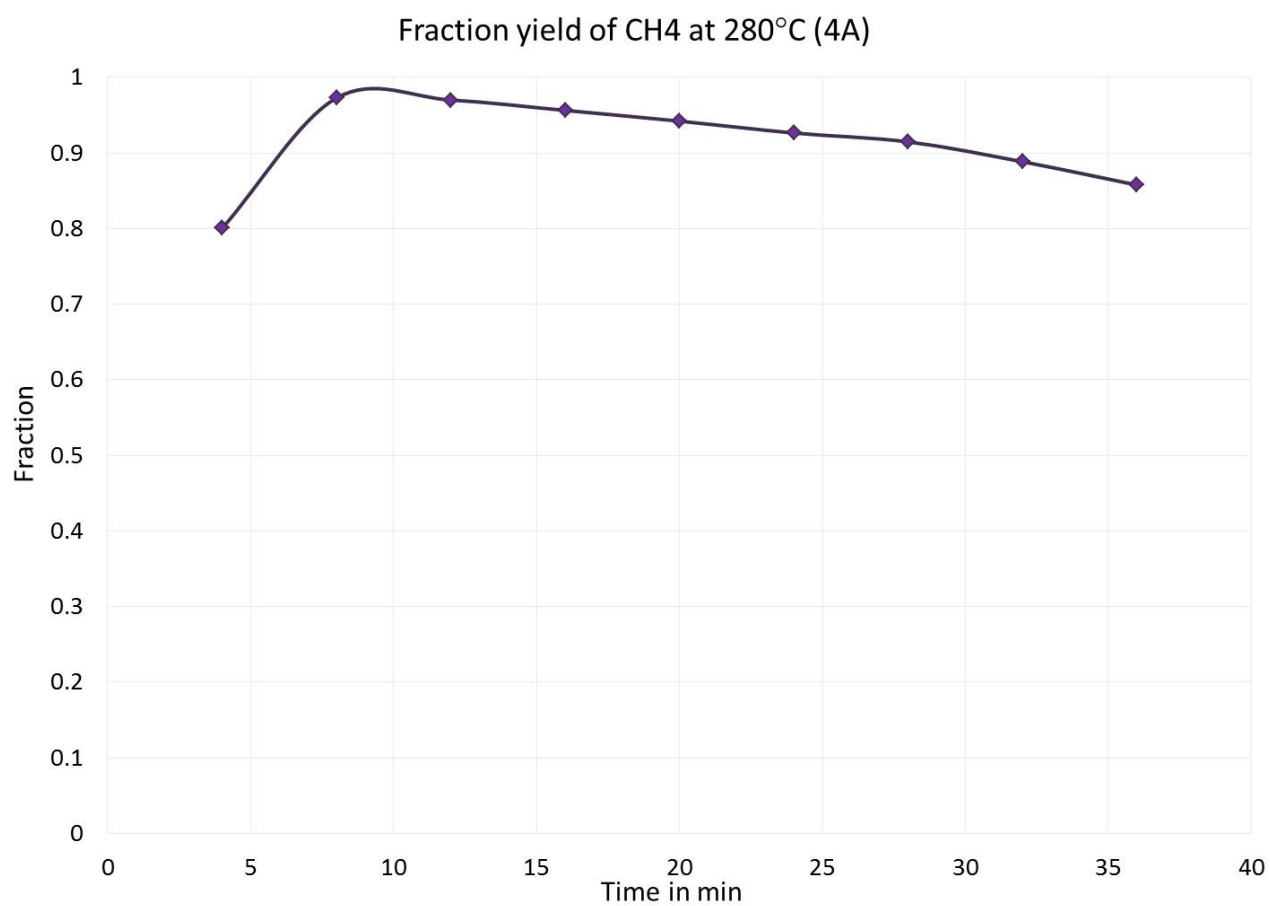


Figure A.8: Fraction yield of CH₄, Ni/Al₂O₃ 1mm-4A, (at 280°C), (GHSV=2400, table 3.7)